FACULTY OF ENGINEERING
Department of Mining & Materials Engineering

Investigating the role of mineralization of bioactive glass in wound healing using a cellular 3D collagen matrix

Rugia Abu A.M.M.A. Alhassan

Supervised by: Showan N Nazhat and Monzur Murshed

A thesis submitted to McGill University, Montreal, in
partial fulfillment of the requirements of the degree of
Master of Engineering

Abstract

Background: Chronic wounds suffer from low blood supply to the wound bed, a condition usually marked by low vascular endothelial growth factor (*Vegf*) levels and subsequently less angiogenesis. While originally designed to repair mineralized tissues, bioactive glasses have recently gained much interest as a treatment to accelerate the healing in chronic wounds. The main argument supporting their use is based on their ionic stimuli by enhancing particular processes, such as angiogenesis, and aiding in the healing stages of inflammation, proliferation, and maturation. However, the majority of in-vitro cell culture research remains based on two-dimensional and ionic release-only models, with little research done on three-dimensional direct contact models; especially with regard to wound healing, bioactive glass and the potential of ectopic mineralization. **Methods:** In this work, a three-dimensional model was developed to study the function of NIH/3T3 fibroblasts when in direct contact with a classical bioactive glass; 45S5 Bioglass®, when amorphous, post pre-conditioning in simulated body fluid (SBF) for 3 and 14 days to induce different extents of mineralization and synthetic hydroxyapatite (HAp). Cells were cultured in dense collagen gels of approximately 13.4 wt%, either alone or when incorporated with amorphous 45S5 Bioglass®, 3- and 14-day conditioned 45S5 Bioglass® or HAp particles for up to 23 days, in-vitro. The proliferation, metabolic activity, viability, matrix mineralization and the expression of genes implicated in would healing, namely *vegf*, alpha-smooth muscle actin (*α-SMA*), transforming growth factor beta (*Tgfb1*), and collagen (*Col1a1*), were investigated along with bone sialoprotein (*Ibsp*) as an indicator of cell-mediated matrix mineralization. **Results:** The 45S5 Bioglass® particle specific surface area increased 900-fold after 14 days of conditioning in SBF. Scanning electron microscopy (SEM), X-ray diffraction and attenuated total reflectance-Fourier-transform infrared spectroscopy analyses confirmed the partial mineralization of the amorphous 45S5 Bioglass® through the formation of a surface hydroxycarbonate apatite layer. Inductively coupled plasma-optical emission spectrometry analysis indicated amorphous 45S5 Bioglass® had the highest release level of alkaline species in deionized water. Its incorporation into fibroblast-seeded dense collagen gels led a decrease in initial cell proliferation, metabolic activity, and viability. Cells in direct contact with partially mineralized 45S5 Bioglass® and HAp had comparable metabolic activities and proliferation. *Vegf* expression levels were highest at day

2 for cells in contact with amorphous and 3-day mineralized 45S5. By day 23, *Vegf* expression significantly decreased in cells when in contact with amorphous 45S5, whereas those in the presence of 14-day mineralized 45S5 displayed the highest expression. HAp conditioning experienced the highest α-SMA expression at day 2 in culture. *Col1a*1 expression levels significantly decreased for both 3-day mineralized glass and HAp. No significant differences were observed for *Tgfb1* under all conditions. By day 23 in culture, 45S5 Bioglass® incorporated dense collagen also underwent greater mineral deposition with its seeded NIH/3T3 cells experiencing highest induction in *Ibsp* expression. This mineralization effect and *Ibsp* expression decreased with an increase in pre-conditioning time of 45S5 Bioglass® in SBF. Furthermore, upon prolonged culturing (up to 23 days), cells seeded in the dense collagen gels showed an upregulation of specific osteogenic markers; alkaline phosphatase (*Alpl*), *Sp7* (encodes osteogenic transcription factor OSX), and runt-related transcription factor 2 (*Runx2*) along with the formation of osteoid-like structures as examined under SEM, and verified by von-Kossa-van Gieson staining. This illustrates the ability of NIH/3T3 cell lines to subscribe to an osteogenic pathway upon prolonged culturing in dense collagen gels and in the absence of osteogenic media. **Conclusions:** The direct contact of 45S5 Bioglass® with fibroblasts in dense collagen gels appeared to reduce their initial proliferation, metabolic activity and delay their transition from an initially rounded to spindle shape morphology. Amorphous 45S5 Bioglass® also induced *Vegf* initially, while in longer term, a significant degree of matrix mineralization through particle deposition and upregulation of bone markers. This mineralization potential seems to decrease with increase in pre-conditioning in SBF. These findings indicate the potential of ectopic mineralization as a result of 45S5 Bioglass® incorporation. Furthermore, the induction of osteogenic differentiation of NIH/3T3 in a dense collagen environment, suggests for their ability to subscribe to the osteogenic pathway.

Résumé

Contexte : Les plaies chroniques souffrent d'un faible approvisionnement en sang au niveau du lit de la plaie, une condition généralement marquée par de faibles taux en facteur de croissance endothélial vasculaire (*Vegf*) et par la suite une moindre angiogenèse. Bien qu'initialement conçus pour réparer les tissus minéralisés, les verres bioactifs ont récemment sollicité beaucoup d'intérêt comme traitement pour accélérer la cicatrisation des plaies chroniques. L'argument principal soutenant leur utilisation repose sur leurs capacités de stimulations ioniques améliorant des procédés particuliers, tels que l'angiogenèse, et facilitant les phases de guérison de l'inflammation, prolifération et maturation. Toutefois, la majorité des recherches sur cultures cellulaires *in vitro* restent basées sur des modèles bidimensionnels et de libération ionique uniquement, alors que peu de recherches portent sur des modèles tridimensionnels à contact direct, notamment en ce qui concerne la cicatrisation des plaies, le verre bioactif et le potentiel de minéralisation ectopique. **Méthodes :** Dans cette étude, un modèle tridimensionnel a été développé pour étudier la fonction de fibroblastes NIH/3T3 lorsqu'ils sont en contact direct avec un verre bioactif classique ; 45S5 Bioglass®, lorsqu'il est sous forme de particules amorphes et après préconditionnement dans un liquide physiologique simulé (SBF) pendant 3 à 14 jours pour induire des degrés différents de minéralisation. Les cellules ont été cultivées dans un gel de collagène dense d'environ 13,4 % en poids, seules ou incorporées avec des particules de 45S5 Bioglass® amorphe, de 45S5 Bioglass® conditionné 3 et 14 jours ou des particules d'hydroxyapatite synthétique (HAp) jusqu'à 23 jours, *in vitro*. La prolifération, l'activité métabolique, la viabilité, la minéralisation de la matrice et l'expression de gènes impliqués dans la cicatrisation des plaies, à savoir *Vegf*, l'actine alpha des muscles lisses (α-SMA), le facteur de croissance transformant bêta (*Tgfb1*) et le collagène (*Col1a*1), ont été analysés avec la sialoprotéine osseuse (*Ibsp)* comme indicateur de la minéralisation de la matrice à médiation cellulaire. **Résultats :** La surface spécifique des particules de 45S5 Bioglass® a augmenté de 900 fois après 14 jours de conditionnement dans le SBF. Les analyses par microscopie électronique à balayage (SEM), diffraction des rayons X et spectroscopie infrarouge à transformée de Fourier (FTIR) par réflectance totale atténuée (ATR) ont confirmé la minéralisation partielle du Bioglass® 45S5 amorphe par la formation d'une couche d'hydroxycarbonate d'apatite de surface. L'analyse par spectrométrie d'émission optique à plasma à couplage inductif (ICP-OES) a indiqué que le Biograss® 45S5 amorphe avait la libération

d'espèces alcalines la plus élevée dans l'eau désionisée. Son incorporation dans les gels de collagène denses ensemencés en fibroblastes entraînait une diminution de la prolifération cellulaire initiale, de l'activité métabolique et de la viabilité. Les cellules en contact direct avec le Bioglass® 45S5 partiellement minéralisé et l'HAp avaient des activités métaboliques et une prolifération comparables. Les niveaux d'expression de *Vegf* étaient les plus élevés au jour 2 pour les cellules en contact avec le 45S5 amorphe et pour celles en contact avec le 45S5 minéralisé pendant 3 jours. Au jour 23, l'expression de *Vegf* avait diminué significativement dans les cellules en contact avec le 45S5 amorphe, alors que celles maintenues en présence de 45S5 minéralisé pendant 14 jours présentaient la plus haute expression de *Vegf*. Les cellules conditionnées à l'HAp présentaient la plus haute expression d'α-SMA au jour 2 en culture. Les niveaux d'expression de Col1a1 diminuaient significativement pour le verre minéralisé 3 jours et l'HAp Aucune différence significative n'a été observée pour le *Tgfb1* dans toutes les conditions expérimentales. Au jour 23 en culture, le collagène dense incorporé dans le 45S5 Biograss® avait également subi une déposition minérale plus importante avec ses cellules NIH/3T3 ensemencées qui présentaient la plus forte induction d'expression d'*Ibsp*. Cet effet de minéralisation et d'expression de l'*Ibsp* diminuait avec l'augmentation du temps de préconditionnement du 45S5 Bioglass® dans le SBF. En outre, lors de la mise en culture prolongée (jusqu'à 23 jours), les cellules ensemencées dans des gels de collagène dense ont montré une régulation à la hausse des marqueurs ostéogéniques spécifiques ; la phosphatase alkaline (*Alpl*), le facteur de transcription *Sp7* et le facteur de transcription 2 lié au runt (RUNX2) en même temps que la formation de structures de type ostéoïde comme examiné sous SEM et vérifiée par coloration von Kossa-van Gieson. Ceci illustre la capacité des lignées cellulaires NIH/3T3 à souscrire à une voie ostéogénique lors d'une permanence prolongée en culture dans des gels de collagène denses et en l'absence de milieux ostéogéniques. **Conclusions :** Le contact direct de 45S5 Bioglass® avec des fibroblastes dans des gels de collagène dense semble réduire leur prolifération initiale, l'activité métabolique et retarde la transition entre une morphologie initialement arrondie vers une morphologie fusiforme. Le 45S5 Bioglass® amorphe induit également initialement le VEGF et, à plus long terme, un degré important de minéralisation de la matrice par dépôt de particules et la régulation à la hausse des marqueurs osseux. Ce potentiel de minéralisation semble diminuer avec l'augmentation de la durée de préconditionnement dans le SBF. Ces résultats indiquent le potentiel de minéralisation ectopique à la suite de l'incorporation de Biograss® 45S5. En outre, l'induction de la

différenciation ostéogénique des NIH/3T3 dans un environnement de collagène dense met en évidence leur capacité à emprunter la voie ostéogénique.

Acknowledgments

First and foremost, I would like to thank my supervisor, Dr. Showan Nazhat, for providing every opportunity to develop my skills and understanding. I also would like to express my deep thanks and appreciation to my co-supervisor Dr. Monzur Murhsed for helping me build a strong hands-on foundation in cell-culture work and making sure I understand the principles behind different techniques applied in this thesis. I would like to also extend my gratitude to my colleagues in both labs, namely, Will Lepry, Hyeree Park, Gabriele Griffanti, Ehsan Rezabeigi, Tiantian Yin and Abhinav Parashar for their advice and time sharing their knowledge in different techniques. I would also like to thank Dr. Jingjing Li for sharing her knowledge and time.

I would also like to thank all staff of the ABIF for training me on confocal microscopy. I extend my gratitude to Barbara Hanley for her support throughout these two years. I would also like to thank Ranjan Roy for sharing his expertise in ICP-OES.

Lastly, I would like to thank my mother for providing me with unlimited emotional support throughout this journey; my best friends Yasmien Emara, Dara Ali, Zainab Khalid and Meera Al Oufi for their company and support. At the end, I would like to dedicate this thesis to my late father for believing in me and encouraging me to pursue whatever interests me.

TABLE OF CONTENT

List of Figures

List of Tables

List of Abbreviations

ADM: Acellular Dermal

ALP: Mouse alkaline phosphatase-2

ASTM: American Society for Testing Materials

ATR-FTIR: Attenuated Total Reflectance-Fourier Transform Infrared Spectroscopy

BET: Brunauer–Emmett–Teller

BMSC: Bone Marrow Stromal Cell

BO: Bridging Oxygen

BSA: Bovine Serum Albumin

CFD: Collagen Gel Fibrillar Density

COL-1A1: Type1 Collagen

DAPI: 4′,6-diamidino-2-phenylindole

DC: Dense Collagen

DIW: Deionized Water

DMEM: Dulbecco's Modified Eagle Medium

EC: Endothelial Cells

ECM: Extracellular Matrix

FBS: Fetal Bovine Serum

FDA: Food and Drug Administration

HCA: Hydroxycarbonated Apatite

HPRT: Hypoxanthine-guanine Phosphoribosyltransferase

IBSP: Bone Sialoprotein

ICP-OES: Inductively Coupled Plasma Optical Emission Spectrometry

LSM: laser Scanning Confocal Microscope

MEM: Minimum Essential Medium

MMPs: Matrix Metalloproteinases

NMR: Nuclear Magnetic Resonance

OPN: Osteopontin

Osx: Sp7 Transcription Factor

PBS: Phosphate-buffered Saline

PC: Plastic Compression

PFA: Paraformaldehyde

PG: Phosphate glass

qRT-PCR: Real-time Polymerase Chain Reaction

RCT: Randomized Controlled Trial

Runx2: Runt-related Transcription Factor2

SBF: Simulated Body Fluid

SEM: Scanning Electron Microscopy

SSA: Specific Surface Area

TC: Tissue Culture

TGF-β: Transforming Growth Factor

VEGF: Vascular Endothelial Growth Factor

XRD: X-ray Diffraction

α-SMA: Alpha-smooth Muscle Actin

1. Introduction

First-generation biomaterials were classically defined as materials with maximum biological inertness when in contact with body fluids [1,2]. In the late 1960s - being motivated to move away from biologically-inert materials characterized by fibrous encapsulation and ultimate rejection after exposure to body fluid - Larry Hench invented a "bioactive" glass composition with a high Ca/P ratio that reacts with carbonate ions from the body fluids to form carbonated hydroxyapatite (HCA) on the surface and similar to the inorganic part of bone [3,4]. Bioactivity, in the context of biomaterials, is defined as the ability of a biomaterial to form an HCA surface layer [3,4,5]. This new grafting material seemed promising to integrate with living tissues. Due to the ability of this biomaterial to form a tissue-implant bond and release ions that can stimulate cellular processes, such as migration, proliferation and manipulate gene expression, it is now recognized that bioactive glasses have defined the way second and third generation biomaterials should respond when in contact with body fluids [3].

The originally bioactive glass, 45S5 Bioglass®, with composition $45SiO_2$-24.5CaO-$24.5Na_2O$-$6.0P_2O_5$, (wt%), has silicate as the network former with calcium, sodium, and phosphate as modifier ions [3]. Motivated by limitations silicate-based glasses possess, such as low solubility and high melting temperatures during processing, the exploration of different compositions have expanded the solubility and bioactivity ranges of bioactive glasses [6]. Two other main types of bioactive glasses in literature are borate-based and phosphate-based glasses. Borate-based glasses are valued for their high bioactivity, solubility, and the bacteriostatic potential of their boron release [7]. Phosphate-based glasses are more known for their higher rates of dissolution, low durability, and low bioactivity [8]. Incorporating and doping bioactive glasses with different metal ions has also been explored heavily. For example, the addition of copper and silver ions have shown to enhance angiogenic and antimicrobial properties, respectively [9,10]

In 2005, Day highlighted the ability of bioactive glasses to promote angiogenesis and vessel formation, both in-vitro and in-vivo [11]. Healthy wound healing requires a good supply of nutrients and oxygen to the wound bed transported in blood vessels. This opened the gate for many specialized bioactive glass formulations to be designed to target slow-healing wounds, or more specifically, chronic skin wounds and ulcers. In April 2017, the United States of America's Food

and Drug Administration (FDA) approved an application by Mo-Sci Corporation (USA) to bring forward their wound healing matrix product; MIRRAGEN™, a borate-based bioactive resorbable glass fiber dressing, to clinical trials. The multi-center randomized controlled trials comparing MIRRAGEN™ Advanced Wound Matrix to a calcium alginate Fibracol ™dressing (Acelity L.P.Inc), started in early 2018 and is anticipated to conclude by June 2020 [12].

The transition of bioactive glasses from hard-tissue repair, primarily bone, to a potential soft-tissue healing product, is interesting and not very well understood. When a bioactive glass is exposed to body fluids, it expels a large concentration of Na^+ ions, which creates an alkaline environment [3]. The most commonly used replica example in-vitro, is simulated body fluid (SBF) This expulsion of alkaline species is followed by the break-up of the glass Si-O-Si bonds and their condensation to form a surface silica-rich layer [13]. The most critical part for the purposes of bone healing is the reaction between Ca^{2+}, PO_4^{3-}, and CO_3^{2-} ions from the body fluid to form HCA mineral that should potentially help in bone regeneration, through the creation of a bone-biomaterial bond and osteoinduction [3, 13]. However, in the context of wound-healing, ionic release and its stimulatory effects on angiogenesis, cell migration, re-epithelialization, and direct ionic anti-bacterial effects, all seem to be the motivating factors behind the use of bioactive glass [14]. The partial mineralization of the bioactive glass is assumed only to be a by-product of this process [14]. Furthermore, the sharp increase in alkalinity due to Na^+ release within a few minutes of exposure to an aqueous environment may in fact compromise cell viability [6, 15]

Synthetic hydroxyapatite (HAp) is a biocompatible, osteoconductive material extensively used to fill bone voids, especially in maxillofacial and dental applications [16]. It is interesting to note that even though most HAp applications have been focused on bone regeneration, it may also have further applications in the soft tissue repair and augmentation, though this has not been explored extensively in literature [16].

Fibroblasts are mesenchymal cells present in connective tissues of the body and are primarily responsible for creating new collagen extracellular matrix (ECM) to support wound healing and contraction [17]. While these cells have been extensively investigated in wound healing, generally, cell studies have traditionally been carried out on 2D systems, e.g., either on treated or collagen coated plastic dishes. However, it has been shown that cell behavior is greatly affected by the substratum it is grown on. In particular, cells grown in three-dimensional (3D)

systems, such as collagen type 1 gels, are believed to be more closely resembling their in-vivo environment [18].

To this end, the goal of this study was to explore the effect of using a mineralizing bioactive glass on wound-healing processes, in-vitro. The function of NIH/3T3 fibroblasts, seeded in 3D dense collagen gels and in direct contact with amorphous 45S5 Bioglass particles as well as partially mineralized glass particles through pre-conditioning in SBF were compared to those exposed to HAp particles. The effect of 45S5 bioactive glass during its course of mineralization on cell metabolic activity, proliferation, viability/death, and the gene expression of markers key to wound healing were explored along with the potential of ectopic mineralization.

2. Research Hypothesis, Aim and Objectives

2.1 Hypothesis

Addition of a mineralizing bioactive glass such as 45S5 Bioglass® in wound healing applications, can potentially:

1. Enhance fibroblastic cell proliferation and expression of wound healing markers due to ionic release within a 3D dense collagen environment.
2. Increase the deposition of calcium and phosphate ions on the collagen fibrils leading to its mineralization.

2.2 Aim

To investigate the function of fibroblastic cells, which hold an essential role in producing several proteins related to the wound healing process, when brought in direct contact with silicate-based bioactive glass at different time points of mineralization in terms of proliferation, gene expression, and matrix mineralization.

2.3 Objectives

1. To create a NIH/3T3 fibroblastic cell seeded dense collagen gel incorporated with amorphous bioactive glass, partially mineralized glass, and synthetic hydroxyapatite particles to examine their direct contact effect on cells, in-vitro.
2. To characterize parameters related to a progression in wound healing, such as cell metabolic activity, viability, and proliferation.
3. To characterize the gene expression of important wound healing markers in NIH/3T3 cells when in direct contact with 45S5 bioactive glass at different time points of mineralization.
4. To characterize the extent of mineralization of the dense collagen matrix with the addition of amorphous bioactive glass, partially mineralized glass, and synthetic hydroxyapatite.

3. Literature Review and Background

3.1 Glass Structure and Chemistry

3.1.1 Definition of Glass

According to the American Society for Testing Materials (ASTM), the classic definition of glass "is a product of fusion and subsequent cooling until a rigid inorganic solid is produced" [19, 20]. However, this definition limits glasses to those prepared by melt-quench only, whereas today, non-crystalline materials can also be made using chemical vapor deposition and sol-gel processing. Therefore, the term "glass'' can cover all non-crystalline solids with a glass transition temperature. Various compositions of soda-lime glass have been used, but the two main components are the network formers (*e.g.,* SiO_2) and the network modifiers (*e.g.,* Na_2O, CaO). Pure SiO_2 is relatively hard with a very high melting point (2000°C), requiring a high energy input and hence cost. To reduce this processing temperature, manufacturers add about 18 mol% soda (Na_2CO_3). Sodium carbonate also causes the glass to dissolve slowly in water; therefore, 10% lime ($CaCO_3$) is added to protect the glass from degradation upon exposure to moisture. Small quantities of $MgCO_3$ and K_2CO_3 are sometimes also added. The carbonates decompose under heat to oxides known as network modifiers, which disturb the strong Si-O bonds responsible for the high melting point of pure silica [21].

3.1.2 Bioactive Glass History

While Dr. Larry Hench was attending a U.S army Materials Research Conference in 1967 to talk about his findings in radiation-resistant electronics, he stumbled upon a request from an army colonel concerned about plastic and metallic implants being rejected by the body of U.S soldiers [22]. The colonel asked him if he can make a material that will not form a fibrous encapsulation when exposed to human tissues [22]. This challenge provided Dr. Hench an incentive to attempt to make a material that will create an interfacial bond with the host tissue rather than an interfacial layer of scar tissue. Inorganic crystalline hydrated hydroxyapatite (HAp) constitutes almost 70 wt% of the bone composition, so Dr. Hench proposed that if he can make a material that synthesized HAp in-vivo, it will not be rejected by the body [22]. It was in 1971, as a result of

research funded through the U.S Army, a group of researchers from the University of Florida published their extraordinary findings of the formation of HAp in solutions that lacked calcium and phosphate ions and the strong bonds the glass formed with bones in rat models. This composition is now known as 45S5 Bioglass® [22]. Figure 1 shows the relationship between the composition and the bone-bonding ability of 45S5 Bioglass®.

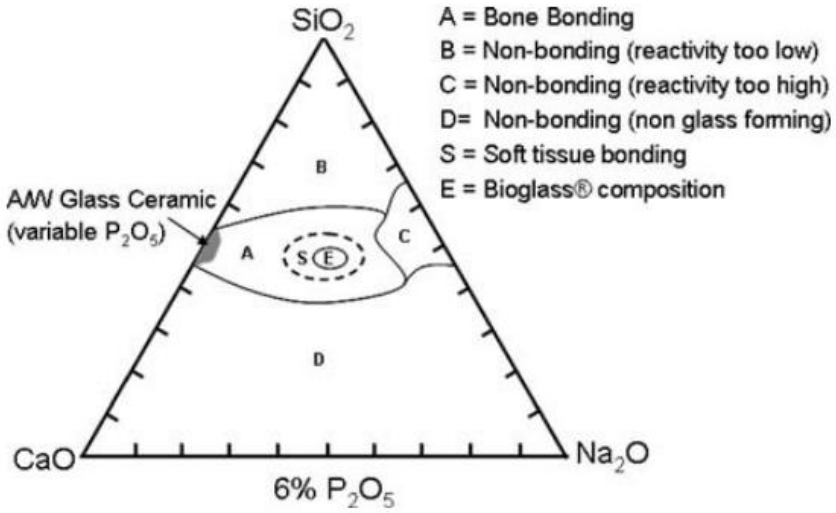

Figure 1: Bioactivity variation with composition of silicate-based glasses [23]

Bioactive glasses are distinct from conventional glasses in that they contain calcium and phosphate in a proportion that is similar to HAp present in bone. The ability of bioactive glass to form a HAp bond to bone is responsible for its osteoconductive and osteoinductive properties when exposed to body fluids, which allows the bioactive glass not only to be biocompatible but also help in bone healing applications [24]. The first bioactive glass and perhaps the most famous formulation to date is 45S5 Bioglass® with composition $45SiO_2$-$24.5CaO$-$24.5Na_2O$-$6.0P_2O_5$, (wt%) where 45 refers to the percentage of silica and 5 refers to the mole ratio of calcium to phosphate [22]. Nowadays, in addition to silicate, other network forming species such as phosphate (P_2O_5), or borate (B_2O_3) are also being explored as bioactive glasses.

The bioactivity of materials, in terms of the ability to stimulate certain processes in tissue regeneration, is dependent on their controlled ionic release kinetics that should ideally be synchronized with the sequence of cellular changes occurring in the site of repair [22]. The composition of the glass plays a vital role in determining this bioactivity. Figure 1 indicates that

silica-based bioactive glasses with the highest level of bioactivity have a composition similar to 45S5 Bioglass®. Compositions with 52 to 60% SiO_2 show slower bonding, and glasses with more than 60% SiO_2 are bio-inert and hence do not bond to the bone.

3.1.3 Silicate-based Glasses

3.1.3.1 Structure

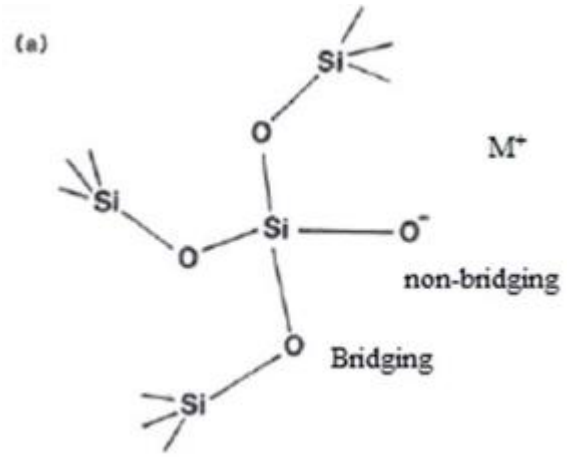

Figure 2: Bridging and non-bridging oxygen atoms in silicate-based glasses [25]

Silicon has a valency of +4 and a coordination number of 4. This results in 4 excess electrons, and hence the basic network former in silicate-based glasses is $[SiO_4]^{4-}$. The tetrahedral units are connected via bridging oxygen atoms. Q^n species are often used to describe the number of bridging oxygen atoms per unit of network former. As network modifying metal oxides are added to the composition, the number of non-bridging oxygen atoms increases, thereby decreasing n. For silicate-based glasses, the connectivity decreases as n decreases. The distribution of this Q^n species can be quantified by Raman and nuclear magnetic resonance (NMR) spectroscopy [26]. Figure 2 shows the formation of non-bridging oxygen atoms as metal oxides (M) are added [26, 27].

3.1.3.2 Dissolution and Bioactivity

When bioactive silicate glass formulations are immersed in body fluid, they form a surface HCA layer. This ability of silicate-based glasses to form a bond with tissues is what makes it biocompatible and able to integrate with hard and soft tissues [23]. The degradation of silicate-based glasses starts with an ion exchange between the Na^+ and H^+ from the glass and body fluid, respectively. This is followed by the solution mediated breaking of Si-O-Si bonds. Soluble $Si(OH)_4$ condensate on the surface and form a silica-rich layer. Lastly, Ca^{2+} and PO_4^{3-} react and crystallize to form HCA layer on top of the silica-rich layer [28].

3.1.3.3 Applications in Soft Tissues

This section gives an overview of several attempts of synthesizing specialized silicate glasses in wound healing applications.

Table 1: Summary of soft tissue applications of silicate -based glasses

Formulation	Bioactive Glass Form	Finding	Year	Reference
$45SiO_2$-$24.5Na_2O$-$24.5CaO$- $6P_2O_5$ (wt%)	Microfibers provided by Mo-Sci Corp (USA)	• 1.6 higher microvascular density than the sham control.	2015	[29]
$53SiO_2$-$6Na_2O$-$20CaO$-$5MgO$-$12K_2O$-$4P_2O_5$ (wt%)	Glass beads provided by Mo-Sci by Mo-Sci Corp (USA)	• 1.3 higher microvascular density than the sham control.	2015	[29]
$58.1SiO_2$-$5.6Na_2O$-$20.3CaO$-$7MgO$-$7.3K_2O$-$1.6P_2O_5$ (mol%)	300-500μm Powder, Melt-Quench	• Lower dissolution rate compared to borosilicates and borate-based glasses.	2018	[30]

$64SiO_2$-26CaO-$5P_2O_5$-$5Ag_2O$ (mol%)	Sol-gel	• 0.02-0.2 mg/ml of silver(I) ion in culture medium inhibited the growth of Escherichia coli bacteria(bacteriostatic). • Bactericidal at the initial stage of incubation. • Undoped silica-based glass did not affect bacterial growth. Possible antibacterial applications.	2008	[31]
$45SiO_2$-$24.5Na_2O$-24.5CaO-$6P_2O_5$ (mol%)	Powder, Provided by the Shanghai Institute of Ceramics, Chinese Academy of Science	• By day 12 of applying 45S5 Bioglass® on the wound site in rat models, higher expression of Cx43, a gap junction alpha-1 protein, was observed in the cells around the newly formed blood vessels compared to the untreated wound site. • Possible mechanism of bioglass wound healing through enhancing cell-cell communication	2016	[32]
$56SiO_2$-30CaO-$4P_2O_5$-$10Ag_2O$ (mol%)	Sol-gel, nanoparticles (50-200) nm	• Hydroxyapatite layer detected Antibacterial effect against S.aureus and E. coli bacteria	2019	[33]
$45SiO_2$-$24.5Na_2O$-24.5CaO-$6P_2O_5$ (mol%)	20 μm Powder, Provided by the Shanghai Institute of Ceramics, Chinese Academy of Science	• 45S5 Bioglass® ionic products activated M2 macrophages phenotype and stimulated macrophages to secrete higher concentrations of anti-inflammatory	2017	[34]

		and angiogenic growth factors compared to endothelial cell medium control. • Accelerated wound healing and reduced inflammation in the initial stage compared to endothelial cell medium control.		

3.1.4 Boron–based bioactive glasses

3.1.4.1 Structure

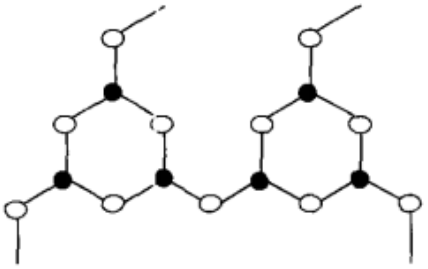

Figure 3: Two boroxyl groups linked by a bridging oxygen. Confirmed Using X-ray diffraction in pure borate glass [35]

The network former in borate glass is a trigonal BO_3 made of one boron atom slightly above three oxygen atoms. In pure borate glass, all three oxygen atoms act as bridges between the nearby triangles. Figure 3 illustrates the vitreous B_2O_3 structure. Since boron has a valency +3, the addition of a modifier oxide will either create non-bridging oxygens, decreasing the connectivity of the network, or increasing the coordination number of boron from 3 to 4. This increase in coordination number of boron does not change the number of bridging oxygens; however, the network former, $[BO_4]^{1-}$ gains one excess negative charge. This increases the connectivity and viscosity of the glass. The addition of up to 16 mol% alkali metal oxide increases connectivity, and a further increase results in the formation of non-bridging oxygen atoms, which decreases the connectivity. This behavior is unique to borate glasses and hence named the "borate anomaly". Figures 4 & 5 illustrate these two behaviors [35, 21, 36].

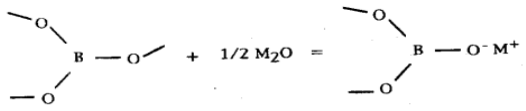

Figure 4: Formation of non-bridging oxygen during the addition of more than 16 mol% metal oxides to borate glass [35]

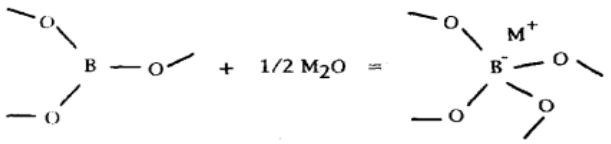

Figure 5: Increase in boron coordination from 3 to 4 during the addition of less than 16 mol% metal oxides to borate glasses [35]

3.1.4.2 Dissolution and Bioactivity

When borate glass is immersed in body fluid, Na^+ is released from the glass network and is exchanged with H^+ from the body fluid. The breakdown of B-O-B bonds is initiated, and $[BO_3]^{3-}$ ions are released into the solution. Ca^{2+} from the glass and PO_4^{3-} ions from the solution or glass complex to form a surface HAp layer, leading to its bioactivity and integration with host tissues [28, 37].

The final pH value of the dissolution of any bioactive glass is dependent on the bond strengths and the species in the glass network. Although the final pH value of the dissolution of borate is basic, it is lower than the final pH value of the dissolution of silicate-based glasses of similar compositions. During dissolution, NaOH is formed in both glasses due to the reaction between released Na^+ and OH^- in the solution. However, the created $B(OH)_3$ has a more potent acidic nature than $Si(OH)_4$, hence lowers the final pH of borate glasses [38, 39]. Due to the simultaneous release of Na^+ and breakage of the B-O-B network, borate-based glasses, in general, have higher bioactivity and lower chemical durability when compared to silicate glasses [37,40].

3.1.4.3 Applications in Soft Tissues

Due to the high bioactivity and low chemical durability of borate glasses when compared to silicate-based glasses, research efforts, and now commercial products, are focused on the use of borate-based glasses in wound healing applications. It has been reported that the higher Ca^{2+} ions release rate by borates promotes the migration of epidermal cells to the wound site, in turn, accelerating soft tissue regeneration [33]. B^{3+} has been shown to have an accelerating effect on the wound healing process, where stimulation of vascularization and angiogenesis leading to faster

wound closure has been reported [36, 37, 38, 39]. Furthermore, the addition of 10wt% B_2O_3 to a SiO_2-Al_2O_3-MgO-K_2O-B_2O_3-F system has been shown to improve the bacteriostatic property of this glass system. This may be due to ability of boric acid to target the bacteria cell wall [40].

Perhaps the biggest revolution in commercially available wound care products is MIRRAGEN™ (previously known as DermaFuse), which is a borate-based bioactive cotton-like fibrous mat developed by Mo-Sci corporation. The fibrin-like network was tested on 13 diabetic patients with chronic ulcer wounds at Phelps County Regional Medical Center, USA. It was shown that after treatment application, the wound completely healed in eight patients, and significant improvements were observed in four other patients. In early 2017, the FDA approved this treatment in animal wounds under the product name Redi-Heal™. In April 2017, MIRRAGEN™ won FDA approval for human wound healing applications [41]. Table 2 summarizes the overall borate-based findings in soft tissue applications.

Table 2: Summary of findings of borate glass in soft tissue applications

Formulation	Bioactive Glass Form/Particle Size/Source	Finding	Year	Reference
$53B_2O_3$-$6Na_2O$-20CaO-5MgO-$12K_2O$-$4P_2O_5$ (mol%)	Microfibers, Mo-Sci	• 2.3 times higher microvascular density than sham control in mouse model.	2015	[29]
$53B_20_3$-$6Na_2O$-20CaO-5MgO-$12K_2O$-$4P_2O_5$ (mol%)	Glass Beads, Mo-Sci	• 1.6 times higher microvascular density than sham control in mouse model.	2015	[29]

52.7B_2O_3-5.98Na_2O-19.92CaO-4.98MgO-11.95K_2O-3.98P_2O_5-0.40CuO (mol%)	Microfibers, Mo-Sci	• 2.7 times higher microvascular density than sham control in mouse model.	2015	[29]
52.79B_2O_3-5.98Na_2O-19.92CaO-4.98MgO-11.95K_2O-3.98P_2O_5-0.40CuO (mol%)	Glass Beads, Mo-Sci	• 2.5 times higher microvascular density than sham control in mouse model. • Vascular endothelial growth factor (*Vegf*) expression promoted in copper doped borate glasses.	2015	[29]
54.5B_2O_3-6.1Na_2O-22.1CaO-7.6MgO-7.9K_2O-1.7P_2O_5 (mol%)	300-500µm Powder, Melt-Quench	• Borate based glasses had higher dissolution rates than borosilicates and silicate glasses. • Release of boron was inhibited in static simulated body fluid	2018	[30]
55.1B_2O_3-6.2Na_2O-18.7CaO-7.7MgO-8.0K_2O-1.8P_2O_5-2.6CuO (mol%)	300-500µm Powder, Melt-Quench	• Copper ions released up to 10mg/L(Critical biological level for fibroblast survival).	2018	[30]
54.7B_2O_3-6.2Na_2O-21CaO-7.67MgO-7.9K_2O-1.8P_2O_5-0.8ZnO (mol%)	300-500µm Powder, Melt-Quench	• Zinc ions could only be released under acidic conditions. • Possible applications in infection treatment.	2018	[30]

$54B_2O_3$-$6Na_2O$-22CaO-8MgO-$8K_2O$-$2P_2O_5$ (mol%) with up to 3%CuO	0.4-1.2 μm microfibers	• Fibers converted to hydroxyapatite within 7 days. • Ca, B, Cu ions released. • No cytotoxicity detected in endothelial cells. • Endothelial cell migration promoted. • VEGF secretion enhanced. • Higher CuO% improved angiogenesis but did not affect collagen deposition.	2015	[42]
$56.6B_2O_3$-$5.5Na_2O$-18.5CaO-4.6MgO-$11.1K_2O$-$3.7P_2O_5$ (wt%)	Nano/microfibers	• Borate-based glasses exhibited higher erosion rates and HAp formation under dynamic SBF flow. • Presoaking fibers up to 48 hours had a positive effect on cell proliferation (35-40) % higher compared to control (only medium) • Higher fiber concentration showed a negative effect on cell viability. • Borate glass had no significant effect on cell proliferation compared to control (only medium)	2015	[43]
$51.6B_2O_3$-$6Na_2O$-20CaO-5MgO-$12K_2O$-$4P_2O_5$-0.4CuO-1.0ZnO (wt%).	Nano/micro fibers	• 20-40% higher cell proliferation for fiber concentrations less than or equal to 250 μg/mL	2015	[43]
$52.7B_2O_3$-$5.98Na_2O$-19.92CaO-4.98MgO-$11.95K_2O$-$3.98P_2O_5$-0.4CuO (wt%).	Microfibers	• Copper ions promoted angiogenesis when compared to silica glass microfibers and control on rat models	2010	[44]

$60B_2O_3$-36CaO-(4-X)P_2O_5-(X)Ag_2O where X= 0.0, 0.3, 0.5 and 1 (mol%).	Sol-gel, 45.7-51.1 (µm)	• AgBGs exhibited dose dependent antibacterial property and were found to be more effective against E. coli than S.aureus.	2018	[45]

3.1.5 Phosphate-based Glasses

3.1.5.1 Structure

Phosphates are common in nature due to a strong phosphorous affinity towards oxygen. The network former of phosphate-based glasses is a tetrahedral unit $[PO_4]^{3-}$, as shown in Figure 6. Phosphorous has a valency of +5. When a phosphate tetrahedral unit forms a charge-balanced 3D binary oxide, the phosphorous atom can only share three of its four oxygen atoms. The oxygen atoms not shared with the other tetrahedral units share their two unpaired electrons with phosphorous, forming terminal double bonds. This terminal double bond limits the phosphate glass network connectivity with fewer cross-links when compared to silicate-based glasses. When phosphate-based glasses are mixed with network modifying metal oxides such as CaO, a high number of terminal oxygens are formed [46].

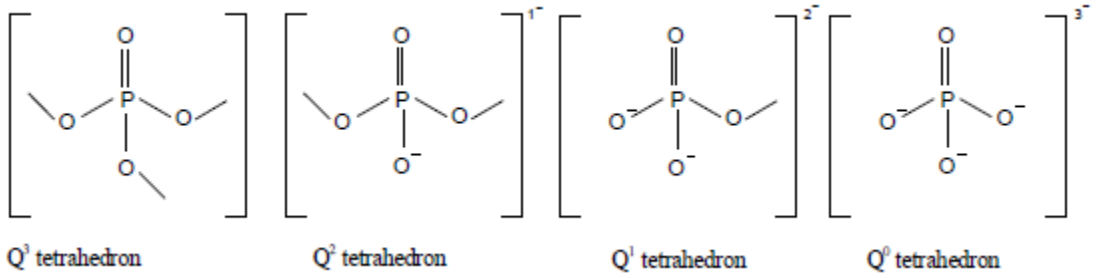

Figure 6: Phosphate glass network former variation with number of non-bridging oxygen atoms [47]

Phosphate glass (PG), in general, is classified in terms of the number of bridging oxygen (BO), between one unit and the other tetrahedral units. This classification is expressed by labeling

PG as Q^i, where i is the number of bridging oxygens. In PG, i ranges from 0 to 3 since one oxygen in the $[PO_4]^{3-}$ tetrahedral unit is terminal oxygen with double bonds to the phosphorous. As the amount of metal oxide added increases, the dominant i species decreases, reflecting the decrease in connectivity. Q^3 species are referred to as ultraphosphates, Q^2 species are referred to as metaphosphates, Q^1 species are referred to as pyrophosphates, Q^0 species are referred to as orthophosphates. In fact, glasses with dominant concentrations of Q^0 and Q^1 are referred to as invert glasses [48].

Unlike pure silica, which is chemically and thermally stable, pure phosphorus pentoxide has very low chemical durability. It is susceptible to hydrolysis of its P-O-P bonds from atmospheric moisture. The addition of metal oxides increases PG chemical durability by creating more stable $P\text{-}O\text{-}M^+$, where M is the metal cation incorporated. Due to this further decrease in connectivity when metal oxides are added, phosphate glasses are good candidates for low-temperature melt-quench processing [46].

3.1.5.2 Dissolution and Bioactivity

When phosphate-based glasses are placed in aqueous media, PG degrades through two main synergistic processes:

1- Ion exchange and hydration: Na^+ ion, which has been shown to have a preferential release from the PG network in aqueous media, is exchanged with H^+, which performs a charge balance action and hydrates the glass surface.
2- Hydrolysis: H^+ and water, now in the glass network, break-up the P-O-P bonds, degrading the network in the process and forming a gel layer where the phosphate chains break [49, 50].

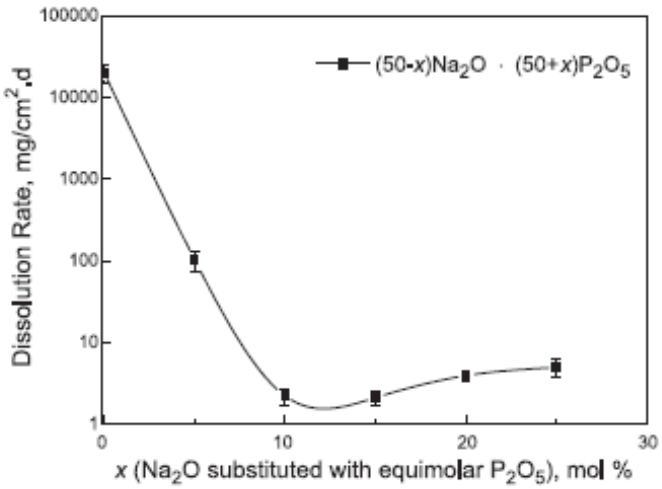

Figure 7: Dissolution rate of PG with different Na_2O mol % [50]

Figure 7 shows the dissolution rate measured by evaluating the weight loss of discs immersed in deionized water as a function of increasing P_2O_5 mol% for a binary system of P_2O_5 and Na_2O [50]. As the percentage of the network former increases, the number of bridging oxygens and cross-linkage increases, which decreases the ability of water molecules to diffuse into the network, hindering the degradation process. On the other hand, as the P_2O_5 mol% increases further, the vulnerability and lack of stability of the branched [PO_4] units are more noticeable, which break to smaller units. This exhibits the potential of tailoring PG composition for controlled release [51]. The change in the pH with time during the dissolution of PG is also highly dependent on the [PO_4] units and the modifying metal oxides concentration. In most bioactive glass systems, the Na^+ and Ca^{2+} ions released react with OH^- raising the pH. However, in PG systems, this is highly dependent on composition. As can be seen in Figure 8, Knowles et al. reported that for a $50P_2O_5$:40CaO:$10Na_2O$ system, the pH increases rapidly then gradually decreases [50]. This can be attributed to the preferential release of Na+, which raises the pH.

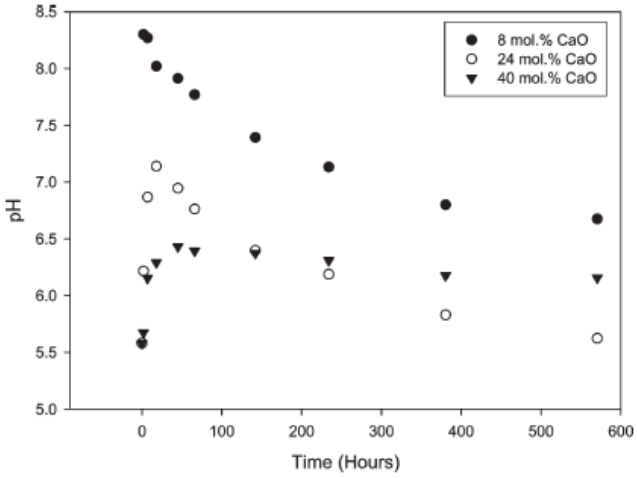

Figure 8: pH Change with Time for Phosphate Glass with Different CaO mol% [50]

Hydrolyzed $[PO_4]^{3-}$ units are released, which form H_3PO_4 in aqueous media leading to a drop in pH [50, 51]. The addition of the CaO has been found to increase the cross-linking of the PG and slow down its rate of hydration by Ca^{2+} blocking water from diffusing into the glass network. Increasing the Na_2O concentration, on the other hand, has been shown to increase the pH [50, 51].

3.1.5.3 Applications in Soft Tissues

For a material to be useful as a carrier of ions of interest for the wound healing process, it is must release ions and degrade at a rate that synchronizes with the concentration required so as not to induce cytotoxicity. Phosphate glasses are relatively unstable due to the weaker cross-linking and less bridging oxygen atoms, which increase their dissolution. In contrast, silica-based glasses which have captured considerable interest in hard tissue engineering, take 1-2 years to completely disappear from the body [52]. Furthermore, polymers and copolymers based on polyglycolic and polylactic acid have had a great interest because they degrade via hydrolysis. However, the main problem with these materials is that they leave behind small crystalline particles that have been reported to cause inflammation [48]. PGs in binary, ternary, and with transition metals

incorporating stability and bioactivity, have been studied by examining their degradation rate and cell adhesion and proliferation [46, 48]. PGs with high P_2O_5, and CaO (*e.g.*, $50P_2O_5$-$48CaO$-$2Na_2O$) have been proven to support cell proliferation [48].

Interest in the use of PGs in soft tissue engineering has mainly been in the form of fibers, whereas most studies assessing their bioactivity have examined the glass in disc form [46, 47, 48, 49, 50, 51]. Fibrous PGs have been reported to act as nerve conduits by supporting cell proliferation, growth, and guiding cell orientation [46]. However, there are challenges in converting PGs from bulk to fiber. Knowles et al. showed that ternary PGs with greater than 50 mol% P_2O_5 undergo higher polymerization and exist in only Q^2 states. The ability of PG to exist in a more polymeric structure allows it to be made into fibers [50].

3.1.6 Glasses Processing

Over the past ten years, 45S5 Bioglass®, $45SiO_2$-$24.5Na_2O$-$24.5CaO$-$6P_2O_5$ (wt%), have had considerable clinical success in mineralized tissue applications [28]. This formulation was first made using the melt-quench technique by blending the oxide precursors and heating the mixture in a furnace up to 1600°C. The melted glass is then quenched in a mold and further annealed at low temperatures to remove residual stress. One advantage of using melt-quench is the flexibility it offers in terms of composition. However, applications that require high purity glasses might not find melt-quench beneficial because refractory materials in the furnace, such as SiO_2 and ZrO_2, which may contaminate the mixture during the heating process. Porous bioactive silicate-based glasses have also been synthesized using the sol-gel method and was found to have a greater surface area and bioactivity [53].

Similarly, the most common and well-studied method of making borate glasses is through melt-quench where the temperature is then increased to 1100°C to melt the glass [54, 55]. In contrast, the first sol-gel borate-based glasses were prepared using binary and ternary glasses modified with Na^+, K^+, and Li^+ [56, 57]. The difficulty in borate glass sol-gel processing is due to its low network connectivity, which makes gel formation relatively more difficult compared to silicate sol-gel. However, sol-gel processing has been found to improve certain qualities attractive

to bioactivity and integration to the host tissue, for example, a higher surface area, porosity, and reduced processing temperatures [58].

Phosphate glasses are also commonly synthesized by melt-quench method [46, 48, 49, 50, 51]. where the temperature is raised to a range of 1000-1200°C, depending on the composition of the phosphate glass [46]. Despite the applicability of sol-gel in low temperature, high surface area processing of borate and silicate glasses, research progress into sol-gel preparation of phosphate glasses has been slow due to difficulty in finding a suitable phosphorous precursor that does not lead to the precipitation of the network forming units, $[PO_4]^{3-}$ [46, 59, 60].

3.2 Wound Healing Process

3.2.1 Wound-Healing Steps

Cutaneous wound healing is a multiple phase process that involves a multitude of interacting growth factors, cytokines, and chemokines, that in a healthy individual, work together in a synchronized and a timely manner [62]. This multistage process should ideally restore tissue integrity [63]. When a stimulus causes a lesion to physically continuous tissues, a sequence of tissue repair events occurs in an overlapping manner. The wound healing stages can be defined as hemostasis, inflammatory reaction leading to tissue restoration, cell proliferation, and tissue remodeling [64].

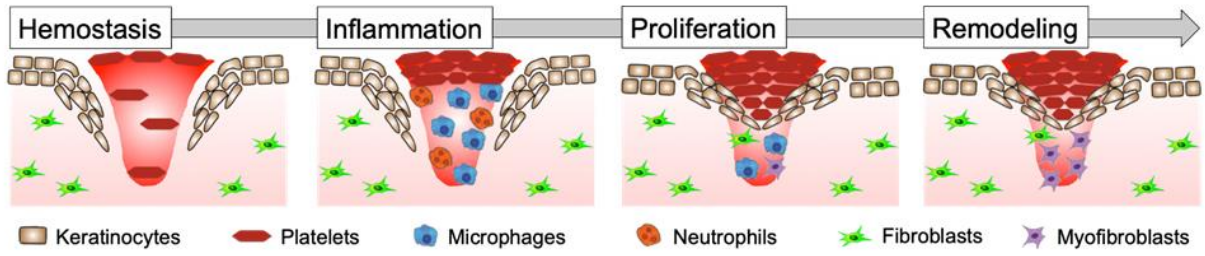

Figure 9: Wound healing stages and different cell roles [61]

Figure 9 shows the different stages of wound healing with the various sequences and cells involved during the overall process. Because of the disruption of blood vessels at the wound site, the body's first response is to block and limit the amount of blood lost through a process known as hemostasis. Hemostasis can be thought of as two major events: development of a fibrin clot and coagulation. The now exposed platelets are activated by the ECM such as fibrillar collagen, and this results in their adherence, aggregation and release of many mediators (*e.g.,* serotonin) and adhesive proteins (*e.g.,* fibrinogen) which induces further platelet aggregation and the conversion of fibrinogen to fibrin by thrombin [62 ,65]. This platelet aggregation triggers a specific enzyme known as the Hageman factor XII to convert prothrombin to thrombin, which leads to the further deposition of the insoluble fibrin. This ends in coagulation, the last step of hemostasis. Ideally, it should take less than 15 minutes for hemostasis to occur [66].

The platelets release diffusible factors that trigger the inflammation phase. Histamine causes redness, and the matrix attracts neutrophils to remove dead cells and control infection. VEGF and transforming growth factor-beta (TGF-β) attract monocytes to the ECM to combat infection. This second, inflammation stage can last up to 6 days after the lesion occurrence [62].

The third phase of wound healing is proliferation. A critical event in proliferation is endothelial, myofibroblastic, and fibroblastic cell migration [67]. This event is initiated approximately two days after the wound occurrence and is stimulated by the release of growth factors, such as VEGF, TGF-β and matrix metalloproteinases (MMPs) and their regulation plays a vital role in angiogenesis. Proliferation takes about two weeks [62].

The last and longest phase in wound healing is remodeling, which can take more than two years for completion. This phase is controlled by mechanisms that attempt to maintain a balance between degradation and synthesis of new cells. The collagen bundles increase in connectivity and tensile strength, regaining up to 80% of their original strength. As the wound heals, apoptosis leads to the decline in the number of fibroblasts, along with the growth rate of capillaries, declining the blood flow and metabolic activity to the wound site. This stage is also highly regulated by TGF-β [68, 69, 70].

3.2.2 Healing of Chronic Wounds

3.2.2.1 Diabetic Ulcer Complications

Approximately 15% of all people with diabetes develop non-healing diabetic foot ulcers during their lifetime [71]. Figure 10 shows the factors related to slower wound healing in diabetic patients. Uncontrolled diabetic patients suffer from low levels of VEGF and hence insufficient angiogenesis at the wound site, which leads to prolonged hypoxia and increases the concentration of oxygen radicals; ultimately amplifies and extends the inflammatory response leading to a slower rate of healing. Furthermore, an imbalance in MMPs levels can lead to tissue destruction inhibiting healthy repair. In chronic diabetic wounds, the level of MMPs is almost 60 times higher than in acute injuries [72, 73, 74, 75].

Unfortunately, neuropathy in diabetic patients not only delay the patient from discovering the wound but also slows down the healing process. Neuropeptides important in wound healing, such as nerve growth factors, are at lower concentrations in diabetic patients. Moreover, Galkowska et al. found that a decrease in neuropeptides exhibits a lowering in leukocyte concentration at the wound site, thereby increasing the chances and severity of infections [76].

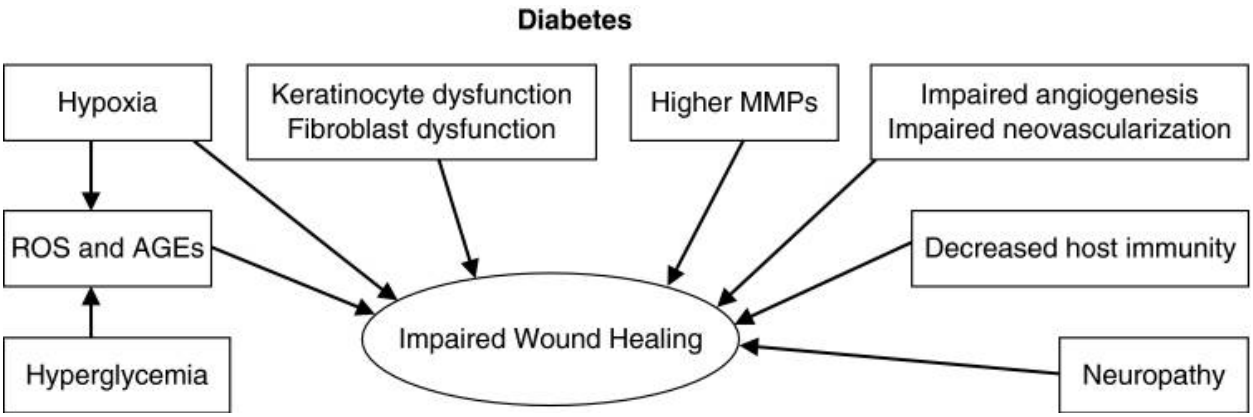

Figure 10: Factors leading to slower wound healing in diabetic patients [23]

3.2.2.2 Standard of Care for Diabetic Wound Healing

In developed countries, 1-2% of the population will experience chronic wounds during their lifetime [77,78]. Chronic wounds can be defined as any wound that fails to undergo a normal reparative process that eventually restores tissue integrity [79]. A chronic wound often presents itself as a comorbid condition associated with obesity or diabetes [77, 80]. Chronic lower limb ulcer is a chronic wound of the leg that does not heal after three months of appropriate treatment. It is estimated that between 19 and 34% of diabetic patients will develop a diabetic foot ulcer in their lifetime [81]. Slow wound healing in diabetic patients comes as a result of conditions triggered by low glycemic control. High blood sugar causes the stiffening of arteries, low angiogenesis, and lower blood supply to tissues, especially at the extremities. This coupled with diabetic neuropathy, which is damage to nerves, makes diabetic patients unaware of a wound, which can lead to infection, and increases the chances of amputations. Up to 40% of all diabetic foot ulcer patients suffer from peripheral arterial disease. Due to low circulation, and hence the ability of white blood cells to move in the wound area, diabetic patients have a weakened immune system; causing wounds to be more prone to infection [82].

Unfortunately, patients with diabetic foot ulcers (DFUs) have more than two times increased risk of death compared to those without DFUs [81, 83]. The standard of care for DFUs established by Dr. Frederick Treves is still used today: wound sharp debridement, off-loading, and educating the diabetic patient about how to take care of their wound and glycemic control. These core practices are still used today coupled with using a wound dressing that promotes a moist environment, which helps reduce discomfort, vascular assessment of blood vessels and arteries in the foot, and active treatment of any infection through antibiotic therapy [81, 84].

The first step in the standard of care is debridement, which is the surgical removal of necrotic tissue; this helps allow new granulation tissue formation, development, and formation of a new epithelial layer. The second step is applying an appropriate dressing. The main reason for the dressing is to create a moist environment that supports granulation tissue formation and angiogenesis. Lastly, wound off-loading usually involves reducing pressure and shear stress from the injured foot. This can be done by total contact casting [81, 85, 86].

In addition to the standard of care, several wound care products and practices are being studied for their efficacy in treating chronic wounds and restoring tissue integrity. One of the methods often used is negative pressure wound therapy, where a vacuum device collects wound exudates keeping the wound clean, reducing the chances of infection, and ultimately the frequency of dressing change [87].

Non-surgical debridement agents are also being considered as alternatives to sharp surgical debridement [88]. However, limited evidence is available regarding their effectiveness. Autolytic debridement with hydrogels utilizes specialized dressings made of insoluble hydrophilic polymers that claim to provide an optimal level of moisture in the wound area to help cell migration and endogenous proteolytic enzymes to breakdown necrotic tissue. A meta-analysis of three randomized controlled trials concluded the ability of hydrogel-based dressings to close wounds more effectively when compared to traditional dressings [88].

Skin grafts are also being used to promote wound healing through the addition of an ECM. The ability of cells to feel and respond to their extracellular environment is evident when decellularized donor dermis is used as a scaffold in the wound bed. This method, also known as the acellular dermal matrix (ADM), has been shown to offer support for vascularization, provide a moist environment, and a barrier to protect the wound from infection. The dermis contains factors that are important in wound healing. An alternative is also being explored, and that is adding specialized human growth factors directly to the subject. For example, VEGF was tested by Kusmanto et al. in a double-blinded randomized controlled trial showing more than 60% reduction in wound size in a significant number of patients with DFUs [81, 89].

Indeed, a wound dressing that can stimulate cells to release growth factors that can promote angiogenesis, release antibacterial factors, protect from infection by creating a barrier, and retain a moist environment will be ideal for chronic wound healing applications [23].

3.3 Collagen and Hydroxyapatite in Tissue Engineering

3.3.1 Collagen

3.3.1.1 Applications in Soft Tissue Engineering

The ECM is the non-cellular component present around all tissues, which acts as a physical scaffold to cells and organs. Collagen is the major protein within the ECM, providing strength, and regulating cell adhesion [90, 91]. In hard tissue engineering, natural polymers are often used as scaffolds due to their close resemblance to the ECM. Naturally derived collagen type 1 has excellent biocompatibility and an essential role in tissue formation [92, 93]. However, in-vitro collagen type 1 scaffolds have low mechanical properties, which Brown et al. improved by developing the plastic compression (PC) technique to synthesize collagen type 1 fibrillar scaffolds with a higher fibrillar density [93]. This technique was later commercialized into a RAFT^{TM} product for use as a realistic tissue model.

Rigid two-dimensional (2D) surfaces used in investigating cellular responses to specific stimuli are constrained by the lack of elastic properties of the fibrillar ECM present in-vivo. Studies have found that cells sense the chemical and physical properties of their culture surface [18]. Cell adherence, migration, angiogenesis, and differentiation have been found to be affected by culture surface [18]. Collagen type 1 is the most abundant protein in the ECM, is used as an in-vitro three-dimensional (3D) assay to help reproduce physiological responses expected in-vivo [94]. Moreover, as the use of in-vitro 3D collagen matrices becomes more prevalent in broadening our understanding of cell behavior when exposed to various cues, the demand for characterization techniques that can visualize both the cellular protein and the surrounding 3D collagen matrix increases. Cellular proteins can be visualized by immunostaining cells with fluorescently labeled antibodies under fluorescence microscopy [94]. Even better, laser-scanning confocal microscopy with control of depth-of-field and ability to create 3D images allowed better visualization of cellular proteins and fibrillar ECM [94].

Marelli et al. used a dense collagen-bioactive glass hybrid to examine the biomineralization of these glasses in SBF [72]. The study concluded with the ability of collagen-45S5 Bioglass® to mineralize in SBF while phosphate glass of the composition $50P_2O_5$-40CaO-$10Fe_2O_3$ mol% and inert alumina did not exhibit any mineralization. Stahli et al. investigated MMPs gene regulation

of endothelial cells (EC) under the controlled release of copper ions from phosphate glass by seeding ECs in collagen type 1 gels [95]. Copper ions are angiogenic agents, and hence the growth of the EC network was examined under a confocal laser microscope to quantify the EC network length, connectivity, and branching with time.

3.3.1.2 Fibroblasts and Collagen

Fibroblastic cell behavior in various collagen gel systems has been studied to explore their role in wound healing. Some of the early works trying to duplicate the collagen connective tissue natural system include that published by Ehrmann and Gey (1956), who successfully attempted to create reconstituted collagen gels and tested the strain created by various cell types within the matrix. The results showed an improved cell growth in 3D collagen matrix compared to glass [96]. In 1972, Elsdale and Bard tested various cell behavior parameters of diploid lung fibroblasts in hydrated collagen lattices. The results showed an improved cell attachment and extension with time when compared to cells grown in soft agar 3D matrices [97]. This illustrated the ability of the cells to "feel" and respond to the substratum they developed in. In 1979, Merrill et al. explored the contraction of the collagen matrix as a result of growing fibroblasts within the matrix. The paper reported a reduction of a fibroblast seeded hydrated collagen gel to 1/28th of its initial surface area. The formation of a tissue-like structure was seen to be regulated by cell number, protein content, and concentration of cell growth inhibitors added to the matrix. The study also highlighted an increase in cell proliferation in the matrix as the stiffness and isometric tension within the matrix increased. Since no gel densification processes were applied, the increase in matrix stiffness was attributed to cell behavior [98].

Fibroblastic cells also respond to the surface chemistry of the matrix. For example, in collagen, they have been found to attach to the fibers and have a polar orientation within hours to a few days [17]. They have also been observed to respond differently, depending on whether the matrix is attached or free-floating [99]. Fibroblastic cells in free-floating collagen were often described as quiescent resembling fibroblasts in the dermis. At the same time, those in attached matrices resemble activated fibroblasts in the granulation tissue during the early stages of wound healing [100]. Seeded cells have been found to modulate the matrix in such a way that the stiffness of the matrix is changed. Brown et al. were able to create a cell-independent method of

densification of the collagen matrix known as PC [101]. In this technique, rapid expulsion of fluid is enabled by applying a weight post gel formation. This densification technique was used by Hadjipanayi et al. to study how changing the stiffness of the matrix affects the proliferation of fibroblastic cells within the 3D structure. It was found that human dermal fibroblasts seeded in free-floating collagen matrices have the lowest proliferation, whereas those seeded in plastically compressed matrices showed the highest proliferation rate [102]. Discher et al. reviewed how the matrix mechanics can change cell orientation and proliferation, in particular, cells were shown to exert higher tension with an increase in matrix stiffness and accumulate more in the stiffer parts of a soft-to-stiff collagen gel gradient [103].

As cell-seeded plastically compressed collagen gel models were developed, Cheema et al. explored the possible effect of this densification process on the oxygen tension cells are exposed to at the surface and core of rolled PC collagen constructs at different cell densities. This study concluded that PC densification produces O_2 gradients that do not significantly damage cell viability. However, it was noticed that VEGF mRNA expression is upregulated to higher levels in the core of the construct compared to the surface of the construct [104]

.

3.3.2 Hydroxyapatite in Tissue Engineering

Bone is composed of collagenous proteins and inorganic mineral in the form of small calcium phosphate crystals known as HAp. HAp, constituting approximately 70 wt% of the mineral composition of bone, has found extensive applications as a biocompatible and biomimetic coating to medical implants, especially titanium-based osteoarticular implants. Synthetically made HAp coating allowed metal implants to promote bone in-growth and hence secure better fixation [105, 106]. Today, the osteoconductive properties of HAp have allowed it to be widely used in bone regeneration in orthopedic, dental, and maxillofacial surgeries. [105, 107]. HAp can also be obtained from sea coral by exposing it to intense heat to remove the organic parts, hence removing chances of an allergic reaction by the recipient body [108, 109, 110].

It is interesting to note that even though most hydroxyapatite applications have been focused on bone regeneration, it may have further application in the soft tissue application realm.

For example, Yu et al. reported using mesoporous hydroxyapatite as carriers for simvastatin to the wound site, and as a result, accelerating the wound closure in-vivo [117]. Even though this supports the biocompatibility of HAp, it does not shed light on the role HAp has on the wound healing process. In another study, Majeed et al. investigated the role HAp plays in the wound healing process in-vivo using rabbits. The study found that applying HAp powder in the wound site before suturing lead to faster wound healing than the control group with no HAp applied. Wound sites were observed using. Figure 11 shows light microscopy images of the wound site, characterized by the formation of fibrous connective tissues between the calcified areas of the wound. It was suggested that this acceleration in the wound healing process was due to HAp attracting macrophages and enhancing fibroblast migration to the wound site [110].

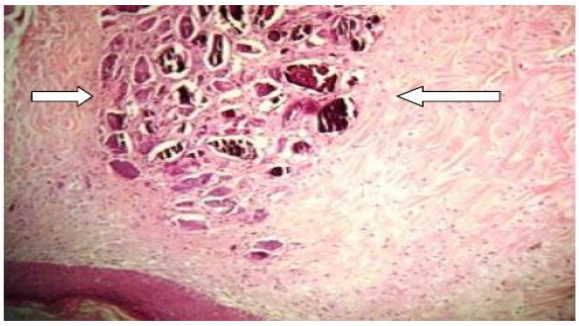

Figure 11: Wound site after 21 days under a microscope [110]

4. Materials and Methods

4.1 Materials

Melt-quenched bioactive glass particles of similar composition to 45S5 Bioglass® ($45SiO_2$-$24.5CaO$-$24.5Na_2O$-$6.0P_2O_5$) (wt%) and particle size range 53 µm was purchased from Mo-Sci Corporation (USA). Synthetic hydroxyapatite of particle size approximately 30 µm and resazurin sodium salt were purchased from Sigma Aldrich (Canada). RAFT 24-well absorbers were purchased from Lonza (Switzerland).

4.2 Simulated Body Fluid (SBF) preparation

Simulated body fluid (SBF) was prepared according to Kokubo's method [119]. The following chemicals were used in the preparation: Sodium chloride (Fisher, USA), sodium hydrogen carbonate (Fisher, USA), potassium chloride (Fisher, USA), di-potassium hydrogen phosphate trihydrate (Sigma-Aldrich, USA), magnesium chloride hexahydrate (Fisher, USA), calcium chloride (Fisher, USA), sodium sulfate (Fisher, USA), tris-hydroxymethyl aminomethane (Fisher, USA), 1M (mol/l) Hydrochloric Acid (Fisher, USA). The final expected ionic concentrations in the SBF solution were: 142 mM Na^+, 5 mM K^+, 1.5 mM Mg^{2+}, 2.5 mM Ca^{2+}, 147.8 mM Cl^-, 4.2 mM HCO_3^-, 1 mM HPO_4^{3-}, and 0.5 mM SO_4^{2-}. The final pH of the solution was 7.4.

4.3 Conditioning of 45S5 bioactive glass in SBF

Bioactive glass particle was immersed in SBF (pH 7.4) in sterile 50 mL falcon tubes at a concentration of 1.5 mg/mL glass in 50 mL SBF solution for 3 and 14 days at 37±1°C (Figure 12). At the end of the conditioning period, the tubes were centrifuged, and the SBF solution removed. The remaining solid was washed twice with deionized water (DIW) and then twice with ethanol and finally dried overnight at 55^{o}C.

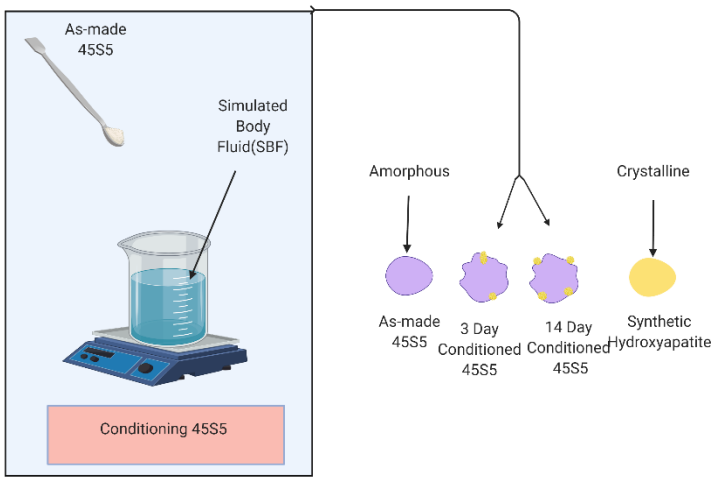

Figure 12: Conditioning of 45S5 bioactive glass in 1x Simulated Body Fluid (SBF) for 3 and 14 days. *45S5 bioactive glass particles were immersed in SBF at a ratio of 45S5/SBF of 1.5 mg/mL and kept at 37ºC for 3 and 14 days. The conditioned samples were then washed with DIW and ethanol and dried at 55ºC*

4.4 Scanning electron microscopy (SEM)

Scanning electron microscopy (SEM) imaging was used to investigate the morphological properties of the as-received glass, conditioned glass and synthetic hydroxyapatite particles. Samples were mounted on metal stubs and sputter-coated with Pt before SEM using a Leica Microsystems EM ACE600. The morphology was examined using a field-emission SEM (Quanta 450 FEG; FEI Corporation, USA) at 5kV.

4.5 X-ray diffraction (XRD)

XRD diffractograms (XRD) of the as-received glass, conditioned glass and synthetic hydroxyapatite particles were generated using a Bruker D8 Discover X-ray diffractometer (Bruker AXSS Inc., USA) equipped with a CuKα ($\lambda = 0.15406$ nm) target set to a power level of 40 mV and 40 mA. Using an area detector, three frames of 25° were collected from 15 – 75, 2 theta (°), and merged in post-processing.

4.6 Attenuated total reflectance-Fourier transform infrared spectroscopy (ATR-FTIR)

Attenuated total reflectance-Fourier transform infrared (ATR-FTIR) spectroscopy was carried out on as-received glass, conditioned glass and synthetic hydroxyapatite particles using a Spectrum 400 (Perkin-Elmer, USA) between 4000 and 650 cm^{-1} with a resolution of 4 cm^{-1} using 64 scans per sample.

4.7 Particle size and surface area

The particle size (D50) of the sieved particle was determined using a Horiba LA-920 particle size distribution analyzer (ATS Scientific Ink., Canada). The specific surface area (SSA) of the particles was measured with nitrogen gas adsorption and desorption isotherms collected with a Micromeritics TriStar 3000 (Micromeritics Instrument Corporation, USA) gas sorption system. SSA values were determined from the isotherm with the Brunauer–Emmett–Teller (BET) method. Samples were run at n=3.

4.8 Inductively coupled plasma optical emission spectrometry (ICP-OES)

Release of silicon, calcium, sodium, and phosphorus ions from as-received glass, conditioned glass and synthetic hydroxyapatite particles in DIW at a concentration of 1.57 mg/mL were quantified at 3 and 72 hours using ICP-OES (Thermo Scientific iCAP 6500, USA). Aliquots of 5 mL were filtered through a 0.2 μm nylon filter and stored in a 15 mL falcon tubes. A volume of 1 mL of 4% (w/v) nitric acid (Fisher Scientific, Canada) was added to 3 mL of the aliquot, and digestion was allowed at 95°C for 3 hours. After digestion and allowing samples to cool down, DIW was added up to 5 mL in all tubes. Calibration standards of Ca, Si, Na and P were prepared in-house at values 50 ppm, 5 ppm, and 0.5 ppm. Samples were run at n=3.

4.9 Sterilization of particles

As-received glass, conditioned glass, and synthetic hydroxyapatite particles were sterilized through dry-heat autoclaving. Particles were placed in glass vials and exposed to dry heat in an oven at 180^{o}C for 4 hours, followed by 10 minutes under U.V. radiation.

4.10 Cell culture

A murine-derived NIH/3T3 fibroblastic cell line (ATCC) was used in this study. Cells were cultured in Tissue cultured-treated 10 cm dishes in Dulbecco's Modified Eagle Medium (DMEM) (High glucose, ThermoFisher) supplemented with 10% fetal bovine serum (FBS) (Hyclone) and 1% penicillin-streptomycin (Invitrogen). Cells were incubated at 37°C under humidified air containing 5% CO_2. At 80% confluency, the cells were washed with sterile phosphate-buffered saline (PBS), detached with 0.25% trypsin ethylenediaminetetraacetic acid solution (Invitrogen), centrifuged for 5 min at room temperature, the supernatant removed, suspended in fresh full DMEM and counted using a hemocytometer. Cells between passages 5 and 9 were used for cell work.

4.11 Direct contact model

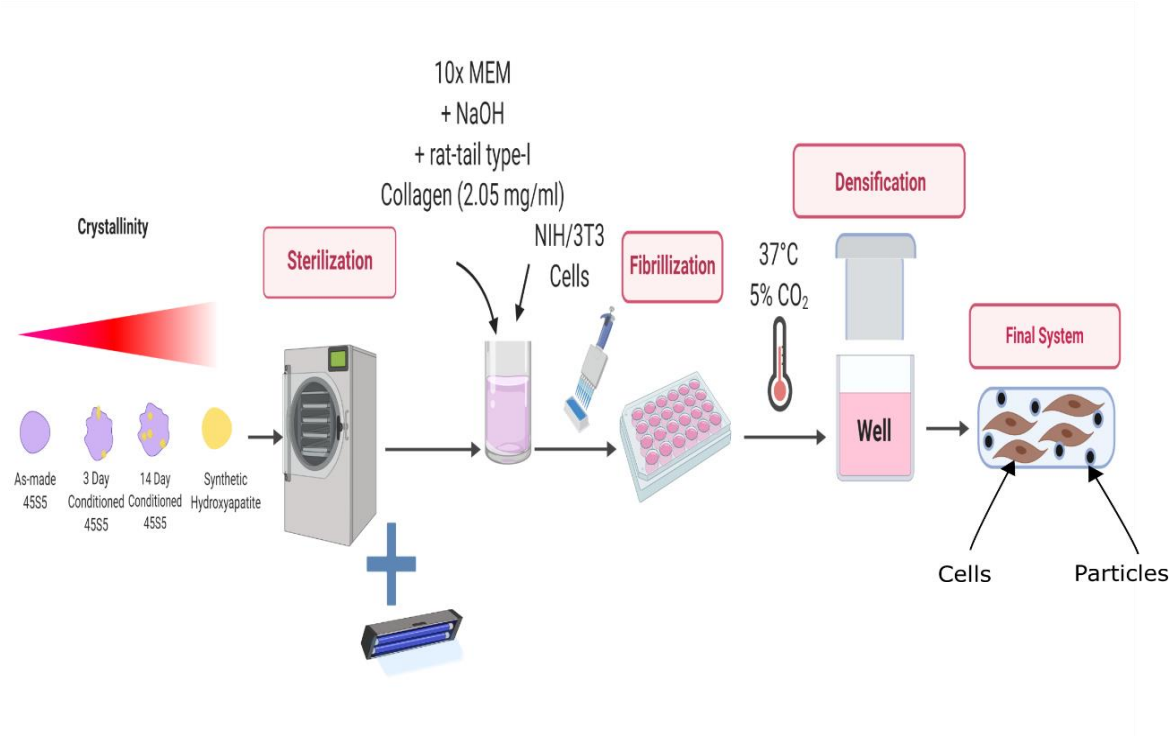

Figure 13: Creation of a direct-contact model to investigate the effect of bioactive glass/ceramic particle incorporation on NIH/3T3 cell viability, death, proliferation, metabolic activity, ability to mineralize collagen and gene expression in a three-dimensional environment. *Particles were dry heat sterilized, followed by a brief UV treatment. Post 10XMEM and collagen solutions addition to sterilized vials containing the particles, the solution was neutralized using NaOH and NIH/3T3 cells were seeded at a density of 250,000 cells/mL collagen solution. Gelling was enabled at 37°C and 5% CO_2 for 30 minutes. RAFT™ 24-well absorbers were applied for 15 minutes. Culture media was added, and gels are physically detached from the base of the wells*

To produce particle incorporated cellular and acellular collagen gels, a 1:4 mixture of 10x Minimum Essential Medium (MEM) (FirstLink Ltd., UK) and 2.00 mg/mL rat-tail tendon derived collagen type I (First Link Ltd., UK) were added to sterile vials containing bioactive glass/ceramic particles. Particle incorporation was carried out at a concentration of 0.8 mg/mL relative to collagen solution. Non-particle incorporated collagen gels were used as Control. The mixture was neutralized by adding sterile-filtered 5 M NaOH. For cellular gels, cells were seeded post collagen neutralization at a density of 2.5×10^5 cells/mL collagen solution while the solution was kept on ice and 1 mL of the solution is dispensed in each well of Costar® 24-well Clear TC-treated multiple well plates (Corning, USA). Gelling was enabled in an incubator with 5% CO_2 atmosphere at 37°C

for 30 minutes. RAFT^{TM} 24-well absorbers were applied for 15 minutes following the incubation. Gels were detached from the bottom of the wells using sterile pipette tips to produce floating gels resembling fibroblasts in the dermis [99]. A volume of 500 µL of full DMEM was added to each well, and the medium was changed at two-day intervals.

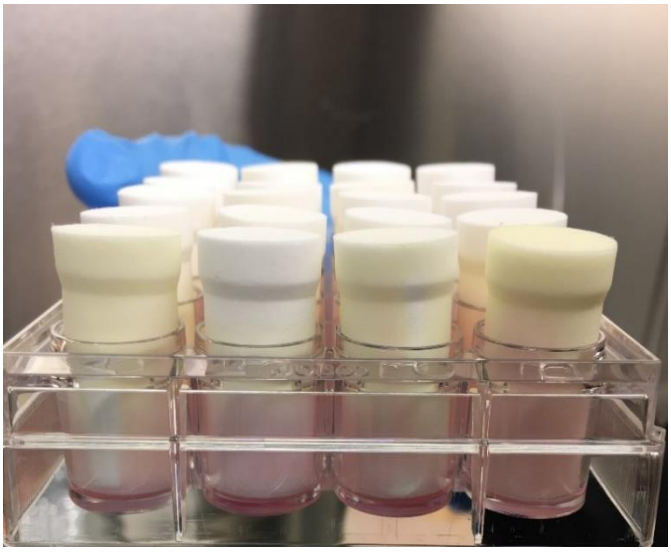

Figure 14: Gel densification using RAFT^{TM}-24 well

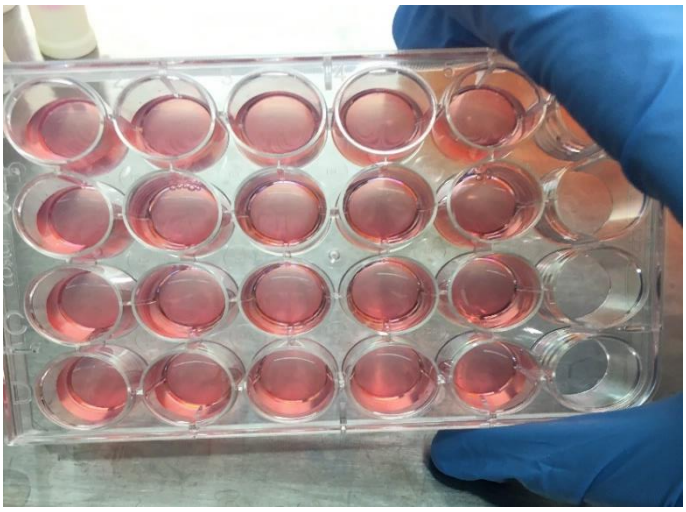

Figure 15: Dense collagen after removal of RAFT^{TM}24-well absorbers and addition of cell culture media

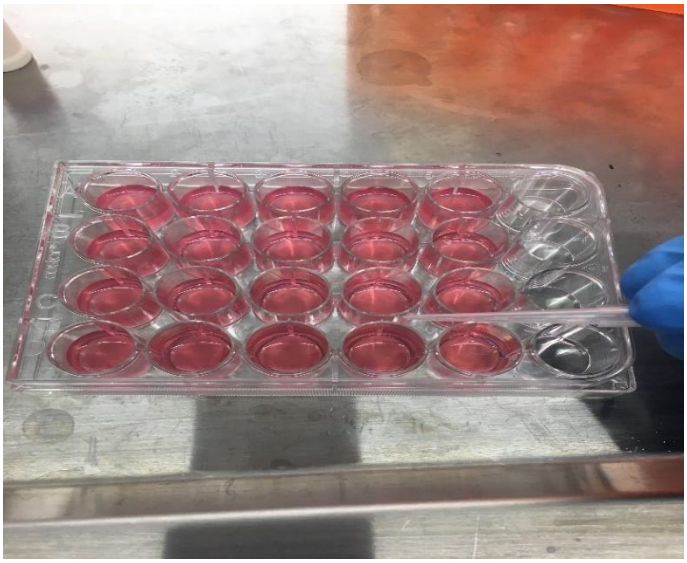

Figure 16: Detachment of dense collagen gels from the bottom of their wells using a sterile tip

Figure 17: Free floating gels in culture

4.12 Determination of collagen gel fibrillar density (CFD)

Collagen content in the gels was quantified through the collagen fibrillar density (CFD; wt%). Collagen gels were frozen in liquid nitrogen, weighed, followed by freeze-drying (FreeZone 2.5 Benchtop Freeze Dryer, Labconco) (Figure 18) overnight and weighed again. The weight percent of collagen was calculated according to Equation 1. Samples were assessed at n=6.

$$\mathrm{CFD} = \frac{W_{Dry}}{W_{Wet}} \times 100\% \qquad \textit{Equation 1}$$

Figure 18: FreeZone 2.5 Benchtop Freeze Dryer from Labconco used in freeze drying dense collagen gels

Figure 19: Parafilm covered 1-ml tubes after freeze-drying

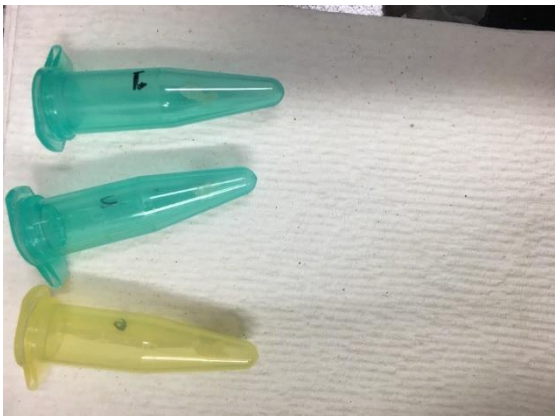

Figure 20: Weighted 1-ml tubes after freeze-drying

4.13 Seeded NIH/3T3 metabolic activity

The metabolic activity of seeded NIH/3T3 as an indicator of cell proliferation/viability was evaluated through the reduction of AlamarBlue®, which was prepared by dissolving 0.03 g of resazurin sodium salt Sigma Aldrich (Canada) in 45 mL 1xPBS and sterile filtered. NIH/3T3-seeded gels were incubated in FBS-free growth medium with 10% AlamarBlue® solution and incubated under darkness in 5% CO_2 and 37°C for 4 hours. An absorbance detection system was employed using a PerkinElmer microplate reader (VICTOR Nivo, USA). Background absorbance measured in medium incubated with acellular gels was subtracted from all values. Absorbance was measured at 570 nm. Analysis was carried out at days 1, 4, 7, 12, 17 and 21. Samples were examined at n=6.

4.14 Ki-67 proliferation assay

At day 15 in culture, cellular gels were fixed in 4% formaldehyde for 30 minutes and washed with 1xPBS for 10 minutes, followed by permeabilization by adding 1% Triton/PBS for 15 minutes. 1% Bovine Serum Albumin (BSA) (Fisher) blocking buffer in 1xPBS solution was then added for 1 hour. Purified Mouse Anti-Ki-67 primary antibody (BD, USA) in blocking solution (1:200) was added, and gels incubated overnight at 4^{o}C. The primary antibody solution was discarded, and gels were washed with 1xPBS for 5 minutes. Lastly, Cy3-conjugated donkey anti-rabbit IgG secondary antibody (Jackson ImmunoResearch, USA) (1:500) was added, and gels were incubated for 2 hours at room temperature with the addition of 1% 4′,6-diamidino-2-phenylindole (DAPI) fluorescent nuclear counterstain in 1xPBS. After the solution was removed, the gels were washed with 1xPBS three times for 5 minutes and imaged using laser scanning confocal microscope, LSM 710 (Zeiss, Germany). Samples were examined at n=3 and the DAPI and KI-67 positive cells per field were quantified by splitting the two channels and manually counted using ImageJ (NIH, USA).

4.15 Live/Dead assay

Seeded cells were stained with 1 μM calcein-AM and 2 μM ethidium homodimer-1 (Live/dead assay; Invitrogen) for 30 minutes. Images of green fluorescent viable cells and red fluorescent dead cell nuclei were acquired in the same well plates through a laser scanning confocal microscope, LSM 710 (Zeiss, Germany). Both viability/death and morphology of seeded NIH/3T3 cells were investigated at days 11 and 23 in culture. All conditions were tested in triplicates.

4.16 Transmitted Light Microscopy

Gels were imaged using EVOS FL Auto Imaging System (Thermo Fisher, USA) at days 1, 7 and 15 in culture.

4.17 Gel sectioning

Gels were fixed for 30 minutes in 4% Paraformaldehyde (PFA)/PBS, embedded in optimal cutting temperature compound, and frozen at -20^{o}C in a precooled cryostat bar (CRYOSTAR NX70, Fisher) (Figure 21) and sectioned (10 µm) using the cryostat. Six sections were collected per sample and stored at 4^{o}C until staining and preserved at 4^{o}C after staining.

Figure 21: CRYOSTAR NX70 cryostat used in sectioning and settings applied

4.18 Alizarin Red S staining

Alizarin Red S was used to identify calcium deposits in sections. Alizarin Red solution was prepared by dissolving 2 g Alizarin Red S powder (Sigma-Aldrich) in 100 mL distilled water. The

solution was mixed on a magnetic stirrer at room temperature, and the pH was adjusted using 10% ammonium hydroxide until pH range of 4.1-4.2 was reached. Sections were briefly dipped in DIW three times, followed by dipping in Alizarin Red S solution for 5 minutes and then briefly three-times in fresh DIW to remove excess stain. Stained sections were then gradually dehydrated through gradient ethanol and finally cleared in Xylene, permanent xylene based mounting media was applied and coverslips placed. Calcium deposits appear as orange-red regions. The resulting stained sections were analyzed by light microscopy (Leica DM2000) at 40× magnification. Sample sections were examined at n = 6.

4.19 Von Kossa van Gieson staining

Von Kossa and van Gieson staining was used to examine phosphate deposition and counterstain targeting the collagen matrix, respectively. Sections were briefly dipped in DIW three times followed by incubation in 1% silver nitrate solution; sodium formamide develops silver ions to black silver and the unreacted silver ions were then removed by reaction with sodium thiosulfate. Sections were then dipped in Van Gieson stain followed by running under tap water. Stained sections were then gradually dehydrated through gradient ethanol and finally cleared in Xylene, permanent xylene based mounting media was applied and coverslips placed. Phosphate deposits appeared as dark black regions whereas collagen appeared as light to dark pink. The resulting stained sections were visualized by light microscopy (Leica DM2000) at 40× magnification. Sample sections were examined at n = 6.

4.20 SEM and ATR-FTIR spectroscopy analyses of collagen gels

SEM and ATR-FTIR analyses were used to characterize the cell seeded gels at day 23 in culture. Gels were fixed in 4% formaldehyde for 30 minutes, rinsed twice with DIW for 10 minutes and then dehydrated through an ethanol gradient followed by immersion in 1,1,1,3,3,3-hexamethyldisilazane (Sigma-Aldrich, Canada). Samples to be examined using SEM were coated with Pt using a Leica Microsystems EM ACE600 sputter coater (Austria), and Images were acquired with a field-emission SEM (Quanta 450 FEG; FEI Corporation, USA) at 5kV. ATR-FTIR spectroscopy was carried out on dried samples using a Spectrum 400 (Perkin-Elmer, USA)

between 4000 and 650 cm^{-1} with a resolution of 4 cm^{-1} using 64 scans per sample. Each sample was scanned on at least three positions and each mineralization assay was run in triplicates.

4.21 Gene expression of seeded fibroblasts

Figure 22: AHS200 homogenizer from VWR

Gene expression analyses were performed using qRT-PCR system (QuantStudio™ 7 Flex Real-Time PCR System; Applied Biosystems). Total RNA was extracted from the gels with TRIZOL reagent (Invitrogen) using a homogenizer (AHS200, VWR) (Figure 22) and subjected to DNase I (Invitrogen) treatment. The first-strand cDNA synthesis and qRT-PCR were performed using a high-capacity cDNA reverse-transcription kit (Applied Biosystems) and SYBR green quantitative PCR master mix (Wisent Bioproducts), respectively. Relative gene expression was analyzed using QuantStudio™ software (Applied Biosystems) using comparative Ct and hypoxanthine-guanine phosphoribosyltransferase (Hprt, a housekeeping gene) expression as an endogenous control. In order to calculate the delta cycle threshold (ΔCt) value, the mean Ct value of the expression of a gene in a sample was first normalized to the mean Ct value of *Hprt* expression in that sample. The ΔCt value of the calibrator sample was subtracted from that of the sample-of-interest to obtain the ΔΔCt value. The relative expression was reported as $2^{-\Delta\Delta Ct}$. Table 3 shows the forward and reverse primers of the genes of interest

Table 3: qRT-PCR primers used to indicate both wound healing and osteogenic differentiation

Gene Name	Forward Primer	Reverse Primer
Transforming growth factor beta (Tgfb1)	5 ’ -CAGCCCTGCTCACCGTCGTG -3 ’	5 ’ -GGTTTGTGGCTCCCGAGGGC-3 ’
Alpha-smooth muscle actin (*α-SMA*)	5 ’ -ATCATGCGTCTGGACTTGG-3 ’	5 ’ -AATAGCCACGCTCAGTCAGG-3 ’
Vascular endothelial growth factor (*Vegf*)	5 ’ -GATCATGCGGATCAAACCTC-3 ’	5 ’ -AATGCTTTCTCCGCTCTGAA-3 ’
Alpha chain of type I collagen (*Col1a1*)	5 ’ -ACATGTTCAGCTTTGTGGACC-3 ’	5 ’ -GGTTTCCACGTCTCACCATT-3 ’
Bone sialoprotein 2 (*Ibsp*)	5 ’ -GAAGAGTCACTGCCTCCCTG-3 ’	5 ’ -TCCATCGAAGAATCAAAGCA-3 ’
Mouse alkaline phosphatase 2 (*Alp*)	5 ’ -GAGCCGGAACAGACCCTC-3 ’	5 ’ -TACCCTGAGATTCGTCCCTC-3 ’
Sp7 transcription factor	5 ’ -GGACTGGAGCCATAGTGAGC-3 ’	5 ’ -CTCTCCATCTGCCTGACTCC-3 ’
Runt-related transcription factor2 (*Runx2*)	5’-GCTCACGTCGCTCATCTTG-3’	5’-TATGGCGTCAAACAGCCTCT-3’
Hypoxanthine-guanine phosphoribosyltransferase (*Hprt*)	5’-GTTGAGAGATCATCTCCACC-3’	5’-AGCGATGATGAACCAGGTTA-3’

4.22 Statistical analysis

Statistical analysis was carried out using ordinary one-way analysis of variance to compare the means of more than two groups with significance levels as follows: *($P \leq 0.05$), **($P \leq 0.01$), ***($P \leq 0.001$) and ****($P \leq 0.0001$).

5. Results

5.1 SEM, XRD and ATR-FTIR analyses of particles in SBF

Figure 23A (i-iv) shows the SEM images of the 45S5 Bioglass®, 3-day conditioned 45S5 Bioglass®, 14-day conditioned 45S5 Bioglass® and HAp particles, which were in the range of 25-75 µm. Figure 23A (v-vi) exhibits higher magnification images showing the surface topography of 45S5 Bioglass® at days 3 and 14 of conditioning in SBF. With longer immersion time in SBF, the surface roughness of 45S5 Bioglass® increased, and more apatite-like spherulitic shaped particles were observed.

In order to verify the formation of HCA on the initially amorphous glass particles, XRD and ATR-FTIR spectroscopy were utilized on the glass particles at days 3 and 14 in SBF. XRD diffractograms confirmed apatite layer formation in the partially mineralized glass due to the appearance of two characteristic peaks located at $2\Theta = 26°, 32°$ which correspond to (002) and (211) crystal planes, respectively, according to standard HCA peaks, ICDD 00-001-1008 (Figure 23B). After 14 days of conditioning, the XRD pattern of the surface was not identical to that of HAp indicating the presence of residual glass phase in addition to the newly formed apatite. This is in line with several studies reporting on the conversion of silicate glasses in SBF [111,112].HCA formation was also confirmed using ATR-FTIR spectroscopy (Figure 23C). The infrared spectra were plotted in the range of 1600–400 cm^{-1}, which is the region of interest. The amorphous 45S5 Bioglass® peaks can be observed through Si-O-Si bending at 460 cm^{-1}; Si-O-Si stretch at 1000 cm^{-1}, and Si-O-(non-bridging-oxygen) at 920 cm^{-1} [113, 114, 115]. These vibrational modes changed with immersion in SBF. Both the 3- and 14-day partially mineralized samples in SBF exhibited similar distinctive peaks related to the formation of a phosphate layer. The P-O stretch appeared at 1028 cm^{-1}; P-O bending peaks associated with the crystal phase emerged at 562 cm^{-1}, and 602 cm^{-1}. The decrease in the Si-O-(non-bridging-oxygen) peak reveals the release of Na^{+} and Ca^{2+} modifying ions into the SBF solution. Furthermore, a C-O peak at 870 cm^{-1} was detected confirming the CO_3^{2-} containing hydroxyapatite (HCA) formation, as previously reported [113, 114, 116, 117].

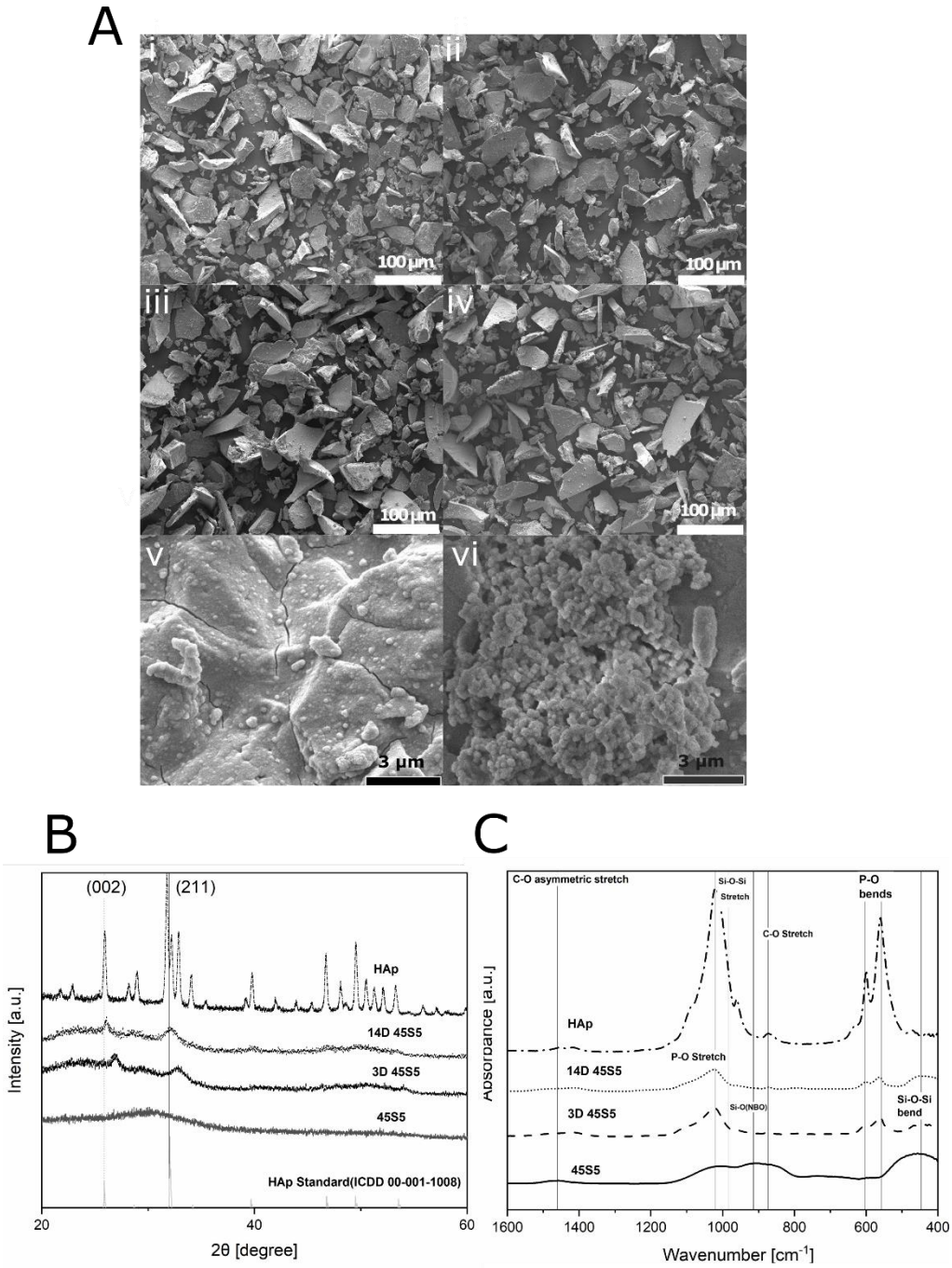

Figure 23: Characterization of conditioned 45S5 Bioglass®. *A. SEM micrographs of 45S5 Bioglass® (i); 3-day conditioned 45S5 Bioglass® (ii); 14-day conditioned 45S5 Bioglass® (iii); and HAp (iv) particles. All particles were of similar size (Table 4). Magnification 5000X (Scale bar = 100 µm). Subset (v and vi) show surface roughening and particle deposition observed on 3-day conditioned 45S5 Bioglass® (v); and formation of apatite-like spherulitic shaped particles on 14-day conditioned 45S5 Bioglass® (vi). Magnification 10,000X (Scale bar = 3 µm). B. XRD diffractograms of amorphous 45S5 Bioglass®, 3-day conditioned 45S5 Bioglass®, 14-day conditioned 45S5 Bioglass®, and HAp. After 3 days conditioning, peaks at 26º and 32º appear, indicating the formation of a crystalline HCA layer. C. ATR-FTIR spectra of amorphous 45S5 Bioglass®, 3-day conditioned 45S5 Bioglass®, 14-day conditioned 45S5 Bioglass®, and Hap particles. Spectra indicated the formation of phosphate groups through the formation of P-O bend peaks characteristic of a crystalline phosphate phase, similarly a C-O bends indicates a carbonate formation*

5.2 Particle size and surface area characterization

The effect of partially mineralizing 45S5 Bioglass® particles in SBF solution on both particle size and specific surface area was examined. Particles were all in the target size range of 25-75 μm. However, there was a 900-fold increase in surface area between as-received glass (45S5) and the 14-day partially mineralized 45S5 (Table 4), which may be due to the roughening of the surface during dissolution and growth of HCA layer.

Table 4: Particle size and specific surface area measurements, n=3.

Sample	Mean Particle Size (μm)	D50 Particle Size (μm)	Specific Surface Area (m^2/g)
45S5 Bioglass®	42.05 ± 27.46	37.82 ± 27.46	0.24 ± 0.02
3 Day Conditioned 45S5	42.39 ± 25.92	38.02 ± 25.92	49.22 ± 0.33
14 Day Conditioned 45S5	45.10 ± 27.03	40.87 ± 27.03	219.50 ± 2.01
HAp	28.91 ± 15.48	25.72 ± 15.48	1.10 ± 0.01

5.3 Ionic dissolution

ICP-OES analysis was carried out to evaluate ionic release from the various glass/ceramic particles in DIW. Figure 24 shows the concentration of silicon, sodium, calcium and phosphorous ions in ppm in DIW after cumulative durations of 3 and 72h. It can be observed that at the longer immersion time point in DIW, there were higher concentrations of sodium and calcium ions in as-received and partially mineralized glasses. The concentrations of both alkaline species were also observed to decrease with an increase in partial mineralization. This was due to the ionic exchange between H^+ and H_3O^+ from the DIW with the glass sodium and calcium cations, respectively [6,

22, 118]. This occurs rapidly within a few minutes in aqueous solutions. Hydrolysis of the Si-O-Si in the glass network leads to the release of soluble silica in the form of $Si(OH)_4$ [118]. However, the concentration of phosphorous ions (likely to be in the form of phosphates) in the solution seems to decrease with time for the Bioglass® samples, both in the amorphous and partially mineralized glasses. However, this was not observed for HAp, where the concentration of phosphorus ions seems to increase with immersion time in DIW. This can be attributed to the lower reactivity of HAp when compared to 45S5 glass [119]. Furthermore, the greater the duration of conditioning of 45S5 Bioglass® in SBF, the lower its release of sodium and calcium cations when immersed DIW. It is also interesting to observe the higher silicon release from these conditioned glasses compared to the as-received glass.

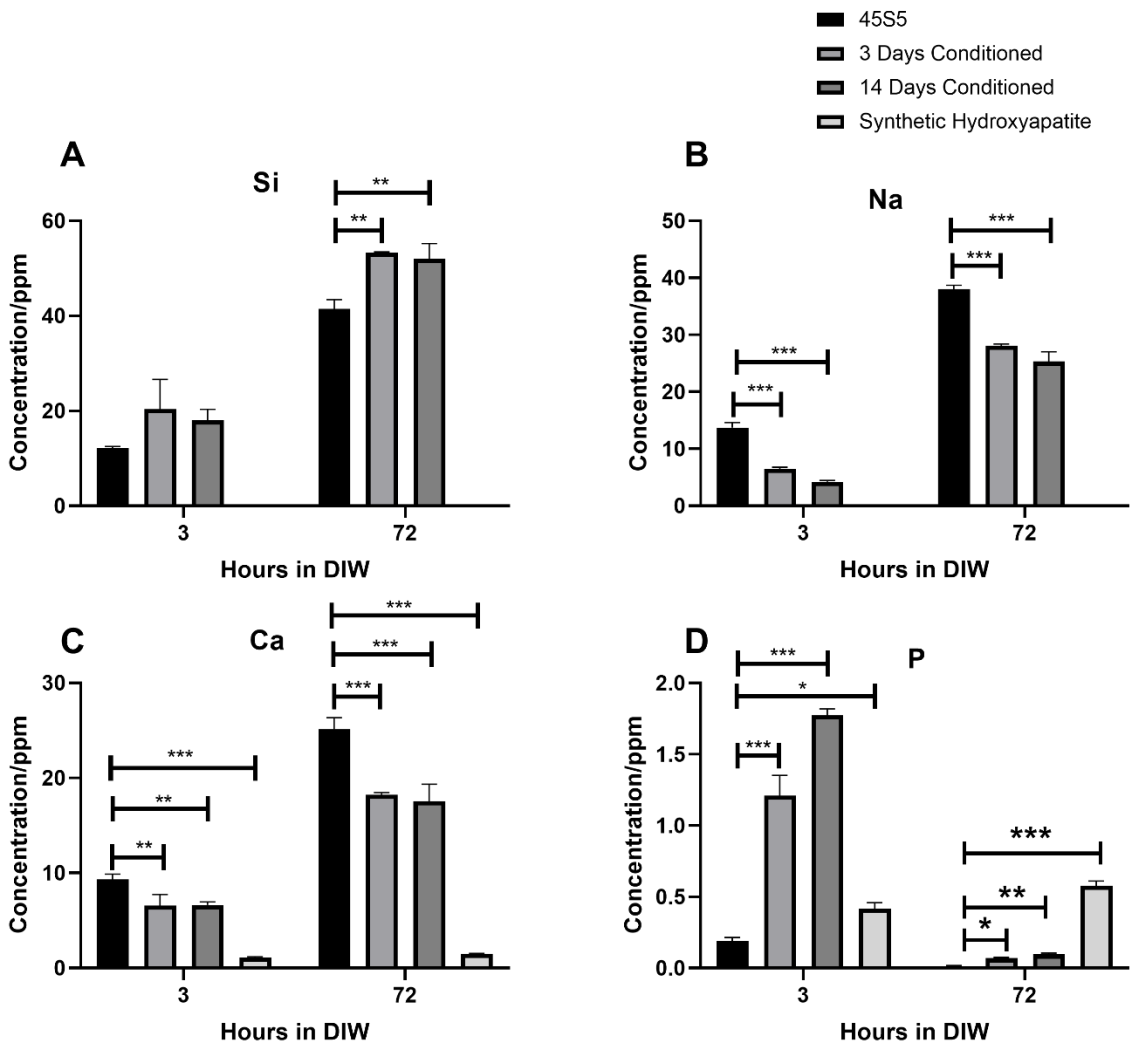

Figure 24: Measurement of ionic dissolution products in DIW through ICP-OES. *A. Silicon B. Sodium C. Calcium D. Phosphorous after cumulative 3 and 72 hours in DIW. A significant decrease in sodium and calcium ion release after 3- and 14-day conditioning of 45S5 Bioglass® in SBF. Higher silicon release was observed from the conditioned glasses. A higher phosphorous concentration was observed after immersion in DIW at 3 hours, which then decreased in all conditions except for HAp. Silicon, Sodium, Calcium and Phosphorous concentrations in DIW, if any, were subtracted from each condition. Samples were evaluated at n=3. *($P \leq 0.05$), **($P \leq 0.01$), ***($P \leq 0.001$)*

5.4 Evaluation of collagen fibrillar density (CFD)

A collagen fibrillar density (CFD) post-RAFT^{TM} densification was evaluated to be 13.38 ± 2.19 wt% (Table 5; Appendix A).

5.5 Metabolic activity, proliferation and viability of seeded NIH/3T3 cells

The metabolic activity of NIH/3T3 cells three-dimensionally seeded in RAFT^{TM} compacted dense collagen gels and in-direct contact with either 45S5 glass, partially mineralized 45S5 glass or HAp particles was evaluated through the AlamarBlue® reduction assay at 6 different time points for up to 21 days in culture (Figure 25). At day 1, the metabolic activity of the cells seeded in the presence of as received 45S5 glass particles was significantly ($P \leq 0.001$) lower when compared to the Control. In contrast, those seeded in the presence of partially mineralized 45S5 glass and HAp particles were significantly ($P \leq 0.001$) higher than the Control. By day 7, the metabolic activity of the cells seeded in the Control, partially mineralized glass and HAp particles were similar ($p>0.05$), while those in the presence of 45S5 glass increased significantly ($P \leq 0.001$), indicating no significant ($p > 0.05$) differences with the control from day 17 and up to day 21.

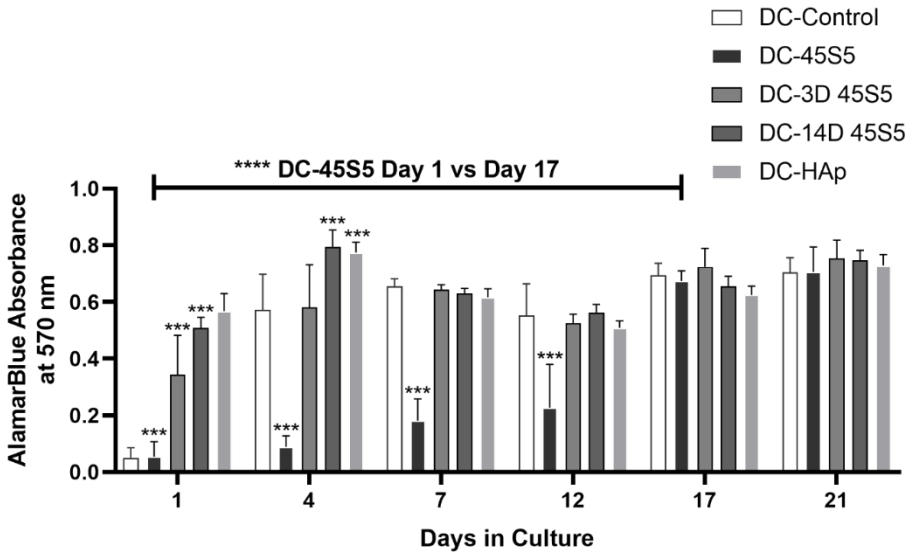

Figure 25: Metabolic activity of seeded NIH/3T3 cells. *AlamarBlue® assay of NIH/3T3 cells seeded in 3D RAFT^{TM} dense collagen gels and in direct contact with incorporated as-received 45S5 Bioglass®, 3-day conditioned 45S5 Bioglass®, 14-day conditioned Bioglass®, and HAp particles at days 1, 4, 7, 12, 17, and 21 in culture. Cell-seeded neat dense collagen gels were used as Control. Acellular neat collagen gels were used as blank. There was a significant increase in the metabolic activity of cells in the presence of the 14-day conditioned 45S5 and HAp particles up to day 4 then the metabolic activities were similar up to day 21 in culture. The metabolic activity of the cells in the presence of the as-received 45S5 Bioglass® particles was significantly lower up to day 12 in culture indicating a slower initial proliferation. Between days 1 and 21 there was a significant ($P \leq 0.0001$) increase in the metabolic activity of cells in the presence of 45S5 Bioglass®. (n=6). *($P \leq 0.05$), **($P \leq 0.01$), ***($P \leq 0.001$), and ****($P \leq 0.0001$)*

In addition to being a direct measure of metabolic activity, AlamarBlue® reduction can also be used as an indirect measure of cell proliferation. After observing a significant ($P \leq 0.0001$) increase in the metabolic activity of cells exposed to as-received 45S5 glass particles between days 12 and 17, the Ki-67 assay was performed at day 15 to further assess this rapid increase in proliferation (Figure 26). Figure 26A exhibits the Ki-67 and DAPI positive cells (indicated by white arrows) while Figure 26B indicates the total number of Ki-67 positive cells per field. To comprehend the number of proliferating cells relative to the total number of cells per field, the ratios of Ki-67 positive cells to DAPI positive cells were evaluated in Figure 26C. There was no difference in the ratios of Ki-67 positive cells to DAPI positive cells at day 15 in culture. A lower number of DAPI positive cells in the presence of as-received 45S5 glass particles indicated a lower total proliferation up to day 15.

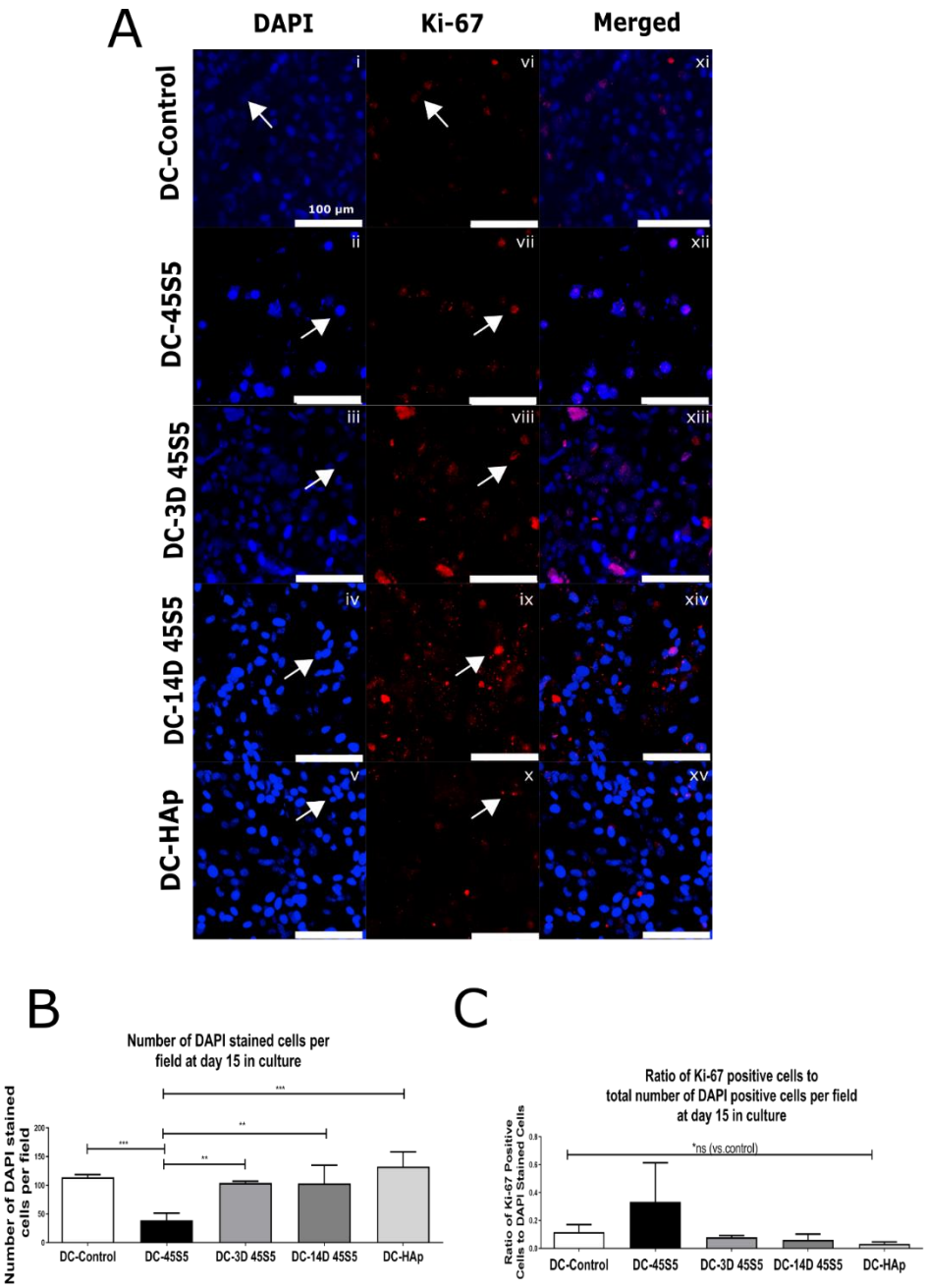

Figure 26: Proliferation of seeded NIH/3T3 cells. *Ki-67 assay of NIH/3T3 cells seeded in 3D RAFT™ dense collagen gels and in direct contact with incorporated as-received 45S5 Bioglass®, 3-day conditioned 45S5 Bioglass®, 14-day conditioned Bioglass®, and HAp particles at day 15 in culture. Cell-seeded neat dense collagen gels were used as Control. A. CLSM images of Ki-67 and DAPI stained cells at day 15 in culture. B. Number of DAPI stained cells indicating the overall proliferation up to day 15. C. Ratio of Ki-67 positive cells to the total number of DAPI stained cells. Overall, a significantly ($P \leq 0.05$), lower overall proliferation rate was observed for as-received 45S5 Bioglass® through a DAPI count. However, at day 15, no significant ($P > 0.05$), difference in Ki-67 positive cells and Ki-67 to DAPI ratio was observed. (n=3). White arrows indicate the Ki-67 positive cells and DAPI positive cells selection. Scale bar = 100 µm*

Cell viability was also evaluated through the Live/Dead Assay and CLSM imaging at days 11 and 23 in culture. The cytoplasm of live cells and nucleic acid of dead cells were visualised by applying fluorescent Calcein-AM and ethidium homodimer-1, respectively (Figure 27). Preliminary CLSM imaging of cell seeded particle-free dense collagen gels at days 2, 11 and 23 indicated a progressive change in viable cell morphology (Figure 27A). Initially, the cells were rounded, which appeared to be increasingly spread by day 11, and at day 23, the structure was denser with well spread cells. Figure 27B shows a Live/dead assay for the different examined conditions with cells in direct contact with the various glass/ceramic particles at days 11 and 23 in culture. At day 11 cells under the different conditions appeared to already assume a spindle-like morphology from their initially rounded morphology as they adhered to the collagen fibers. This was observed for all conditions, except for the as received 45S5 glass particle incorporated gels, which exhibited a rounded morphology. Between days 11 and 23 there seemed to be a substantial increase in cell number in this condition, which may be an indication of improved proliferation after day 11 in culture. Denser structures were also observed in all other conditions.

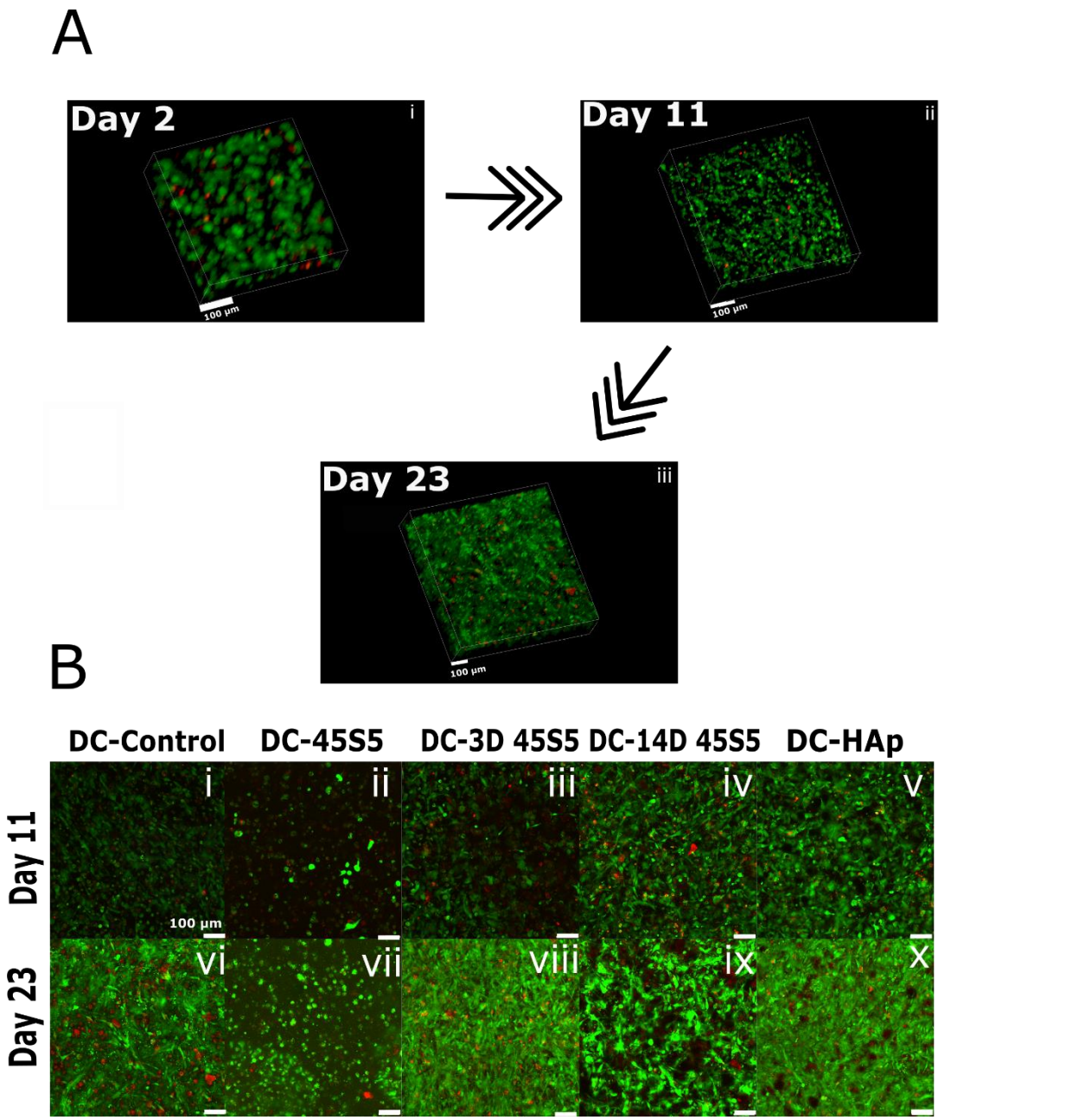

Figure 27: Viability and morphology of seeded NIH/3T3 cells. *A. Live/Dead™ assay of NIH/3T3 cells seeded in 3D in particle-free RAFT™ dense collagen gels visualized using Calcein-AM and Ethidium Homodimer-1 after 2, 11 and 23 days in culture. B. Live/Dead™ assay of NIH/3T3 cells seeded in 3D RAFT™ dense collagen gels and in direct contact with incorporated as-received 45S5 Bioglass®, 3-day conditioned 45S5 Bioglass®, 14-day conditioned Bioglass®, and HAp particles at days 11 and 23 in culture. Cell-seeded neat dense collagen gels were used as Control. Cells were well spread into a spindle-like morphology at day 11 in culture. However, lower cell viability was observed for the as received 45S5 Bioglass® condition with less cell spreading, indicating a lower proliferation rate. A higher cell density was observed in all conditions at day 23 in culture. When compared to day 11, the as received 45S5 Bioglass® showed a higher cell viability. Scale bar = 100 µm. (n=3)*

5.6 Particle deposition and mineralization examined using Transmission Light Microscopy, SEM, von Kossa van Gieson, Alizarin Red stainings, and ATR-FTIR spectroscopy

Figure 28A shows the growth progression of NIH/3T3 cells in dense collagen at days 2, 11 and 23 in culture. Two changes can be observed: First, the change from rounded to well spread cell morphology; second, cell cytoplasm appear to occupy more area with less gaps observed. Figure 28B shows transmission light microscopy images of the collagen gels seeded with NIH/3T3 cells in direct contact with 45S5 glass, partially mineralized glass and HAp particles. At day 1, cells were rounded and well distributed throughout the gel matrix. By day 7, cells appeared well spread assuming their fibroblastic characteristic spindle shaped morphology [18]. This was observed for all conditions except for 45S5, where cells appeared rounded at day 11. Cells in direct contact with HAp particles appeared to maintain their spindle shaped morphology up to day 15. Images of the matrix of the cell-only control gel indicated well distributed dark spots from day 15 in culture. The matrix containing 45S5 glass seemed to start darkening from day 7, and at day 15 the matrix was very dark making it difficult to observe the cell body through light microscopy. Images of the cell-seeded gels incorporated with the 3- and 14-day conditioned glass particles showed darkened patches at days 7 and 15 in culture, but to a lesser extent than those incorporated with as-received 45S5 glass particles.

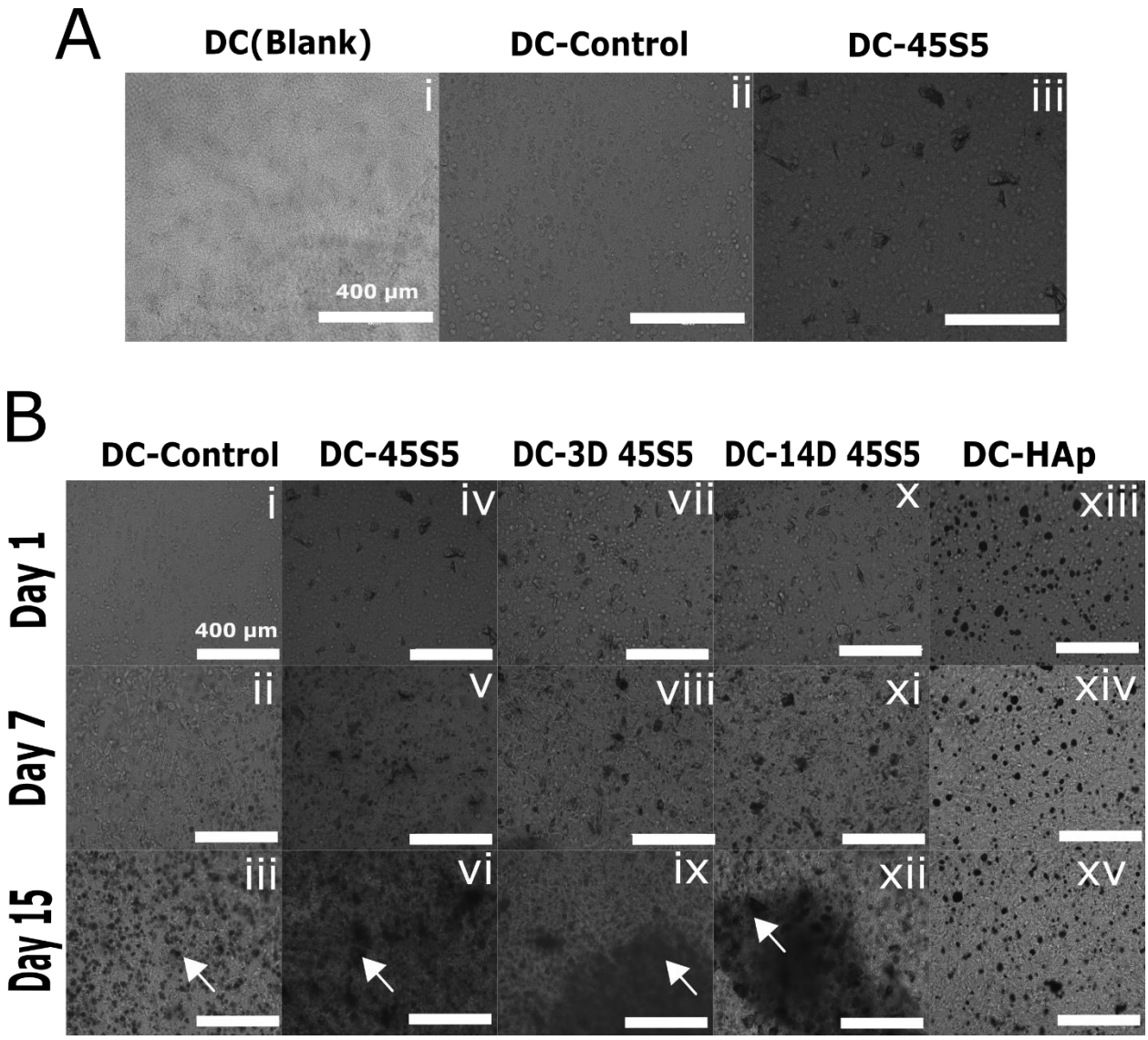

Figure 28: Transmission light micrographs of mineral deposition in dense collagen gels. *A. Cell-seeding and glass incorporation in 3D RAFT^{TM} dense collagen gels at day 1 in culture. DC(Blank) indicates neat acellular dense collagen (i), DC-Control indicates neat cellular collagen (ii) and DC-45S5 indicates cellular dense collagen with incorporated 45S5 particles. B. Inverted microscope images of NIH/3T3 cells seeded in 3D RAFT^{TM} dense collagen models and in direct contact with incorporated as-received 45S5 (iv,v,vi), 3-day conditioned 45S5 Bioglass® (vii,viii ix), 14-day conditioned Bioglass® (x, xi,xii), and HAp particles (xiii, xiv, xv) at days 1, 7 and 15 in culture. Cell-seeded neat dense collagen gels were used as Control (i,ii, iii). At day 15 in culture, suspect mineral darkened regions (indicated in white arrows) are observed in the matrix for the cell-only control, and the 45S5 conditions both amorphous and conditioned. The same spots are not observed for the HAp-incorporated gels. Scale bar 400 µm*

SEM micrographs at low magnification (5000x) showed well spread cells on the surface of the DC gels. Higher magnification micrographs (10,000x) allowed the visualization of any mineralized nodule formation or particle deposition on the collagen fibrils as seen in Figure 29A.

At day 23, mineralized nodules were visible in the DC-Control sample. Particle deposition was also observed in DC gels incorporated with as-received 45S5 Bioglass® particles, as well as 3 day- and 14-day conditioned 45S5 Bioglass® particles (DC-45S5, DC- 3D 45S5 and DC-14D 45S5, respectively). The highest level of mineral deposition was observed in 45S5-DC sample. In contrast, there was no particle deposition observed in HAp particle incorporated DC gels.

Von Kossa and Alizarin Red S stainings shown in Figure 30 A&B allowed the identification of the extent of matrix-wide mineralization through reaction with phosphate and complexing with calcium deposition, respectively [120]. A positive von Kossa is dark black, whereas a positive Alizarin Red S stain is orange red in colour. At day 23, acellular dense collagen gels incorporated with as-received 45S5, as well as 3 day- and 14-day conditioned 45S5 particles exhibited high positive von Kossa and Alizarin red stains. DC-Control and DC-HAp also exhibited a deposition but to a lesser extent. Cellular dense collagen gels with incorporated particles also exhibited similar results with the DC-45S5, DC- 3D 45S5 and DC-14D 45S5 samples, with more calcium deposition was exhibited in the cellular DC-Control than the acellular DC-Control. Also, small nodules of phosphate deposition can be observed in the cellular DC-Control samples rather than matrix wide phosphate accumulation. Cellular DC-HAp on the other hand did not show any significant phosphate deposition on the matrix.

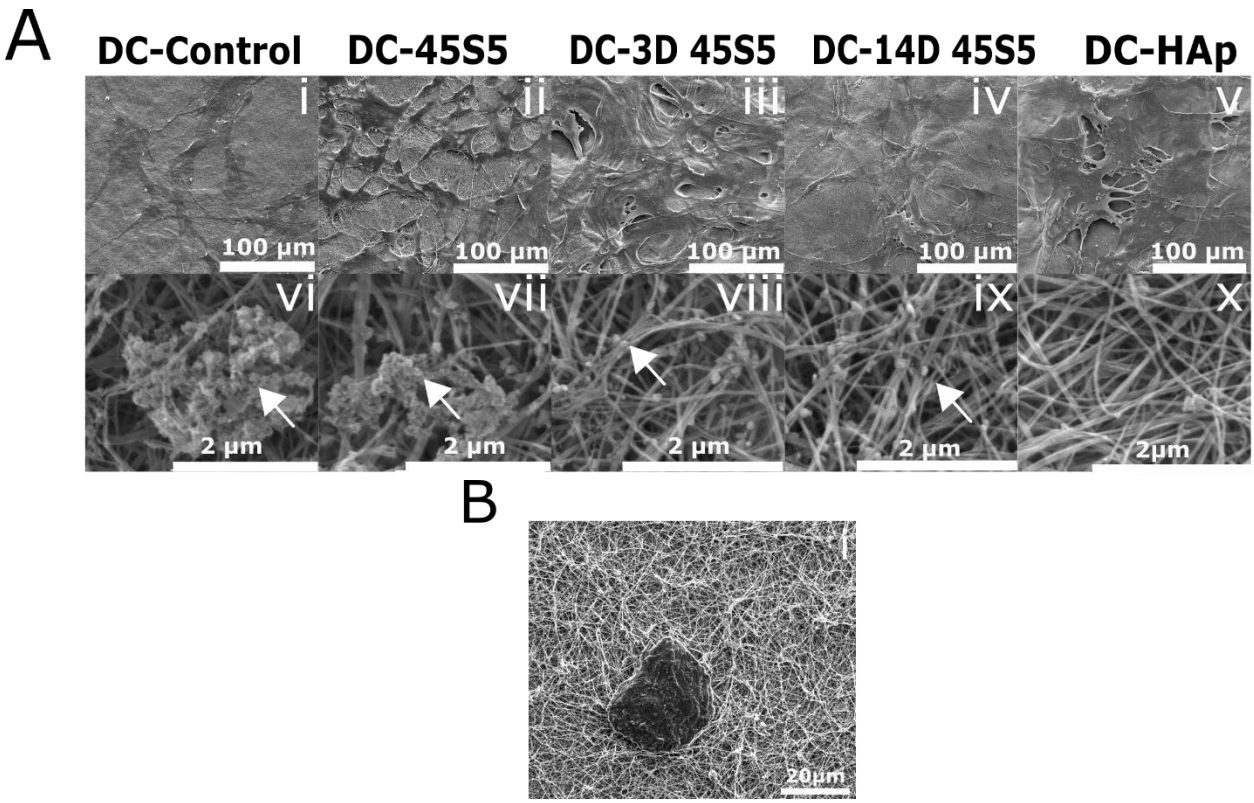

Figure 29: SEM characterization of mineralized dense collagen (DC) gels. *Histology analysis of NIH/3T3 cells seeded in 3D RAFT™ dense collagen gels and in direct contact with incorporated as-received 45S5 Bioglass®, 3-day conditioned 45S5 Bioglass®, 14-day conditioned Bioglass®, and HAp particles at day 23 in culture. Cell-seeded neat dense collagen gels were used as Control. A. SEM micrographs of NIH/3T3 seeded in particle-incorporated DC gels at day 23 in culture. Magnification 5000X (Scale bar = 100 µm for i-v; and subsets (vi-x) 10,000X (Scale bar = 3 µm) at 5kV. Cells well spread over DC surface (i-v); Higher magnification images highlighted mineral deposition on the DC-Control, DC-45S5, DC-3D and DC-14D (vi-ix). No particle deposition on collagen observed in DC-HAp (x). B. 45S5 glass particle captured on the surface of the DC-45S5 matrix at day 23 in culture (scale bar = 20 µm). White arrows indicate areas of mineral deposition*

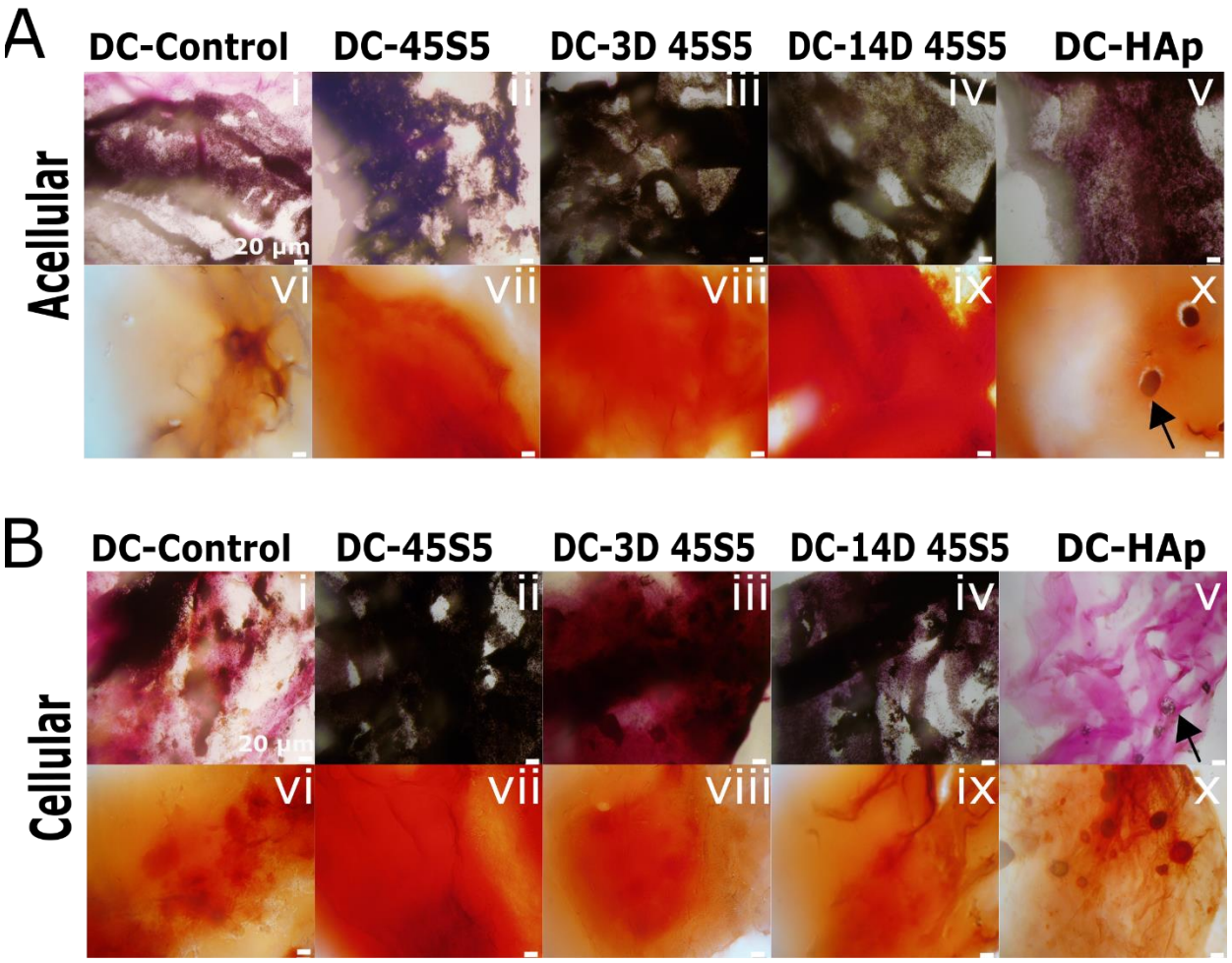

Figure 30: Histology characterization of calcium and phosphate ions deposition in dense collagen (DC) gels. *A. Von Kossa (i-v) & Alizarin Red (vi-x) staining of acellular dense collagen gels with incorporated particles. Higher calcium and phosphate deposition on DC gels observed for amorphous (DC-45S5) and partially mineralized conditions (DC-3D and DC-14D) than DC-Control and DC-HAp. B. Von Kossa (i-v) & Alizarin Red (vi-x) staining of cell seeded DC gels with incorporated particles. Also, higher calcium and phosphate ions deposition on DC gels observed for amorphous (DC-45S5) and partially mineralized conditions (DC-3D and DC-14D) than DC-Control and DC-HAp. DC-HAp did not show a positive Von-Kossa staining except at regions where particle agglomerates were present. HAp particles highlighted using black arrows*

ATR-FTIR spectroscopy was used to confirm the type of mineral deposition in dense collagen. If the mineral deposition led to the formation of HCA, characteristic HCA peaks can be observed as shown in Figure 31. This method also allowed the identification of collagen specific peaks. For example, amide I peak at 1650, amide II (N-H bending, C-N stretching) at the range 1542 cm^{-1} and amide III (N-

H in-plane bending) at 1238 cm^{-1} of collagen [121]. Addition of Bioglass® allowed the development of a weak absorbance peak at 750 cm^{-1} [20] Phosphate peaks at 960 cm^{-1} and 1030 cm^{-1} were observed in the HAp sample. There were no noticeable changes in the FTIR spectra of the cellular and acellular DC-control after 23 days in culture medium when compared to the as-made collagen gel. However, a substantial increase in the intensity and sharpness of the phosphate peak at 1030 cm^{-1} was observed for cellular DC-45S5, DC- 3D 45S5 and DC-14D 45S5 samples. This is not observed in the acellular samples. No change is observed in the cellular and acellular HAp incorporated collagen gels after 23 days of culturing in media.

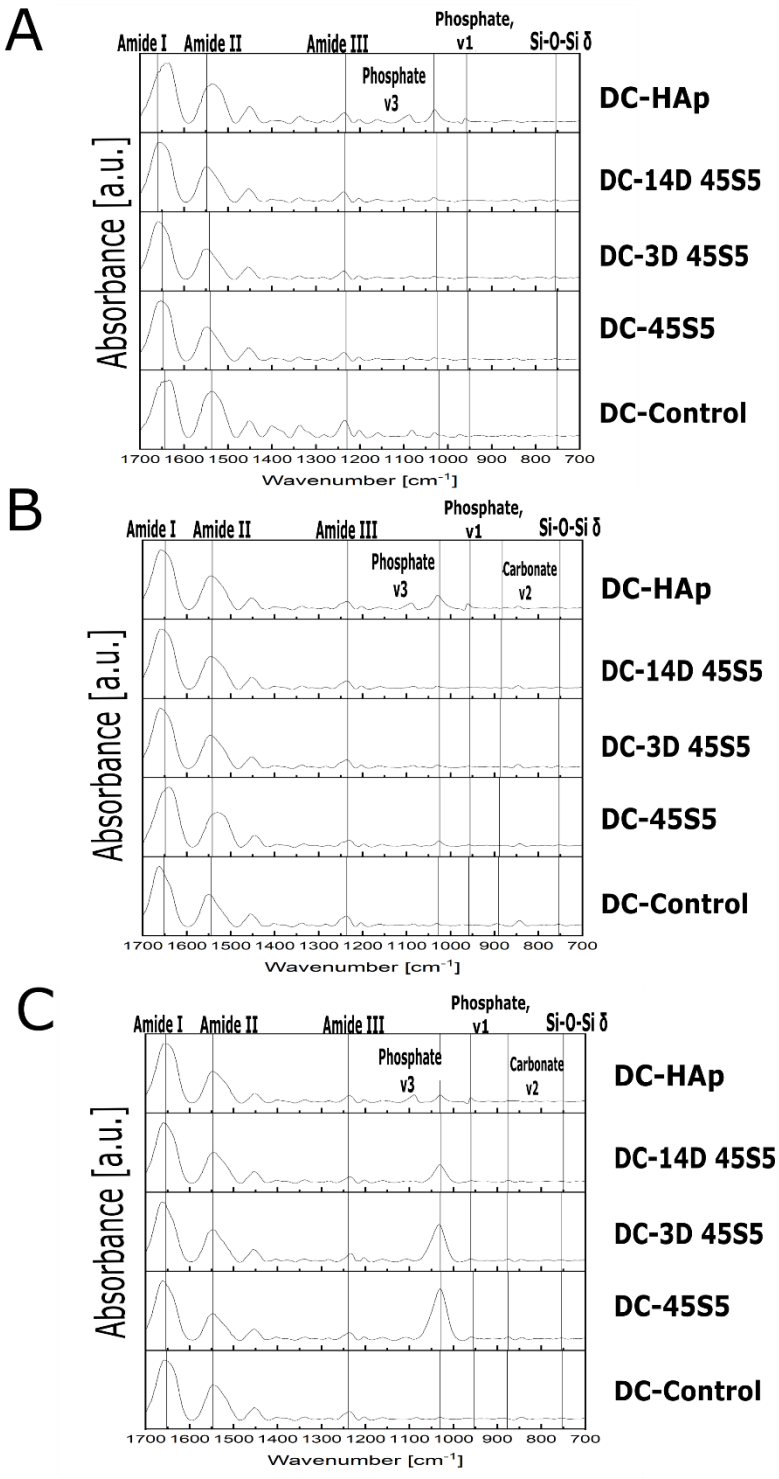

Figure 31: ATR-FTIR spectroscopy of DC gels. *ATR-FTIR spectra of NIH/3T3 cells seeded in 3D RAFT™ dense collagen models and in direct contact with incorporated as-received 45S5, 3-day conditioned 45S5 Bioglass®, 14-day conditioned Bioglass®, and HAp particles at day 23 in culture. Cell-seeded neat dense collagen gels were used as Control. A. ATR-FTIR spectra of the acellular as-made gels. B. ATR-FTIR spectra of the acellular gels after 23 days in culture. C. ATR-FTIR spectra of the NIH/3T3 seeded gels after 23 days in culture. Cell seeding of the DC-45S5-DC, DC-3D and DC-14D appeared to enhance HCA deposition on collagen fibrils when compared to control and HAp. This is indicated through the sharp phosphate v3 peak at 1017 cm $^{-1}$, which is typical of hydroxyapatite*

5.7 Gene expression

5.7.1 Wound healing markers and *Ibsp* gene expression

qRT-PCR analysis shown in Figure 32 undertaken at days 2 and 23 allowed the identification of genes implicated in wound healing, as expressed by NIH/3T3 cells in direct contact with the as-received 45S5 glass, partially mineralized glass and HAp particles within the dense collagen matrix. α-SMA expression at day 2 was significantly ($p<0.05$) higher for HAp versus 3-day partially mineralized and 45S5 glass incorporated gels. Similar levels of α-SMA expression were observed for all conditions at day 23. *Tgfb1* expression showed no significant ($P > 0.05$) changes over time. *Vegf* expression seemed to be upregulated in the cells in direct contact with the as-received 45S5 Bioglass® and 3-day conditioned Bioglass® particles at day 2 compared to day 23 in culture. On the other and, a significantly ($P \leq 0.05$), higher expression of *Vegf* was also observed at day 23 days in culture for the cells in direct contact with the 14-day conditioned Bioglass® particles compared to all other conditions at the same time point. Collagen expression significantly decreased between days 2 and 23 for both the 3-day conditioned Bioglass® particles and HAp particle incorporated gels. Bone sialoprotein gene expression significantly increased for as-received 45S5 and the partially mineralized glass particles with a residual glass phase. This expression level seemed to decrease with an increase in the degree of mineralization of the 45S5 glass, whereas negligible expression of *Ibsp* (encodes bone sialoprotein, (IBSP) was detected for the HAp-in-cooperated DC gel. It was also surprising to observe a significant expression of bone sialoprotein in the cell-only (Control samples) both at days 2 and 23. The expression of a bone marker such as *Ibsp*, the observation of calcium phosphate depositions and the positive von Kossa and Alizarin Red assays in the cell-only dense collagen gel led to further investigate other bone markers such as *Alpl*, and *Sp7* gene expression.

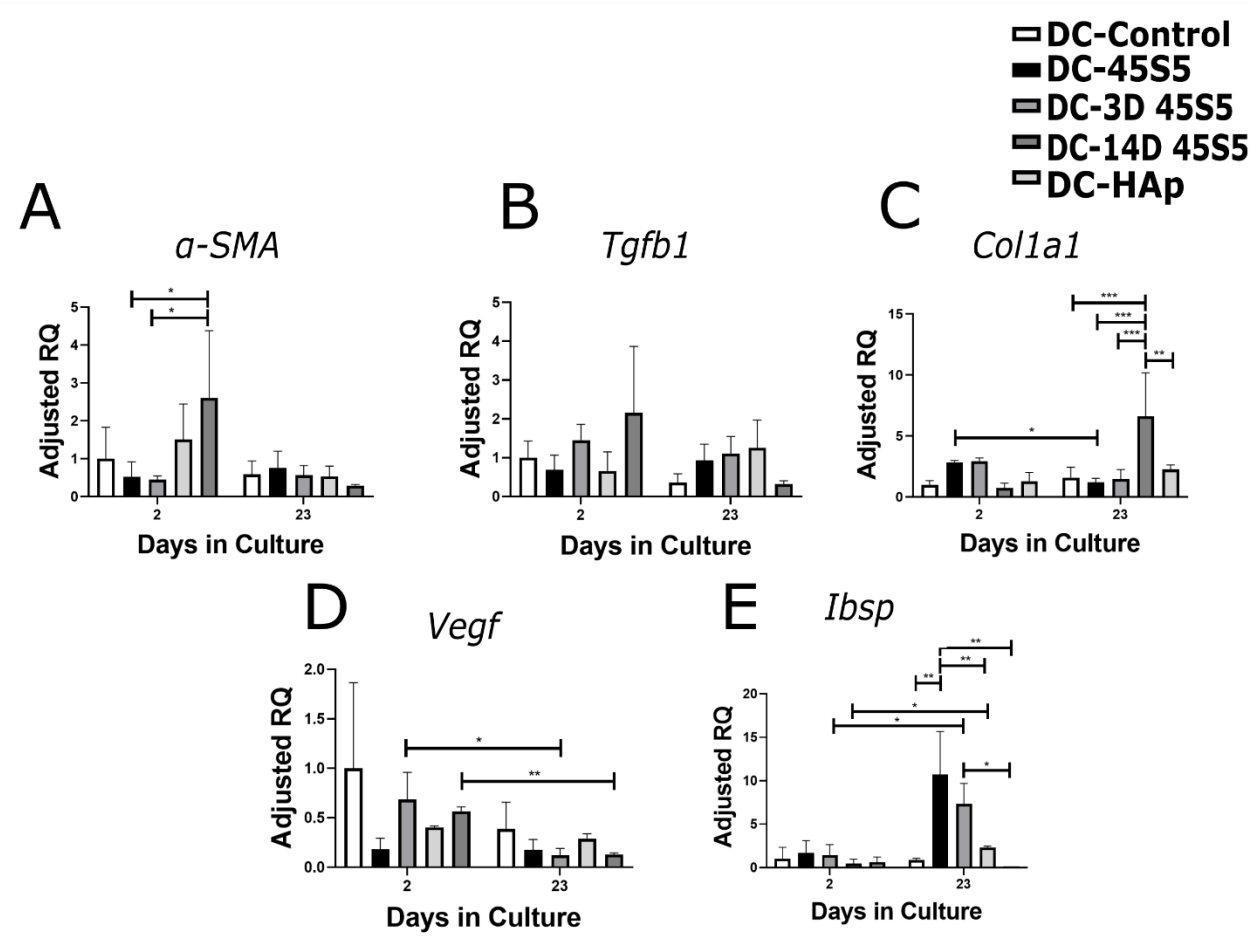

Figure 32: Gene expression of wound healing markers and bone sialoprotein (Ibsp) at days 2 and 23 in culture. *A. α-SMA B. Tgfb1 C. Vegf D. Col1a1 and E. Ibsp. Results indicate an induction in α-SMA levels for the HAp condition at day 2, however at day 23 all conditions reach similar expression levels. Similar Tgfb1 expression levels are observed for all conditions at both time points. 45S5-DC condition shows an induction in Vegf which decreases by day 23. Significantly higher Vegf expression levels are observed for the 14D-DC at day 23 when compared to other conditions. A significant decrease in the expression of Col1a1 is observed for cells seeded in the 14D-DC and HAp-DC between days 2 and 23. A significant upregulation of bone sialoprotein (Ibsp) is observed for the 45S5-DC, 3D-DC and 14-DC conditions. This expression level seems to decrease in the order 45S5-DC>3D-DC>14D-DC. No expression of Ibsp is detected for the HAp-DC condition. Samples examined at (n=3)*

5.7.2 Bone markers gene expression in control sample

qRT-PCR analysis at days 2, 11 and 19 shown in Figure 33 indicated an upregulation in the expressions of *Alp*, *Runx2* and *Sp7* in regular DMEM culture media (10% FBS, 1% P/S), indicating osteoblastic differentiation. Specifically, between days 11 and 19, the level of expression of *Alp* increased significantly. Similarly, the level of expression of *Sp7* increased significantly between days 2 and 11 and days 11 and 19. *Sp7* expression levels increased significantly between days 11 and 19.

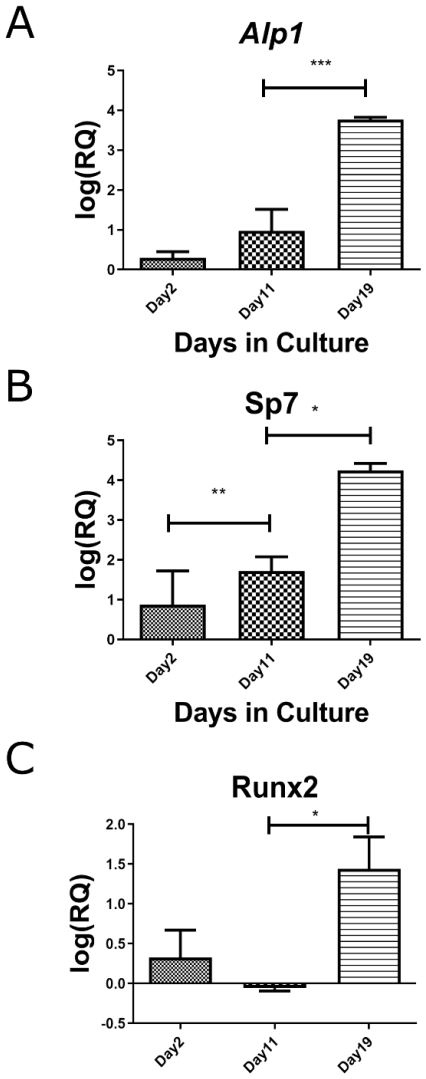

Figure 33: ***Gene expression of osteogenic differentiation markers at days 2, 11 and 23 in culture***. *A. Alpl B. Sp7 C. Runx2. Results indicate a significant induction in in all three markers between days 11 and 19 in culture*

6. Discussion

6.1 Effect of SBF conditioning on particle topography, particle size, surface area, crystallinity and ionic release

SEM images of the 45S5 Bioglass® particles indicated an increase in surface roughness with an increase in conditioning time SBF (Figure 23A v, vi). Similarly, the data given in Table 4 showed a 900-fold increase in specific surface area between the amorphous, as-received 45S5 and 14-day conditioned 45S5 Bioglass® particles. HCA layer is not smooth in nature, instead it usually appears as cauliflower shaped agglomerations when examined using electron microscopy imaging techniques [122]. This can explain the rapid increase in specific surface area. Furthermore, there was no significant ($p > 0.05$) change in the overall particle size between the two time points (days 3 and 14) of conditioning and that of the amorphous 45S5.

Cerruti et al. investigated the early-stage dissolution behaviour of 45S5 Bioglass® in DIW [123]. Within a few minutes, a sharp rise in pH was observed in DIW. By measuring the ICP-OES ionic concentrations, this was attributed to the Na^+/H^+ exchange from the glass/solution, respectively. This spike in Na^+ concentration can be observed in Figure 24B, which then seems to decrease. There were no significant ($p > 0.05$) differences between the concentrations of Na^+ and Ca^{2+} ions released by the 3- and 14-day partially mineralized 45S5 when immersed in DIW for 3h and 72h, as observed in Figures 24B&C. However, the pH decreased slightly within 2 days, which was attributed to uptake of carbonates and phosphate ions which shift the following equilibrium $HCO_3^- \leftrightarrow CO_3^{2-} + H^+$ and $HPO_4^{2-} \leftrightarrow PO_4^{3-} + H^+$ to the product side, increasing the H^+ concentration and subsequently lowering the pH slightly from the initial sharp rise [123]. The reaction between atmospheric CO_2 and Ca^{2+} ions on the surface allows the formation of carbonates in this solution.

Cerruti et al. also presented one of the first ATR-FTIR investigations of Bioglass® dissolution behaviour [123]. Similar findings can be observed here, where the non-bridging oxygen (NBO) peak observed here around 920 cm^{-1} was observed at 930 cm^{-1} and the sharp peak attributed to the newly formed phosphate species on the surface at 1030 cm^{-1} was observed at 1028 cm^{-1}. However, the authors observed a broad band at 1210 cm^{-1} which was attributed to Si-O-Si stretch, which was not observed here. Similar to the reported v_2 carbonate peak at 872 cm^{-1}, a peak

was observed at this wavenumber in the spectra of 3- and 14-day conditioned 45S5 Bioglass® particles. Furthermore, Jones et al. also investigated the dissolution behaviour of bioactive glass at different concentrations in SBF [124]. It was concluded that an optimal concentration of 1.5 mg/mL for 58S was required for HCA deposition, whereas a higher concentration may lead to a preferential calcium carbonate (calcite) deposition due to the higher calcium ion concentration when compared to phosphorous [124]. In this study, a similar concentration of Bioglass®:SBF was used to condition and partially mineralize the as-received 45S5 Bioglass® particles. In the same study, X-ray diffraction was carried out to identify the phases deposited [124]; the peak used to identify HCA formation was approximately at 31º which was also identified at 32º here.

Jones et al. also investigated the ionic release from melt-derived 45S5 in SBF for up to 22 hours using Inductively Coupled Plasma (ICP) [124]. In this study, a similar pattern was observed for the as-received, amorphous 45S5 Bioglass® particles after 3 and 72h. Calcium and silicon concentrations seemed to increase with incubation time while that of phosphorous decreased with time, which was attributed to the scarcity of phosphorous leading to it being the limiting factor to mineralization. However, the concentration of silicon in the solution was found to be dependent on the starting Bioglass® concentration in SBF [124]. To the best of our knowledge, there has been no reports on the ionic dissolution of 45S5 Bioglass® post-conditioning in SBF.

The increase in silicon release in the conditioned 45S5 Bioglass® after 72h in DIW when compared to the initially as-received amorphous 45S5 Bioglass® could be attributed to the breakage of the Si-O-Si network. It can be postulated that conditioning 45S5 Bioglass® in SBF for 3 and 14 days allowed for more Si-O-Si bonds to break, making it potentially easier for further hydrolysis to occur. Another possible explanation is that an equilibrium in silicon concentration is reached during SBF conditioning and when particles are immersed in DIW, the equilibrium is shifted towards forming more silanol groups. In contrast, HAp has a low solubility when compared to bioactive glass, and calcium has a lower solubility than phosphorous [119]. This can explain the relatively lower concentration of calcium after 3 and 72h. During bioactive glass mineralization, a silica rich layer is formed, which is thought to act as a nucleation site for HCA deposition [125]. It has been suggested that the formation of calcium phosphate complexes such as apatite on both glasses and glass-ceramics is due to the formation of a negatively charged surface on residual glass developed by corrosion in aqueous media [23]. HAp has low solubility and resorbability in neutral and alkaline environments and is known to have a lower bioactivity than bioactive glasses [119].

In this study, culture media and DIW have near neutral pH. This can explain the lack of drop in phosphorous concentration after 72h usually associated with calcium phosphate deposition [126]. The higher concentration of phosphorous release at 3h from the conditioned samples compared to 45S5 Bioglass® is likely due to some of the HCA dissolving in DIW when first immersed. Furthermore, the decrease in the release of alkaline species such as Na^+ and Ca^{2+} in the partially mineralized 45S5 Bioglass® is likely due to the initial rapid release of these species in SBF, which are then washed away during sample preparation.

6.2 Effect of amorphous 45S5 Bioglass®, partially mineralized 45S5 Bioglass® and HAp on metabolic activity, proliferation, and viability of seeded fibroblastic cells, in vitro.

Collagen fibrillar density (CFD) is an important parameter in determining if a collagen construct realistically resembles the extracellular environment around a cell type[127]. For example, here the CFD of the collagen matrices post-RAFT™ densification was evaluated to be 13.38 ± 2.19 wt%, Table 5 (Appendix A). RAFT™ densification is similar to plastic compression (PC) densification, with the difference between the two being instead of applying a weight on top of the gels and the casting fluid removal is through a mesh, a hydrophilic absorber is applied atop which densifies the collagen hydrogel through upward fluid removal [127, 128]. PC has been shown to produce dense collagen matrices that can potentially mimic the skin and also allow for particle incorporation [101]. However, RAFT™ absorbers can allow for more reproducibility and is a less "messy" process in general [128].

The original bioactive glass, 45S5 Bioglass®, has been previously investigated on different cell lines (e.g., osteoblasts, stem-cells, endothelial cells and fibroblasts) as well as primary cells [129, 130, 131]. Results have shown that silicon and calcium ion release from 45S5 Bioglass® can lead to cell activation and increase in metabolism [132, 133]. For example, Deb et al. attempted to seed both osteoblasts and human umbilical vein endothelial cells (HUVECs) on Bioglass®-based scaffolds. An increase in proliferation was observed in both co-cultured cell types, whereas this increase in proliferation was not observed on HAp-based scaffolds [134]. In another study, Keshaw et al. investigated the effect of Bioglass®-containing media on growth factor release from

fibroblast cells (CCD-18Co) and the subsequent culturing of endothelial cells in the media. It was found that compared to the control, an increased amount of VEGF and basic fibroblastic growth factor (bFGF) released from fibroblasts which was seen to directly correlate with a higher endothelial cell proliferation [135]. Similarly, Silver et al. reported higher adenosine triphosphate generation in 45S5 Bioglass® -containing culture media [129]. Yu et al. investigated the effect of different ionic dissolution products of 45S5 Bioglass® in media on the proliferation, cell migration, viability, and gene expression of human dermal fibroblasts. It was found that a dilution of 1/128 provided the best proliferation and upregulation of bFGF, VEGF and epidermal growth factor (EGF) gene expression in fibroblasts. Furthermore, a 45S5 Bioglass® activated fibroblast skin tissue graft was investigated in-vivo, which were shown to facilitate enhanced fibroblast migration into the wound bed. This enhancement was attributed to the stimuli provided by Bioglass® ionic release, where a faster wound closure was observed in cell sheets cultured in 1/128 Bioglass® diluted samples [32].

As mentioned above, silicon and calcium ions have been cited as the biggest contributors to the increase in the activity of cells in contact with bioactive glass. Silicon is known to be essential for metabolic activities. For example, Sun et al. cultured osteoblasts in Bioglass® conditioned media, where a shorter osteoblastic growth cycle was recorded, and a higher proliferation were attributed to silicon release [136]. Calcium ion release is also important, which is known to enhance cell proliferation especially in osteoblasts. However, a very high calcium concentration has been reported to be cytotoxic [136].

Most published cell culture work research relating to 45S5 Bioglass® has been carried out using indirect methods. The most common method has been immersing a measured weight of Bioglass® in culture media for a set amount of time and sterile filtering the solution in which the cells are later cultured [132]. While this method allows for the investigation of the ionic release alone, it might not resemble what is happening in a wound site when bioactive glass particles or fibers are used as wound dressings and consequently coming into contact with the cells and collagen ECM. Therefore, direct contact methods such as the one explored in this study, where NIH/3T3 fibroblastic cells are seeded in bioactive glass/ceramic incorporated dense collagen gels, allow for close proximity investigation of cell behaviour and function. This developed model is particularly relevant to mineralizing glasses with potential applications in wound healing because of their ionic release stimuli [10].

However, the concentration of the incorporated bioactive glass can have a drastic effect on the seeded cell metabolic activity. In this study a concentration of 0.8 mg/mL amorphous 45S5 Bioglass® in collagen solution precompression was used. Interestingly, Qazi et al. investigated the effect of 45S5 Bioglass® and 1393 bioactive glasses on human mesenchymal stromal cell (hMSC) proliferation, metabolic activity and cell morphology at different concentrations, in-vitro, either through direct 2D contact, indirectly through retaining the 45S5 Bioglass® in transwell inserts, or encapsulating the hMSCs in alginate beads [138]. Hampering in cell activity with increase in Bioglass concentration in direct contact suggests a dose-dependent response [138]. The results of 3D cultures utilized in that study closely resemble patterns observed in this investigation. The low proliferation of the cells in direct contact with 45S5 Bioglass® up to day 12 (Figure 25) could be due to the high "burst" release of alkaline species (Na^+, Ca^{2+}) from the amorphous glass when exposed to aqueous-based media [15]. This "Burst" in alkaline species is commonly observed when studying the behaviour of cells in direct contact with bioactive glass compositions of high sodium content. For example, Hill et al. reported a reduction in cell metabolic activity with an increase in sodium content in bioactive glasses, which was correlated with a more alkaline medium, in-vitro [142]. More widely, a local pH above the neutral range of 7.2-7.4 has been reported to negatively change the transmembrane electric potential, the Na/K and Ca ion pumps and an altered concertation of metabolic ion protein denaturation can take place, all leading to cell death [148, 149]. This effect could be magnified in direct contact models, at high bioactive glass concentrations, with an increase in sodium concentration and under static cell culture environments – similar to the conditions used in this study [15]. Pre-conditioning the bioactive glass in an aqueous-based medium or solution for a period of time can be a potential remedy to this problem, e.g., in SBF, as used in this investigation [15]. During cell culturing, the media was changed every two days, where the excess alkaline ion released was gradually removed allowing cells to proliferate. Since the partially mineralized glass particles were already preconditioned in SBF for 3 and 14 days, the excess alkaline species was already washed out before their use in direct contact with cells. This can be seen from the ICP-OES data (Figure 24), where the concentrations of sodium and calcium ions significantly ($P < 0.05$) decreased with an increase in conditioning time in SBF. This can explain the similarity in cell metabolic activity when in the presence of partially mineralized glass and HAp particles. Similarly, El Ghannam et al. examined osteoblastic cell activity and spreading on bioactive glass disks post conditioning in Tris-buffer for 20 and 48h.

Although cells were attached to the 20h conditioned disks, a limited amount of ECM components was observed, whereas cells were found to completely cover the 48h conditioned disks and a significant amount of ECM produced [141].

Unlike bioactive glass, HAp is one of the most stable calcium phosphate compounds which is also biocompatible and osteoconductive [107]. Its biocompatibility against fibroblasts has been demonstrated [107,143], which explains the lack of any cytotoxic effect or retarded proliferation when NIH/3T3 cells were cultured with HAp for 21 days. However, HAp lacks solubility and surface reactivity, whereas 45S5 Bioglass® lacks structural integrity, which can be attributed to its high solubility. Partially mineralized 45S5 Bioglass® exhibited higher metabolic activity compared to amorphous 45S5 Bioglass® up to day 12 in culture. A different approach to investigate a partially amorphous, partially crystalline material was investigated by Demirkiran et al., where combinations of sintered Bioglass® and HAp (concentrations of between 0-25 wt% 45S5 Bioglass® in HAp) and were prepared for the purpose of optimizing the osteoconductive/osteoinductive behaviour and strengthening the mechanical properties of the resulting matrix. An increasing trend in bone marrow stromal cell (BMSC) proliferation was observed with an increase in 45S5 Bioglass® percentage up to a maximum at 10 wt%, which then decreased upon further increase in content [144]. This supports the results of this study, by confirming that higher Bioglass® concentrations might not be beneficial in the context of cell metabolic activity and proliferation.

6.3 Effect of amorphous 45S5 Bioglass®, partially mineralized 45S5 Bioglass® and HAp on ECM mineralization in a wound healing context

Ectopic mineralization is defined as the pathological deposition of calcium phosphate complexes in the ECM of the skin, tendons and arterial blood vessels as a result of injury or mineral imbalance [145, 146]. Despite the presence of calcium and phosphate ions in the blood and extracellular fluid being at solubility levels for apatite formation, ectopic mineralization at non-bony sites is avoided through a balance established by the pro-calcific and anti-calcific molecules. Four main categories of molecules play key roles in ectopic mineralization: (i) circulating factors such as calcium and

phosphate ions; (ii) ion transporters and homeostatic enzymes such as alkaline phosphatase; (iii) ECM components such as collagen; (iv) cell signaling molecules such as Runx2 and Bone Morphogenetic Protein 7 (BMP7) [145]. However, certain pathological conditions can result in the calcification of soft tissue, e.g., through diabetes and atherosclerosis [147]. In this investigation, the effect of 45S5 Bioglass®, a known mineralizing glass, which has been investigated for wound healing applications due to its pro-angiogenic properties, on the wound bed properties was explored. Specifically, the extent by which 45S5 Bioglass® can mineralize the collagen ECM was investigated.

Collagen is known to play a promotional role in ectopic mineralization, which when coupled with a high concentration of calcium and phosphate ions, can provide a good environment of mineral deposition [145]. In fact, in 2011, Marelli et al. concluded a more favorable mineralization environment was enabled in collagen gels of higher CFD values. In 2010, Marelli et al. also investigated the mineralizing ability of dense collagen-45S5 Bioglass® hybrid scaffolds in SBF for up to 14 days. Mineralization in the Bioglass® incorporated collagen gels was detected at as early as day 1 in SBF and was seen to increase as a function of Bioglass® to collagen ratio [72]. 45S5 Bioglass®, which is known to be both osteoinductive (can induce osteogenesis), releases silicon, sodium, calcium, and phosphorous associated ions when immersed in a water based medium [132]. Hydrolysis of the Si-O-Si network and condensation of the silanol groups on the glass surface creates a nucleation site for calcium and phosphorous ions released to precipitate into mineral crystals; coupled with the carbonate from the solution, ultimately forming HCA [22,118]. However, a high calcium, high phosphorous environment may also cause a mineral imbalance that may lead to ectopic mineralization if the embedded Bioglass® concentration is not carefully chosen. Furthermore, the effect of this dense collagen environment upon prolonged culturing with and without Bioglass® on the fibroblastic cell phenotype has not been previously explored. Here, it was observed that significant calcium and phosphorous deposition in the amorphous and partially mineralized 45S5 Bioglass® samples in both cellular and acellular gels led to HCA formation, which was more prominent in the cellular samples, as indicated through ATR-FTIR analysis. On the other hand, minimal mineralization was observed with the cellular HAp sample. This could be due to pyrophosphates released by NIH/3T3 in response to HAp presence that could potentially retard mineral deposition [145]. In Figure 28, the increased darkening of the gel aligns with the increase in mineral deposition within the dense collagen

matrix. The lower the residual glass content within the partially pre-mineralized particles, coupled with their lower solubility led to less mineral deposition in the matrix. This can explain the decreasing trend in mineral deposition from 45S5 Bioglass® to HAp. The cell-only control sample may also capture calcium and phosphate from the media leading to complexing and deposition on the collagen fibers [112].

Unlike the osteoinductive Bioglass®, HAp is of low-solubility and a relatively stable calcium phosphate bioceramic with a Ca/P ratio of 1.67 [107]. Interestingly, Filho et al. explored the effect of crystallizing 45S5 Bioglass® (by thermal treatment up to 680^{o}C) on its ability to mineralize on SBF. It was concluded there was no effect of thermal treatment on the 45S5 Bioglass® mineralization potential. However, the duration required for the onset of mineralization to be detected increased from 10 h for the amorphous 45S5 Bioglass® to 22 h for the 100% crystallized ceramic [114]. The findings of this study align with those here, in that a soluble amorphous glass phase accelerates mineral deposition.

6.4 45S5 Bioglass® induces the gene expression of bone sialoprotein (*Ibsp*) in NIH/3T3 fibroblast cell line

Important wound healing markers were investigated such as *α-SMA, Col1a1, Tfgb1 and Vegf*. During the proliferative and remodelling stages of wound healing, fibroblastic cells are triggered by *Tfgb1* levels to undergo fibroblastic differentiation [62,66]. Myofibroblasts are responsible for wound contraction by producing collagen. Increasing population of myofibroblasts and an increase in collagen release could be reflected in an induction of α-SMA levels and *Col1a1* levels, respectively [62,66,68]. *Vegf* is an important angiogenesis marker. Wound healing in most stages require good blood supply [62].

While no significant ($p > 0.05$) changes in *Tfgb1*expression levels were observed, α-SMA expression levels were significantly higher at day 2 in HAp compared to the amorphous and 3-day partially mineralized glass. However, at day 23, all conditions seem to have similar α-SMA levels. This initial α-SMA induction in the HAp condition and spreading detected by Calcein-AM staining compared to amorphous glass could be related to the retardation of proliferation due to the direct contact between NIH/3T3 cells and amorphous glass. *Col1a1* expression dropped significantly ($p<0.05$) for

both 3 day partially mineralized glass and HAp conditions. *Vegf* upregulation for the as-received 45S5 Bioglass® and the 3-day partially mineralized glass has been previously reported [11, 135, 149]. For instance, one of the first reports on this valuable potential of 45S5 Bioglass® was published by Day et al. in 2005, where CCD18Co human fibroblasts experienced an induction of *Vegf* after being cultured on 45S5 Bioglass® coated surfaces [135].

Compared to stem cells, the potential osteoinductive properties of bioactive glass in direct contact with fibroblastic cells have not been extensively studied. The major finding here is the induction of bone sialoprotein in fibroblasts when seeded in dense collagen gels and in direct contact with 45S5 Bioglass® particles. This induction level seems to decrease significantly the longer the 45S5 Bioglass® was conditioned in SBF before incorporation into the collagen gels. This could be related to the ionic release from the glass particles. Amorphous Bioglass® has a higher solubility than HAp with the ability to release ions such as silicon and calcium, which have been shown to enhance ECM mineralization [72]. The local increase in pH from the sodium ion release might also support mineralization and the release of osteogenic markers [15, 150]. This has been explored before but only with stem cells. For example, Ojansivu et al. reported an induction ALP activity, and of certain osteogenic marker genes such as RUNX2a and Osx upon culturing human adipose stem cells (hASCs) on silica-based bioactive glass without the addition of osteogenic media [151]. In contrast, in this study, there was no expression of bone sialoprotein detected in cells cultured with synthetic HAp (Figure 32), which is not known to be osteoinductive [107]. In 2009, Demirkiran et al. reported a direct correlation between the 45S5 Bioglass® content in a Bioglass®45S5-HAp sintered matrix and the extent of ALP activity activity by bone marrow stromal cell (BMSC). In the same study, the lowest ALP activity was observed in HAp only samples [135].

6.5 Induction of osteogenic differentiation markers expression in NIH/3T3 cells cultured in dense collagen matrix.

Collagen is known as an ECM mineralization promoter in the presence of calcium and phosphate ions at solubility level sufficient for apatite formation, which can come form the cell culture media [145]. In 2015, Nishimura et al. investigated the osteogenic differentiation potential of human mesenchymal stem cells (hMSCs) cultured within collagen I sheets in the presence of osteogenic

differentiation media under both static and dynamic flow conditions. After two weeks, in both static and dynamic flow conditions a significantly higher ALP activity was detected in samples cultured in osteogenic media compared to growth media [152]. Similarly, in another study, human periodontal ligament fibroblast (hPDLF) were seeded in three-dimensional collagen type 1 with osteogenic media. Osteopontin (*Spp1*) , *Runx2* gene expression was significantly higher on 3D cultures compared with control surface and *Alp1* and *Col1a1* gene expression were significantly higher in 3D collagen compared to 2D cultures [153]. It is worth noting that both studies were carried out in the presence of osteogenic media. However, in this research work, no osteogenic media was added and the gene expression levels of key osteogenic markers (*Alpl, sp7 amd Runx2*) were significantly upregulated upon prolonged culturing. The presence of fibroblastic cells in dense collagen could be activating certain mineralization pathways.

7. Conclusions

- Conditioning 45S5 Bioglass® particles in SBF allowed the formation of an HCA layer, significantly reducing the release of sodium and calcium ions in DIW and increasing the particle surface area 900-fold after 14 days of conditioning.
- Seeding NIH/3T3 cells in a 3D RAFT^{TM} dense collagen gels allowed for direct contact investigation with incorporated glass/ceramic particles.
- Proliferation, metabolic activity, and viability of fibroblast NIH/3T3 cells seeded in 3D RAFT^{TM} dense collagen gels was initially hindered by incorporating 0.8 mg/mL amorphous 45S5 Bioglass®.
- 45S5 Bioglass® incorporation resulted in elevated *Vegf* gene expression at early time points, which decreased with time in culture.
- Dense collagen gels incorporated with amorphous 45S5 Bioglass® experienced the highest level of mineral deposition and its seeded NIH/3T3 cells experienced the highest induction in *Ibsp* expression in culture.
- Mineralization deposition and *Ibsp* expression decreased with the increase in pre-conditioning time of 45S5 Bioglass® in SBF before incorporation in dense collagen gels.
- The ability of NIH/3T3 cell lines to subscribe to an osteogenic pathway upon prolonged culturing in dense collagen even in the absence of osteogenic media was also examined. Cells seeded in dense collagen with 13.4% collagen fibrillar density (CFD) without glass/ceramic particles showed a significant upregulation in specific osteogenic markers, *Alp1, sp7, and Runx2* and the formation of osteoid like structures as examined under SEM, and verified by von-Kossa van Gieson staining.
- The results indicate a retardation effect of 45S5 Bioglass® on proliferation of NIH/3T3 cells in a dense collagen model. It also indicates the potential of ectopic mineralization and upregulation of osteogenic markers such as *Ibsp* in the wound bed.

8. Future Directions

In this work, a concentration of 0.8 mg/mL of glass/ceramic in collagen solution pre-compression was used. Experimenting with different concentrations of 45S5 Bioglass® particles in the dense collagen matrix might yield a different proliferation profile, which can help in reaching an optimum concentration. Similarly, different densification levels of collagen by applying RAFT^{TM} absorber for different amounts of time may be investigated to understand the effect of collagen density on the mineralization potential both on a cellular level as well as collagen ability to attract mineral deposition in a wound healing context. This work can also be extended in-vivo. For example, investigating gene expression profile of fibroblasts and epithelial cells in direct contact with different concentrations of 45S5 Bioglass® at different time points of application. A pyrophosphate assay can also be utilized to measure the concentration released from cells to confirm the theory behind lack of mineralization of HAp condition.

9. References

[1] L. Hench and I. Thompson, "Twenty-first century challenges for biomaterials", Journal of The Royal Society Interface, vol. 7, no. 4, 2010.

[2] N. Huebsch and D. J. Mooney, “Inspiration and application in the evolution of biomaterials,” Nature, vol. 462, no. 7272, pp. 426–432, 2009.

[3] L. L. Hench, “The story of Bioglass®,” Journal of Materials Science: Materials in Medicine, vol. 17, no. 11, pp. 967–978, 2006.

[4] J. Jones, D. Brauer, L. Hupa and D. Greenspan, "Bioglass and Bioactive Glasses and Their Impact on Healthcare", International Journal of Applied Glass Science, vol. 7, no. 4, pp. 423-434, 2016.

[5] L. Hench, "Biomaterials: a forecast for the future", Biomaterials, vol. 19, no. 16, pp. 1419-1423, 1998.

[6] M. N. Rahman, D. E. Day, B. S. Ball, "Bioactive glass in tissue engineering", Acta Biomaterialia, vol. 7, no. 6, pp. 2355-2373, 2011.

[7] W. C. Lepry and S. N. Nazhat, “Highly Bioactive Sol-Gel-Derived Borate Glasses,” Chemistry of Materials, vol. 27, no. 13, pp. 4821–4831, 2015.

[8] E. A. A. Neel, D. M. Pickup, S. P. Valappil, R. J. Newport, and J. C. Knowles, “Bioactive functional materials: a perspective on phosphate-based glasses,” J. Mater. Chem., vol. 19, no. 6, pp. 690–701, 2009.

[9] L. Weng, S. K. Boda, M. J. Teusink, F. D. Shuler, X. Li, and J. Xie, “Binary Doping of Strontium and Copper Enhancing Osteogenesis and Angiogenesis of Bioactive Glass Nanofibers while Suppressing Osteoclast Activity,” ACS Applied Materials & Interfaces, vol. 9, no. 29, pp. 24484–24496, 2017.

[10] S. Naseri, W. C. Lepry, V. B. Maisuria, N. Tufenkji, and S. N. Nazhat, “Development and characterization of silver-doped sol-gel-derived borate glasses with anti-bacterial activity,” Journal of Non-Crystalline Solids, vol. 505, pp. 438–446, 2019.

[11] R. M. Day, “Bioactive Glass Stimulates the Secretion of Angiogenic Growth Factors and Angiogenesis in Vitro,” Tissue Engineering, vol. 11, no. 5-6, pp. 768–777, 2005.

[12] "Technology", ETS Wound Care, 2020. [Online]. Available: http://www.etswoundcare.com/technology.html.

[13] T. Kokubo and H. Takadama, “How useful is SBF in predicting in vivo bone bioactivity?,” Biomaterials, vol. 27, no. 15, pp. 2907–2915, 2006.

[14] S. Naseri, W. C. Lepry, and S. N. Nazhat, “Bioactive glasses in wound healing: hope or hype?,” Journal of Materials Chemistry B, vol. 5, no. 31, pp. 6167–6174, 2017.

[15] F. E. Ciraldo, E. Boccardi, V. Melli, F. Westhauser, and A. R. Boccaccini, “Tackling bioactive glass excessive in vitro bioreactivity: Preconditioning approaches for cell culture tests,” Acta Biomaterialia, vol. 75, pp. 3–10, 2018.

[16] J. W. Frame and C. L. Brady, “The versatility of hydroxyapatite blocks in maxillofacial surgery,” British Journal of Oral and Maxillofacial Surgery, vol. 25, no. 6, pp. 452–464, 1987.

[17] B. P., “Wound healing and the role of fibroblasts,” Journal of Wound Care, vol. 22, no. 8, pp. 407–412, 2013.

[18] J. Kanta, “Collagen matrix as a tool in studying fibroblastic cell behavior,” Cell Adhesion & Migration, vol. 9, no. 4, pp. 308–316, Mar. 2015.

[19] R. Wood, "The Physics of Amorphous Solids", Physics Bulletin, vol. 35, no. 7, pp. 276-276, 1984.

[20] H. Scholze, "Glass: nature, structure, and properties", Choice Reviews Online, vol. 29, no. 05, pp. 29-2717-29-2717, 1992.

[21] R. Wood, "Glasses for photonics", Optics and Lasers in Engineering, vol. 33, no. 5, pp. 383-384, 2000.

[22] L. Hench, "The story of Bioglass®", Journal of Materials Science: Materials in Medicine, vol. 17, no. 11, pp. 967-978, 2006.

[23] E. Fiume, J. Barberi, E. Verne, "Bioactive Glasses: From Parent 45S5 Composition to Scaffold-Assisted Tissue-Healing Therapies", Journal of Functional Biomaterials, vol. 9, no. 1, p. 24, 2018.

[24] D. Brauer, "Bioactive Glasses-Structure and Properties", Angewandte Chemie International Edition, vol. 54, no. 14, pp. 4160-4181, 2015.

[25] P. McMillan, "Structural studies of silicate glasses and melts—applications and limitations of Raman spectroscopy", American Mineralogist, vol. 69, no. 7-8, pp. 622–644, 1984.

[26] J. Shelby, Introduction to glass science and technology, Royal Society of Chemistry, 2005.

[27] A. K. Yadav and P. Singh, "A review of the structures of oxide glasses by Raman spectroscopy," RSC Advances, vol. 5, no. 83, pp. 67583–67609, 2015.

[28] L. Hench, R. Splinter, W. Allen and T. Greenlee, "Bonding mechanisms at the interface of ceramic prosthetic materials", Journal of Biomedical Materials Research, vol. 5, no. 6, pp. 117-141, 1971.

[29] R. Watters, R. Brown and D. Day, "Angiogenic effect of bioactive borate glass microfibers and beads in the hairless mouse", Biomedical glasses, vol. 1, no. 1, 2015.

[30] K. Schuhladen, X. Wang, L. Hupa, and A. R. Boccaccini, "Dissolution of borate and borosilicate bioactive glasses and the influence of ion (Zn, Cu) doping in different solutions," Journal of Non-Crystalline Solids, vol. 502, pp. 22–34, 2018.

[31] A. Balamurugan, G. Balossier, D. Laurent-Maquin, S. Pina, A. Rebelo, J. Faure, and J. Ferreira, "An in vitro biological and anti-bacterial study on a sol–gel derived silver-incorporated bioglass system," Dental Materials, vol. 24, no. 10, pp. 1343–1351, 2008.

[32] H. Li, J. He, H. Yu, C. R. Green, and J. Chang, "Bioglass promotes wound healing by affecting gap junction connexin 43 mediated endothelial cell behavior," Biomaterials, vol. 84, pp. 64–75, 2016.

[33] A. Vale, P. Pereira, A. Barbosa, E. Torrado, and N. Alves, "Optimization of silver-containing bioglass nanoparticles envisaging biomedical applications," Materials Science and Engineering: C, vol. 94, pp. 161–168, 2019.

[34] X. Dong, J. Chang, and H. Li, “Bioglass promotes wound healing through modulating the paracrine effects between macrophages and repairing cells,” Journal of Materials Chemistry B, vol. 5, no. 26, pp. 5240–5250, 2017.

[35] J. Shelby,” Introduction to glass science and technology”, Royal Society of Chemistry, pp. 249–261, 2005.

[36] J. Biscoe and B. Warren, "X-ray diffraction study of soda-boric oxide glass *", Journal of the American Ceramic Society, vol. 21, no. 8, pp. 287-293, 1938.

[37] W. Huang, D. Day, K. Kittiratanapiboon and M. Rahaman, "Kinetics and mechanisms of the conversion of silicate (45S5), borate, and borosilicate glasses to hydroxyapatite in dilute phosphate solutions", Journal of Materials Science: Materials in Medicine, vol. 17, no. 7, pp. 583-596, 2006.

[38] R. Brown, M. Rahaman and A. Dwilewicz, "Effect of borate glass composition on its conversion to hydroxyapatite and on the proliferation of MC3T3-E1 cells", Journal of Biomedical Materials Research Part A, vol. 88, no. 2, pp. 392-400, 2009.

[39] M. Laczka, K. Cholewa-Kowalska, A. Laczka-Osyczka, M. Tworzydlo and B. Turyna, "Gel-derived materials of a CaO-P2O5-SiO2 system modified by boron, sodium, magnesium, aluminum, and fluorine compounds", Journal of Biomedical Materials Research, vol. 52, no. 4, pp. 601-612, 2000.

[40] S. Kalmodia, A. R. Molla, and B. Basu, “In vitro cellular adhesion and antimicrobial property of SiO2–MgO–Al2O3–K2O–B2O3–F glass ceramic,” Journal of Materials Science: Materials in Medicine, vol. 21, no. 4, pp. 1297–1309, 2009. Med. 21, 1297–1309, 2010.

[41] P. Wray, Wound healing an update on Mo-Sci’s novel borate glass fibres, Am. Ceram. Soc. Bull. 92, 33–35, 2013.

[42] S. Zhao, L. Li, H. Wang, Y. Zhang, X. Cheng, N. Zhou, M. N. Rahaman, Z. Liu, W. Huang, and C. Zhang, “Wound dressings composed of copper-doped borate bioactive glass microfibers stimulate angiogenesis and heal full-thickness skin defects in a rodent model,” Biomaterials, vol. 53, pp. 379–391, 2015.

[43] Q. Yang, S. Chen, H. Shi, H. Xiao and Y. Ma, "In vitro study of improved wound-healing effect of bioactive borate-based glass nano-/micro-fibers", Materials Science and Engineering: C, vol. 55, pp. 105-117, 2015.

[44] S. Jung, "Borate based bioactive glass scaffolds for hard and soft tissue engineering", Ph.D, Missouri University of Science and Technology, 2010.

[45] S. Naseri, "Highly Reactive Silver Doped Sol-Gel-Derived Borate Glasses for Wound Healing Applications", Ph.D, McGill University, 2018.

[46] E. A. A. Neel, V. Salih, and J. Knowles, “Phosphate-Based Glasses,” Comprehensive Biomaterials, pp. 285–297, 2011.

[47] RJ. Kirkpatrick, RK. Brow, Solid State Nuclear Magnetic Resonance, 1995.

[48] I. Ahmed, M. Lewis, I. Olsen, and J. Knowles, “Phosphate glasses for tissue engineering: Part 1. Processing and characterisation of a ternary-based P2O5–CaO–Na2O glass system,” Biomaterials, vol. 25, no. 3, pp. 491–499, 2004.

[49] K. Skelton, J. Glenn, S. Clarke, G. Georgiou, S. Valappil, J. Knowles, S. Nazhat, and G. Jordan, “Effect of ternary phosphate-based glass compositions on osteoblast and osteoblast-like proliferation, differentiation and death in vitro,” Acta Biomaterialia, vol. 3, no. 4, pp. 563–572, 2007.

[50] J. C. Knowles, “Phosphate based glasses for biomedical applications,” Journal of Materials Chemistry, vol. 13, no. 10, p. 2395, 2003.

[51] H. Gao, T. Tan, and D. Wang, “Effect of composition on the release kinetics of phosphate controlled release glasses in aqueous medium,” Journal of Controlled Release, vol. 96, no. 1, pp. 21–28, 2004.

[52] E. A. A. Neel, D. M. Pickup, S. P. Valappil, R. J. Newport, and J. C. Knowles, “Bioactive functional materials: a perspective on phosphate-based glasses,” J. Mater. Chem., vol. 19, no. 6, pp. 690–701, 2009.

[53] G. Kaur, G. Pickrell, N. Sriranganathan, V. Kumar, and D. Homa, “Review and the state of the art: Sol-gel and melt quenched bioactive glasses for tissue engineering,” Journal of Biomedical Materials Research Part B: Applied Biomaterials, vol. 104, no. 6, pp. 1248–1275, 2015.

[54] W. Lepry, S. Smith and S.N. Nazhat, "Effect of sodium on bioactive sol-gel-derived borate glasses", Journal of Non-Crystalline Solids, vol. 500, pp. 141-148, 2018

[55] D. Carta, J.C Knowles, P. Guerry, M.E. Smith., “Sol-gel and melt-quenched borophosphate glasses for biomedical applications”, Handbook on Borates: Performance, Environmental Health and Safety, Nova Science Publishing, pp. 409-419, 2010.

[56] R.L. Ciceo, D.-L. Trandafir, T. Radu, O. Ponta, V. Simon, ‘’Synthesis, characterisation and in vitro evaluation of sol–gel derived SiO2–P2O5–CaO –B2O3 bioactive system’’, Ceram. Int., vol. 40, pp. 9517-9524, 2014.

[57] H.C. Li, D.G. Wang, J.H. Hu, C.Z. Chen, ‘’Effect of the partial substitution of K2O, MgO, B2O3 for CaO on crystallization, structure and properties of Na2O–CaO–SiO2–P2O5 system glass-ceramics’’ Mater. Lett., vol. 106, pp. 373-376, 2013.

[58] R. Ota, N. Asagi, J. Fukunaga, N. Yoshida, T. Fujii ‘’Variation of the gel region with heat-treatment in the B2O3-Na2O-TiO2 system compared with the melt-quenched glass region’’ J. Mater. Sci., vol. 25, pp. 4259-4265, 1990.

[59] X. Lei, B. Yu, H.-L. Cong, C. Tian, Y.-Z. Wang, Q.-B. Wang, and C.-K. Liu, “Synthesis of Monodisperse Silica Microspheres by a Modified Stöber Method,” Integrated Ferroelectrics, vol. 154, no. 1, pp. 142–146, 2014.

[60] W. C. Lepry, S. Smith, and S. N. Nazhat, “Effect of sodium on bioactive sol-gel-derived borate glasses,” Journal of Non-Crystalline Solids, vol. 500, pp. 141–148, 2018.

[61] K. Rieger, N. Birch and J. Schiffman, "Designing electrospun nanofiber mats to promote wound healing – a review", Journal of Materials Chemistry B, vol. 1, no. 36, p. 4531, 2013..

[62] S. Kanji and H. Das, "Advances of Stem Cell Therapeutics in Cutaneous Wound Healing and Regeneration", Mediators of Inflammation, vol. 2017, pp. 1-14, 2017.

[63] L. Braiman-Wiksman, I. Solomonik, R. Spira and T. Tennenbaum, "Novel Insights into Wound Healing Sequence of Events", Toxicologic Pathology, vol. 35, no. 6, pp. 767-779, 2007.

[64] P. Anima, "A Review on Wound Healing", Open Access Journal of Pharmaceutical Research, vol. 1, no. 4, 2017.

[65] R. S. Kirsner and W. H. Eaglstein, “The Wound Healing Process,” Dermatologic Clinics, vol. 11, no. 4, pp. 629–640, 1993.

[66] K. A. Rieger, N. P. Birch, and J. D. Schiffman, “Designing electrospun nanofiber mats to promote wound healing – a review,” Journal of Materials Chemistry B, vol. 1, no. 36, p. 4531, 2013.

[67] T. Velnar, T. Bailey, and V. Smrkolj, “The Wound Healing Process: An Overview of the Cellular and Molecular Mechanisms,” Journal of International Medical Research, vol. 37, no. 5, pp. 1528–1542, 2009.

[68] R. A. Clark, “Regulation of Fibroplasia in Cutaneous Wound Repair,” The American Journal of the Medical Sciences, vol. 306, no. 1, pp. 42–48, 1993.

[69] J. L. Andresen and N. Ehlers, “Chemotaxis of human keratocytes is increased by platelet-derived growth factor-BB, epidermal growth factor, transforming growth factor-alpha, acidic fibroblast growth factor, insulin-like growth factor-I, and transforming growth factor-beta,” Current Eye Research, vol. 17, no. 1, pp. 79–87, 1998.

[70] M. C. Robson, D. L. Steed, and M. G. Franz, “Wound healing: Biologic features and approaches to maximize healing trajectories,” Current Problems in Surgery, vol. 38, no. 2, 2001.

[71] V. V. Artym and K. Matsumoto, “Imaging Cells in Three-Dimensional Collagen Matrix,” Current Protocols in Cell Biology, vol. 48, no. 1, 2010.

[72] B. Marelli, C. E. Ghezzi, J. E. Barralet, A. R. Boccaccini, and S. N. Nazhat, “Three-Dimensional Mineralization of Dense Nanofibrillar Collagen−Bioglass Hybrid Scaffolds,” Biomacromolecules, vol. 11, no. 6, pp. 1470–1479, 2010.

[73] H. Brem and M. Tomic-Canic, “Cellular and molecular basis of wound healing in diabetes,” Journal of Clinical Investigation, vol. 117, no. 5, pp. 1219–1222, Jan. 2007.

[74] D. Mathieu, Handbook on hyperbaric medicine. Dordrecht: Springer, 2010.

[75] K. T. Keylock, V. J. Vieira, M. A. Wallig, L. A. Dipietro, M. Schrementi, and J. A. Woods, “Exercise accelerates cutaneous wound healing and decreases wound inflammation in aged mice,” American Journal of Physiology-Regulatory, Integrative and Comparative Physiology, vol. 294, no. 1, 2008.

[76] K. Woo, E. A. Ayello, and R. G. Sibbald, “The Edge Effect,” Advances in Skin & Wound Care, vol. 20, no. 2, pp. 118–119, 2007.

[77] F. Gottrup, "A specialized wound-healing center concept: importance of a multidisciplinary department structure and surgical treatment facilities in the treatment of chronic wounds", The American Journal of Surgery, vol. 187, no. 5, pp. S38-S43, 2004.

[78] C. Sen, G. Gordillo and S. Roy, "Human skin wounds: A major and snowballing threat to public health and the economy", Wound Repair and Regeneration, vol. 17, no. 6, pp. 763-771, 2009.

[79] R. Frykberg and J. Banks, "Challenges in the Treatment of Chronic Wounds", Advances in Wound Care, vol. 4, no. 9, pp. 560-582, 2015.

[80] P. Ackermann and D. Hart, "Influence of Comorbidities: Neuropathy, Vasculopathy, and Diabetes on Healing Response Quality", Advances in Wound Care, vol. 2, no. 8, pp. 410-421, 2013.

[81] E. Everett and N. Mathioudakis, "Update on management of diabetic foot ulcers", Annals of the New York Academy of Sciences, vol. 1411, no. 1, pp. 153-165, 2018.

[82] R. Ikem, I. Ikem, O. Adebayo and D. Soyoye, "An assessment of peripheral vascular disease in patients with diabetic foot ulcer", The Foot, vol. 20, no. 4, pp. 114-117, 2010.

[83] J. Walsh, O. Hoffstad, M. Sullivan and D. Margolis, "Association of diabetic foot ulcer and death in a population-based cohort from the United Kingdom", Diabetic Medicine, vol. 33, no. 11, pp. 1493-1498, 2016.

[84] C. Naves, "The Diabetic Foot: A Historical Overview and Gaps in Current Treatment", Advances in Wound Care, vol. 5, no. 5, pp. 191-197, 2016.

[85] B. Lipsky, A. Berendt and P. Cornia, "2012 Infectious Diseases Society of America Clinical Practice Guideline for the Diagnosis and Treatment of Diabetic Foot Infections", Clinical Infectious Diseases, vol. 54, no. 12, pp. e132-e173, 2012.

[86] S. Bus, "The Role of Pressure Offloading on Diabetic Foot Ulcer Healing and Prevention of Recurrence", Plastic and Reconstructive Surgery, vol. 138, pp. 179S-187S, 2016.

[87] Z. Liu, J. Dumville and R. Hinchliffe, "Negative pressure wound therapy for treating foot wounds in people with diabetes mellitus", Cochrane Database of Systematic Reviews, 2018.

[88] J. Dumville, S. O'Meara, S. Deshpande and K. Speak, "Hydrogel dressings for healing diabetic foot ulcers", Cochrane Database of Systematic Reviews, 2013.

[89] F. Game, J. Apelqvist and C. Attinger, "Effectiveness of interventions to enhance healing of chronic ulcers of the foot in diabetes: a systematic review", Diabetes/Metabolism Research and Reviews, vol. 32, pp. 154-168, 2016.

[90] S. Guo and L. Dipietro, “Factors Affecting Wound Healing,” Journal of Dental Research, vol. 89, no. 3, pp. 219–229, 2010.

[91] H. Galkowska, W. L. Olszewski, U. Wojewodzka, G. Rosinski, and W. Karnafel, “Neurogenic Factors in the Impaired Healing of Diabetic Foot Ulcers,” Journal of Surgical Research, vol. 134, no. 2, pp. 252–258, 2006.

[92] T. Rozario and D. DeSimone, "The extracellular matrix in development and morphogenesis: A dynamic view", Developmental Biology, vol. 341, no. 1, pp. 126-140, 2010.

[93] C. Frantz, K. Stewart and V. Weaver, "The extracellular matrix at a glance", Journal of Cell Science, vol. 123, no. 24, pp. 4195-4200, 2010.

[94] P. Mogha, A. Srivastava and S. Kumar, "Hydrogel scaffold with substrate elasticity mimicking physiological-niche promotes proliferation of functional keratinocytes", RSC Advances, vol. 9, no. 18, pp. 10174-10183, 2019.

[95] C. Stähli, M. James-Bhasin and S. N. Nazhat, "Three-dimensional endothelial cell morphogenesis under controlled ion release from copper-doped phosphate glass", Journal of Controlled Release, vol. 200, pp. 222-232, 2015.

[96] R. Ehrmann and G. Gey, "The Growth of Cells on a Transparent Gel of Reconstituted Rat-Tail Collagen", JNCI: Journal of the National Cancer Institute, 1956.

[97] T. Elsdale and J. Bard, "Collagen substrata for studies on cell behavior", The Journal of Cell Biology, vol. 54, no. 3, pp. 626-637, 1972.

[98] E. Bell, B. Ivarsson, and C. Merrill, "Production of a tissue-like structure by contraction of collagen lattices by human fibroblasts of different proliferative potential in vitro.," Proceedings of the National Academy of Sciences, vol. 76, no. 3, pp. 1274–1278, 1979.

[99] S. Rhee, "Fibroblasts in three dimensional matrices: cell migration and matrix remodeling," Experimental and Molecular Medicine, vol. 41, no. 12, p. 858, 2009.

[100] F. Grinnell, C.-H. Ho, E. Tamariz, D. J. Lee, and G. Skuta, "Dendritic Fibroblasts in Three-dimensional Collagen Matrices," Molecular Biology of the Cell, vol. 14, no. 2, pp. 384–395, 2003.

[101] R. A. Brown, M. Wiseman, C.-B. Chuo, U. Cheema, and S. N. Nazhat, "Ultrarapid Engineering of Biomimetic Materials and Tissues: Fabrication of Nano- and Microstructures by Plastic Compression," Advanced Functional Materials, vol. 15, no. 11, pp. 1762–1770, 2005.

[102] E. Hadjipanayi, V. Mudera, and R. A. Brown, "Close dependence of fibroblast proliferation on collagen scaffold matrix stiffness," Journal of Tissue Engineering and Regenerative Medicine, vol. 3, no. 2, pp. 77–84, 2009.

[103] D. E. Discher, "Tissue Cells Feel and Respond to the Stiffness of Their Substrate," Science, vol. 310, no. 5751, pp. 1139–1143, 2005.

[104] U. Cheema, R. A. Brown, B. Alp, and A. J. Macrobert, "Spatially defined oxygen gradients and vascular endothelial growth factor expression in an engineered 3D cell model," Cellular and Molecular Life Sciences, Jul. 2007.

[105] M. Akram, R. Ahmed, I. Shakir, W. Ibrahim and R. Hussain, "Extracting hydroxyapatite and its precursors from natural resources", Journal of Materials Science, vol. 49, no. 4, pp. 1461-1475, 2013.

[106] B. Clarke, "Normal Bone Anatomy and Physiology", Clinical Journal of the American Society of Nephrology, vol. 3, no. 3, pp. S131-S139, 2008.

[107] V. Kattimani, S. Kondaka and K. Lingamaneni, "Hydroxyapatite–-Past, Present, and Future in Bone Regeneration", Bone and Tissue Regeneration Insights, vol. 7, 2016.

[108] D. Straub, "Calcium Supplementation in Clinical Practice: A Review of Forms, Doses, and Indications", Nutrition in Clinical Practice, vol. 22, no. 3, pp. 286-296, 2007.

[109] E. Rigo, A. Boschi, M. Yoshimoto, S. Allegrini, B. Konig and M. Carbonari, "Evaluation in vitro and in vivo of biomimetic hydroxyapatite coated on titanium dental implants", Materials Science and Engineering: C, vol. 24, no. 5, pp. 647-651, 2004.

[110] AA Majeed, RA Al Naimi ,"Role of hydroxyapatite in healing of experimentally induced cutaneous wound in rabbits",- Al-Anbar Journal of Veterinary Sciences, 2012.

[111] Y. Rezaei, F. Moztarzadeh, S. Shahabi, and M. Tahriri, "Synthesis, Characterization, and In Vitro Bioactivity of Sol-Gel-Derived SiO2–CaO–P2O5–MgO-SrO Bioactive Glass," Synthesis and Reactivity in Inorganic, Metal-Organic, and Nano-Metal Chemistry, vol. 44, no. 5, pp. 692–701, 2013.

[112] A. Kumar, S. Murugavel, A. Aditya, and A. R. Boccaccini, "Mesoporous 45S5 bioactive glass: synthesis, in vitro dissolution and biomineralization behavior," Journal of Materials Chemistry B, vol. 5, no. 44, pp. 8786–8798, 2017.

[113] H. Aguiar, J. Serra, P. González, and B. León, "Structural study of sol–gel silicate glasses by IR and Raman spectroscopies," Journal of Non-Crystalline Solids, vol. 355, no. 8, pp. 475–480, 2009.

[114] O. P. Filho, G. P. L. Torre, and L. L. Hench, "Effect of crystallization on apatite-layer formation of bioactive glass 45S5," Journal of Biomedical Materials Research, vol. 30, no. 4, pp. 509–514, 1996.

[115] J. Qian, Y. Kang, Z. Wei, and W. Zhang, "Fabrication and characterization of biomorphic 45S5 bioglass scaffold from sugarcane," Materials Science and Engineering: C, vol. 29, no. 4, pp. 1361–1364, 2009.

[116] E. S. Freeman, "The Kinetics of the Thermal Decomposition of Sodium Nitrate and of the Reaction between Sodium Nitrite and Oxygen," The Journal of Physical Chemistry, vol. 60, no. 11, pp. 1487–1493, 1956.

[117] L. Lefebvre, L. Gremillard, J. Chevalier, and D. Bernache-Assollant, “Sintering Behavior of 45S5 Bioglass®,” Bioceramics 20 Key Engineering Materials, pp. 265–268, 2007.

[118] J. R. Jones, “Review of bioactive glass: From Hench to hybrids,” Acta Biomaterialia, vol. 9, no. 1, pp. 4457–4486, 2013.

[119] V. Krishnan and T. Lakshmi, "Bioglass: A novel biocompatible innovation", Journal of Advanced Pharmaceutical Technology & Research, vol. 4, no. 2, p. 78, 2013.

[120] K. Leung, A practical manual for musculoskeletal research. Singapore: World Scientific, pp. 225-228, 2008.

[121] B. Marelli, C. Ghezzi and D. Mohn, "Accelerated mineralization of dense collagen-nano bioactive glass hybrid gels increases scaffold stiffness and regulates osteoblastic function", Biomaterials, vol. 32, no. 34, pp. 8915-8926, 2011.

[122] W. Lepry, E. Rezabeigi, S. Smith and S. Nazhat, "Dissolution and bioactivity of a sol-gel derived borate glass in six different solution media", Biomedical Glasses, vol. 5, no. 1, pp. 98-111, 2019.

[123] M. Cerruti, D. Greenspan and K. Powers, "Effect of pH and ionic strength on the reactivity of Bioglass® 45S5", Biomaterials, vol. 26, no. 14, pp. 1665-1674, 2005.

[124] J. Jones, P. Sepulveda and L. Hench, "Dose-dependent behavior of bioactive glass dissolution", Journal of Biomedical Materials Research, vol. 58, no. 6, pp. 720-726, 2001.

[125] L. L. Hench, "Molecular Control of Bioactivity in Sol-Gel Glasses", Journal of Sol-Gel Science and Technology, no. 13, pp. 245–250, 1998.

[126] L. Souza, J. Lopes and D. Encarnação, "Comprehensive in vitro and in vivo studies of novel melt-derived Nb-substituted 45S5 bioglass reveal its enhanced bioactive properties for bone healing", Scientific Reports, vol. 8, no. 1, 2018.

[127] G. Griffanti and S. Nazhat, "Dense fibrillar collagen-based hydrogels as functional osteoid-mimicking scaffolds", International Materials Reviews, pp. 1-20, 2020. In press.

[128] H. Levis, A. Kureshi, I. Massie, L. Morgan, A. Vernon and J. Daniels, "Tissue Engineering the Cornea: The Evolution of RAFT", Journal of Functional Biomaterials, vol. 6, no. 1, pp. 50-65, 2015.

[129] I. A. Silver, J. Deas, and M. Erecińska, “Interactions of bioactive glasses with osteoblasts in vitro: effects of 45S5 Bioglass®, and 58S and 77S bioactive glasses on metabolism, intracellular ion concentrations and cell viability,” Biomaterials, vol. 22, no. 2, pp. 175–185, 2001.

[130] F. Westhauser, M. Karadjian, C. Essers, A.-S. Senger, S. Hagmann, G. Schmidmaier, and A. Moghaddam, “Osteogenic differentiation of mesenchymal stem cells is enhanced in a 45S5-supplemented β-TCP composite scaffold: an in-vitro comparison of Vitoss and Vitoss BA,” Plos One, vol. 14, no. 2, 2019.

[131] L. Haiyan, “Bioglass promotes wound healing by affecting behaviors of endothelial cells, fibroblasts,” Frontiers in Bioengineering and Biotechnology, vol. 4, 2016.

[132] A. Hoppe, N. Güldal and A. Boccaccini, "A review of the biological response to ionic dissolution products from bioactive glasses and glass-ceramics", Biomaterials, vol. 32, no. 11, pp. 2757-2774, 2011.

[133] E. M. Carlisle, “Silicon: A Possible Factor in Bone Calcification,” Science, vol. 167, no. 3916, pp. 279–280, 1970.

[134] S. Deb, R. Mandegaran, and L. D. Silvio, “A porous scaffold for bone tissue engineering/45S5 Bioglass® derived porous scaffolds for co-culturing osteoblasts and endothelial cells,” Journal of Materials Science: Materials in Medicine, vol. 21, no. 3, pp. 893–905, 2009.

[135] H. Keshaw, A. Forbes, and R. M. Day, “Release of angiogenic growth factors from cells encapsulated in alginate beads with bioactive glass,” Biomaterials, vol. 26, no. 19, pp. 4171–4179, 2005.

[136] J.-Y. Sun, Y.-S. Yang, J. Zhong, and D. C. Greenspan, “The effect of the ionic products of Bioglass® dissolution on human osteoblasts growth cyclein vitro,” Journal of Tissue Engineering and Regenerative Medicine, vol. 1, no. 4, pp. 281–286, 2007.

[137] S. Maeno, Y. Niki, H. Matsumoto, H. Morioka, T. Yatabe, A. Funayama, Y. Toyama, T. Taguchi, and J. Tanaka, “The effect of calcium ion concentration on osteoblast viability,

proliferation and differentiation in monolayer and 3D culture," Biomaterials, vol. 26, no. 23, pp. 4847–4855, 2005.

[138] T. H. Qazi, S. Hafeez, J. Schmidt, G. N. Duda, A. R. Boccaccini, and E.t Lippens, "Comparison of the effects of 45S5 and 1393 bioactive glass microparticles on hMSC behavior," Journal of Biomedical Materials Research Part A, vol. 105, no. 10, pp. 2772–2782, 2017.

[139] D. Bellucci, V. Cannillo, A. Sola, F. Chiellini, M. Gazzarri, and C. Migone, "Macroporous Bioglass®-derived scaffolds for bone tissue regeneration," Ceramics International, vol. 37, no. 5, pp. 1575–1585, 2011.

[140] A. Li, Y. Lv, H. Ren, Y. Cui, C. Wang, R. A. Martin, and D. Qiu, "In vitro evaluation of a novel pH neutral calcium phosphosilicate bioactive glass that does not require preconditioning prior to use," International Journal of Applied Glass Science, vol. 8, no. 4, pp. 403–411, 2017.

[141] A. El-Ghannam, P. Ducheyne, and I. M. Shapiro, "Bioactive material template for in vitro, synthesis of bone," Journal of Biomedical Materials Research, vol. 29, no. 3, pp. 359–370, 1995.

[142] K. Wallace, R. Hill and J. Pembroke, "Influence of sodium oxide content on bioactive glass properties", Journal of Materials Science: Materials in Medicine, vol. 10, no. 12, pp. 697-701, 1999.

[143] H. Shahoon, "The Comparison of Silver and Hydroxyapatite Nanoparticles Biocompatibility on L929 Fibroblast Cells: An In vitro Study," Journal of Nanomedicine & Nanotechnology, vol. 04, no. 04, 2013.

[144] H. Demirkiran, A. Mohandas, M. Dohi, A. Fuentes, K. Nguyen, and P. Aswath, "Bioactivity and mineralization of hydroxyapatite with bioglass as sintering aid and bioceramics with $Na_3Ca_6(PO_4)_5$ and $Ca_5(PO_4)_2SiO_4$ in a silicate matrix," Materials Science and Engineering: C, vol. 30, no. 2, pp. 263–272, 2010.

[145] C. M. Giachelli, "Ectopic Mineralization: New Concepts in Etiology and Regulation," Handbook of Biomineralization, pp. 349–360, 2007.

[146] Q. Li, Q. Jiang, and J. Uitto, "Ectopic mineralization disorders of the extracellular matrix of connective tissue: Molecular genetics and pathomechanisms of aberrant calcification," Matrix Biology, vol. 33, pp. 23–28, 2014

[147] U. Okonkwo and L. Dipietro, “Diabetes and Wound Angiogenesis,” International Journal of Molecular Sciences, vol. 18, no. 7, p. 1419, 2017.

[148] O. P. Filho, G. P. L. Torre, and L. L. Hench, “Effect of crystallization on apatite-layer formation of bioactive glass 45S5,” Journal of Biomedical Materials Research, vol. 30, no. 4, pp. 509–514, 1996.

[149] R. M. Day, A. R. Boccaccini, S. Shurey, J. A. Roether, A. Forbes, L. L. Hench, and S. M. Gabe, “Assessment of polyglycolic acid mesh and bioactive glass for soft-tissue engineering scaffolds,” Biomaterials, vol. 25, no. 27, pp. 5857–5866, 2004.

[150] K. K. Kaysinger and W. K. Ramp, “Extracellular pH modulates the activity of cultured human osteoblasts,” Journal of Cellular Biochemistry, vol. 68, no. 1, pp. 83–89, 1998.

[151] M. Ojansivu, A. Mishra, S. Vanhatupa, M. Juntunen, A. Larionova, J. Massera, and S. Miettinen, “The effect of S53P4-based borosilicate glasses and glass dissolution products on the osteogenic commitment of human adipose stem cells,” Plos One, vol. 13, no. 8, 2018.

[152] I. Nishimura, R. Hisanaga, T. Sato, T. Arano, S. Nomoto, Y. Ikada, and M. Yoshinari, “Effect of osteogenic differentiation medium on proliferation and differentiation of human mesenchymal stem cells in three-dimensional culture with radial flow bioreactor,” Regenerative Therapy, vol. 2, pp. 24–31, 2015.

[153] L. B. Alves, V. C. Mariguela, M. F. D. M. Grisi, S. L. S. D. Souza, A. B. N. Junior, M. T. Junior, P. T. D. Oliveira, and D. B. Palioto, “Expression of osteoblastic phenotype in periodontal ligament fibroblasts cultured in three-dimensional collagen gel,” Journal of Applied Oral Science, vol. 23, no. 2, pp. 206–214, 2015.

Appendix A

Table 5: Evaluation of acellular as-made collagen fibrillar density by freeze drying, n=6

Sample no.	**Tube wt [g]**	**Wet gel + tube wt [g]**	**Wet gel wt [g]**	**Dry gel + tube wt [g]**	**Dry gel wt [g]**	**CFD [wt%]**
1	0.9913	1.0004	0.0091	0.9923	0.0010	10.9890
2	0.9851	0.9913	0.0062	0.9862	0.0011	17.7419
3	1.0019	1.0103	0.0084	1.0029	0.001	11.9048
4	0.9955	1.0045	0.009	0.9966	0.0011	12.2222
5	0.9962	1.0026	0.0064	0.9971	0.0009	14.0625
6	0.9908	0.999	0.0082	0.9919	0.0011	13.4146
					Mean	13.3892
					S.D	2.1881